U.S. Department of Commerce
National Technical Information Service

N77 240 59

THEORETICAL STUDY OF THE EFFECT OF GROUND PROXIMITY ON THE INDUCED EFFICENCY OF HELICOPTER ROTORS

NATIONAL AERONAUTICS & SPACE ADMINISTRATION
WASHINGTON, D.C

MAY 77

(NASA-TM-X-71951) THEORETICAL STUDY OF THE EFFECT OF GROUND PROXIMITY ON THE INDUCED EFFICIENCY OF HELICOPTER ROTORS (NASA) 90 p HC A05/MF A01 CSCL 01A

N77-24059

Unclas
G3/02 30311

NASA TECHNICAL MEMORANDUM

NASA TM X- 71951

NASA TM X- 71951

THEORETICAL STUDY OF THE EFFECT OF GROUND PROXIMITY ON THE INDUCED EFFICIENCY OF HELICOPTER ROTORS

by Harry H. Heyson
NASA Langley Research Center

May 3, 1977

This informal documentation medium is used to provide accelerated or special release of technical information to selected users. The contents may not meet NASA formal editing and publication standards, may be revised, or may be incorporated in another publication.

National Aeronautics and Space Administration

Langley Research Center
Hampton, Virginia 23665

REC
NASA ST
INPUT BRANCH

1. Report No.	2. Government Accession No.	3. Recipient's Catalog No.
TM X-71951		

4. Title and Subtitle	5. Report Date
THEORETICAL STUDY OF THE EFFECT OF GROUND PROXIMITY ON THE INDUCED EFFICIENCY OF HELICOPTER ROTORS	May 3, 1977
	6. Performing Organization Code 31.600
7. Author(s) Harry H. Heyson	8. Performing Organization Report No.
	10. Work Unit No. 791-40-08-01
9. Performing Organization Name and Address NASA Langley Research Center Hampton, Virginia 23665	11. Contract or Grant No.
	13. Type of Report and Period Covered Technical Memorandum
12. Sponsoring Agency Name and Address National Aeronautics & Space Administration Washington, DC 20546	14. Sponsoring Agency Code

15. Supplementary Notes

16. Abstract

A theoretical study of rotors in forward flight within ground effect shows that the ground-induced interference is an upwash and a decrease in forward velocity. The interference velocities are large, oppose the normal flow through the rotor, and have large effects on the induced efficiency. Hovering with small ground clearances may result in significant blade stall. As speed is increased from hover in ground effect, power initially increases rather than decreases. At very low heights above the ground, the power requirements become nonlinear with speed as a result of the streamwise interference. The streamwise interference becomes greater as the wake approaches the ground and eventually distorts the wake to form the ground vortex which contributes to certain observed directional stability problems. The effects of the streamwise interference are of large magnitude and cannot be ignored in ground effect analysis.

17. Key Words (Suggested by Author(s))	18. Distribution Statement
AERODYNAMICS, HELICOPTERS, GROUND EFFECT, INDUCED POWER	UNCLASSIFIED UNLIMITED

19. Security Classif. (of this report)	20. Security Classif. (of this page)	21. No. of Pages	22. Price*
UNCLASSIFIED	UNCLASSIFIED	88	$5.00

* For sale by the National Technical Information Service, Springfield, Virginia 22161

THEORETICAL STUDY OF THE EFFECT OF GROUND PROXIMITY ON THE INDUCED EFFICIENCY OF HELICOPTER ROTORS

by Harry H. Heyson

Langley Research Center
Hampton, VA 23665

SUMMARY

A theoretical study of rotors in forward flight within ground effect shows that the ground-induced interference is an upwash and a decrease in forward velocity. The interference velocities are large, oppose the normal flow through the rotor, and have large effects on the induced efficiency. Hovering with small ground clearances may result in significant blade stall. As speed is increased from hover in ground effect, power initially increases rather than decreases. At very low heights above the ground, the power requirements become nonlinear with speed as a result of the streamwise interference. The streamwise interference becomes greater as the wake approaches the ground and eventually distorts the wake to form the ground vortex which contributes to certain observed directional stability problems. The effects of the streamwise interference are of large magnitude and cannot be ignored in ground effect analysis.

INTRODUCTION

Performance in forward flight close to the ground has significant effects on the operational utility of helicopters. The decrease in ground effect with forward speed has an important role in determining the maximum take-off performance of an overloaded helicopter from a confined area (refs. 1,2). Directional control instabilities at very low speed in ground effect have become a significant problem (ref. 3), and have required extensive experimental studies (refs. 4-7). References 4 and 5 have shown that the directional control problems result from a combination of effects including the ground-induced distortions of the wake and the increased power required as the helicopter is accelerated from hover in ground effect.

The favorable ground effect of the hovering rotor has been the subject of numerous experimental (refs. 8 to 10) and theoretical (refs. 11 to 14) studies. Theoretical analysis of the rotor in forward flight has received less attention (refs. 15,16); furthermore, even the available treatments are approximate and omit significant features of the problem. For example, reference 15 models the rotor wake as a single directional source with a flow pattern that is unrepresentative of the columnar nature of a real rotor wake. Although reference 16 uses a more plausible vortex cylinder to model the wake, the analysis was restricted to the interference at the center of the rotor and it omitted the streamwise interference velocities.

Little theoretical work has been done on the ground-effect problem subsequent to the publication of references 15 and 16; however, substantial effort has been applied to the related problem of wind-tunnel interference (refs. 17 to 23). The results of the wind-tunnel interference studies indicate the need for considering a number of features omitted in the earlier ground-effect analyses. First, when very close to a boundary such as the ground, the configuration must be represented in detail including its attitude and its load distribution (refs. 18 to 20). Second, the horizontal or streamwise interference velocities (refs. 18,19) can not be omitted since they can be so large as to determine the overall character of the flow (refs. 22,23) Indeed, the magnitude of the interference velocities can be great enough to influence the induced performance in a nonlinear manner similar to that described in reference 24. Finally, the wake skew angle used for the calculations should not be that of momentum theory but should be an effective skew angle adjusted to account for the vertical displacements associated with wake roll-up (refs. 21 to 23).

The present study attempts to include many of the foregoing features into an analysis of rotary wing ground effect in forward flight. The effect of the ground is obtained in terms of horizontal and vertical components of interference velocity. These interference velocities are distributed nonuniformly over the rotor disk; however, the average horizontal interference velocity opposes the forward velocity, and the average vertical interference velocity opposes the rotor induced velocity. Thus, the interference decreases the mass flow through the rotor and, at heights above the ground of practical interest, has a major effect on induced power and also on the wake skew angle. These effects are treated by suitably modifying the momentum theory of references 24 and 25 so that it applies to forward flight in ground effect. The induced shaft powers are calculated and presented as functions of forward speed, height above the ground, and rotor angle of attack.

Numerous experimental and theoretical studies (refs. 4 to 7, 9, 12 to 14, 23) have described wake distortion effects which have significant influence on the utility of helicopters in ground effect. The simple rigid wake models used in the present analysis are not capable of actually computing such distortions with any degree of accuracy. Nevertheless, calculated flow-fields using these models do predict the nature of such distortions and are of value in presenting a coherent explanation of the observed distortions and the factors which cause them. Some discussion of wake distortion effects is included and is illustrated by theoretically calculated examples.

SYMBOLS

D	Rotor drag, positive rearward
$\bar{F}$	Force vector produced by rotor
H	Distance of rotor above ground
L	Rotor lift, positive upward
P	Power
P_h	Induced shaft power required to hover in free air with no drag force
P_s	Induced shaft power
$P_{s,h}$	Induced shaft power required to hover with no drag force in the presence of the ground
R	Rotor radius
u_0	Mean, or momentum, value of the streamwise component of rotor induced velocity, positive rearward
V	Rotor forward velocity
$\bar{V}$	Total aerodynamic velocity vector at the rotor
V_R	Resultant aerodynamic velocity at rotor (absolute value of $\bar{V}$)
w	Net vertical velocity, $w_\ell + \Delta w$
w_0	Mean, or momentum, value of the vertical component of rotor induced-velocity, positive upward (also induced velocity at center of a uniformly loaded wing)

w_h Value of w_0 when hovering in free air with no drag force.

w_ℓ Local value of rotor induced velocity

X,Y,Z Cartesian coordinate axes centered in the rotor, X horizontal and positive rearward, Z vertical and positive upward, Y horizontal to the side to form a right-hand system (see figure 1)

x,y,z Distance measured from the origin along the X,Y,Z axis system

α Rotor tip-path-plane angle of attack, the angle measured positive upward from the flight direction to the leading edge of the rotor disk (see figure 1)

Γ Circulation

Δu Incremental streamwise interference velocity caused by the presence of the ground, positive rearward

Δw Incremental vertical interference velocity caused by the presence of the ground, positive upward

δ Interference factor (general)

$\delta_{u,D}$ Factor proportional to the streamwise component of ground interference resulting from the rotor drag force.

$\delta_{u,L}$ Factor proportional to the streamwise component of ground interference resulting from the rotor lift force.

$\delta_{w,D}$ Factor proportional to the vertical component of ground interference resulting from the rotor drag force

$\delta_{w,L}$ Factor proportional to the vertical component of ground interference resulting from the rotor lift force

ρ Mass density of air

χ Wake skew angle, measured positive rearward from the vertical (negative Z-axis) to the centerline of the wake (see figure 1)

χ_e Effective value of χ in consideration of wake roll-up effects.

THEORY

GENERAL APPROACH

While the final form of the analysis must constitute a unified treatment, it is more convenient to discuss a number of individual items separately at the outset. Consequently, the present paper will discuss first the representation of the wake in free air. Then the modification to the free-air wake necessary to represent ground effect will be considered. Next, momentum-theory considerations necessary to obtain the effect on the rotor are derived, and then the roll-up of the wake is considered. Finally, all of these separate considerations are combined into a systematic approach to computing the effect of ground proximity on the performance of the rotor.

ROTOR WAKE IN FREE AIR

Directional source. - A number of rotor wake models are available for use in the analysis. Of these models, the directional source of reference 15 is the simplest. Unfortunately, this wake model does not lead to a wake with the columnar nature of a real rotor wake. Furthermore, its use (ref. 15) leads to a complete elimination of ground effect at high speed which is contrary to the obvious result that ground effect for a rotor at high speed should be similar to that for a wing. Because of these deficiencies, this wake model is not used in the present analysis.

Skewed vortex cylinder. - In contrast to the directional source, the skewed vortex cylinder wake of reference 26 does represent reasonably well the nature of a real rotor wake. Furthermore, reference 27 has shown that, when extended to representative disk-load distributions, the skewed vortex-cylinder wake results in calculated induced flows which match the measured flows over most of the rotor disk. Prior to the advent of modern computers, the computational difficulties associated with this wake model limited its application to regions where calculated results were available in chart form (refs. 26 to 28, for example). Currently, it is more appropriate and more economical to compute the flow-field by direct numerical integration of the equations given in reference 29. Sutiable FORTRAN subroutines will be found in Appendix C of reference 23.

Inclined doublet string. - If the rotor producing the skewed vortex-cylinder is very small, or if the point of interest is far from the rotor and its wake, each of the vortex rings making up the cylinder effectively becomes small until, in the limit, each ring becomes a point doublet, and the entire wake becomes an inclined string of doublets. This representation of the rotor wake was used for the "vanishingly-small" rotor of reference 17 and is the fundamental building block of the system of wind-tunnel corrections developed in references 18 to 20.

Obviously, a rotor is not small with respect to its height above the ground for heights of practical interest (say, 0.5 to 2.0 rotor radii). On the other hand, the simplicity of this wake model leads to closed-form expressions for the flow, both in free air and in the presence of the ground (refs. 17,18). Although the numerical results may contain substantial errors, the simplicity of the results allows one to draw conclusions as to the magnitude and importance of several effects.

Nest of doublet strings. - As indicated in reference 18, and carried to fruition in references 19 and 20, the restriction to a vanishingly small rotor inherent in the inclined doublet string can be removed by superposing the flow fields of a nest of such doublet strings. The superposed flow fields of the doublet strings will approximate the flow field of the skewed vortex cylinder more closely as the number of strings comprising the nest is increased. When 20 doublet strings are used, as in references 19 and 20, the flow field is essentially equivalent to that of the vortex cylinder at distances as small as a few tenths of a rotor radius from the wake.

Although the substitution of a nest of doublet strings for a vortex cylinder may seem superfluous at first glance, several advantages are inherent in the procedure. First, computational time is significantly reduced - by an order of magnitude for a uniformly loaded rotor, and by two orders of magnitude for nonuniformly loaded rotors. Furthermore, additional flexibility is obtained since, as will be shown subsequently, this representation avoids certain restrictions inherent in the vortex-cylinder representation.

INTERFERENCE IN GROUND EFFECT

Wake. - The rotor wake in ground effect is presumed to flow along straight inclined path from the rotor disk to its intersection with the ground. It is then allowed to flow off along the ground to infinity in the free-stream direction. This behavior is extremely linearized when compared to the real rotor wake, and it is obviously in contrast to the required axisymmetric flow on the ground in hover. Nevertheless, it is at least crudely representative of the true behavior of the wake when the rotor has a forward velocity. Furthermore, references 22 and 23 have demonstrated that these assumptions result in a flow field which would produce the observed wake flow patterns if the theoretical wake were allowed to deform.

Ground effect by superposition. - Under the assumption that the free-air wakes do not deform other than in the stylized bend at the ground, the flow field in ground effect can be obtained by a systematic superposition of any of the free-air wakes considered herein. This procedure is illustrated schematically in figure 2.

The free air wake, shown in figure 2(a), is translated, together with its flow field, downward along the wake axis to the location of the ground as in figure 2(b). Subtraction of the translated semi-infinite wake and its flow field from the original wake and flow field results in the finite length of wake shown in figure 2(c). The portion of the wake running along the ground is obtained by increasing the wake skew angle to 90^{o} (figures 2(d) and 2(e)) and then translating this flat wake and its flow field to coincide with the lower end of the truncated cylinder (figure 2(f)). The indicated addition of wakes and flow fields results (figure 2(g)) in the required above-ground portion of the wake.

The wake of figure 2(g) requires an image system in the ground to meet (by symmetry) the required condition of zero flow through the ground. For the present study, where the disk loading is assumed axisymmetric, the image system in the ground is achieved by a rotation about the intersection of wake and ground (figure 2(h)). Addition of the wakes and flow fields of figures 2(g) and 2(h) results in the complete wake system and its flow field as sketched in figure 2(i).

The foregoing sequence would require an additional step if the rotor loading was not at least laterally symmetric. In that case, it would be necessary to invert the Y-axis and the direction of the lateral velocities of the image vortex system prior to the final addition.

The field resulting from the superpositions is that for the entire wake and image system. Ground effect is specifically defined as the difference in flow between free air and in the presence the ground; that is, ground effect is the difference in the flows caused by the vortex systems of figures 2(a) and 2(i). Thus, it could be obtained from an additional subtraction; however, it is simpler to omit the original free-air wake from the calculation at the outset. Indeed, any other course can lead to numerical difficulties with singularities when using some of the current wake models.

Choice of wake model. - If the rotor angle of attack is not zero, the initial translation of the wake (figure 2(b)) results in a wake whose plane of origin does not coincide with the plane of the ground. In this case, the total superposition scheme of figure 2 fails completely. Thus, the skewed vortex-cylinder model is restricted to the study of conditions where $\alpha = 0^{o}$. Since an inclined doublet string has no finite diameter, it can be used when α is not zero; however, that representation is inadequate for most quantitative purposes. Provided that each doublet string involved is carried through the ground-effect superpositions

individually prior to nesting the set of strings comprising the total nested wake model, that model can be used for any angle of attack.

Computer programs. - The initial applications of this method (refs. 12, 13) were accomplished by manual calculations based on charts of induced velocity contours near a rotor. Such methods are too cumberson in the light of current computer capabilities. A FORTRAN program, needing only minor changes, given in Appendix C of reference 23, is suitable for calculations involving wakes modelled as inclined vortex cylinders. Similarly, reference 20 gives FORTRAN programs usuable when the wake model is either a single doublet string or a nest of doublet strings. In all of these programs the main objective was to calculate wind-tunnel interference. Considerable computer time can be saved by disabling the DO-loops which provide the additional images required to represent the three additional boundaries of a wind tunnel.

MOMENTUM THEORY IN GROUND EFFECT

Initial considerations. - Even in the absence of ground effect, the induced velocities at the rotor may be large compared to the free stream velocity. Consequently, the induced performance of the rotor (refs. 25, 30, 31) becomes decidedly nonlinear at low speeds. Even the alterations in the resultant flow which result from small descent rates (ref. 24) magnify the nonlinearities in performance. A ground-induced upwash is the equivalent of an aerodynamic sink rate and may be expected to have effects similar to those shown in reference 24.

Since it will be shown that the ground induces large interference velocities, it is necessary to provide a systematic procedure for the evaluation of the resulting nonlinear induced performance. In the present study, these effects will be evaluated using suitable modifications to the momentum theory presented in references 24 and 25. The derivations are rather simple and provided herein in their entirety.

Induced velocities. - Figure 3 shows the force and velocity vectors at the rotor. It is assumed, following "Glauert's Hypothesis" (ref. 32) that the total mass flow of the rotor, at any forward speed, is that flowing through a circle of radius R with a velocity of V_R. This hypothesis may be justified by observing that simple vortex theory leads to the identical result (ref. 33). For a rotor, the induced velocities in the far wake are twice those at the rotor. Thus, since the vertical and horizontal forces are equal to the timewise rate of change of momentum in the vertical and horizontal directions

$$L = -2\rho\pi R^2 V_R w_0 \qquad (1)$$

$$D = -2\rho\pi R^2 V_R u_0 \qquad (2)$$

The relationship between the forces and the induced velocities is obtained by dividing equation (2) by equation (1) to yield

$$\frac{D}{L} = \frac{u_0}{w_0} \tag{3}$$

The resultant force vector of a rotor is essentially perpendicular to the rotor disk, thus

$$\frac{D}{L} = \frac{u_0}{w_0} = \tan \alpha \tag{4}$$

The resultant velocity V_R through the rotor is obtained from figure 3 as

$$V_R = \sqrt{(V + u_0 + \Delta u)^2 + (w_0 + \Delta w)^2} \tag{5}$$

Now, divide each side of equation (5) by $-w_0$ and then use equation (4) to obtain

$$\frac{V_R}{w_0} = -\sqrt{\left(\frac{V}{w_0} + \frac{u_0}{w_0} + \frac{\Delta u}{w_0}\right)^2 + \left(1 + \frac{\Delta w}{w_0}\right)^2} \tag{6a}$$

$$\frac{V_R}{w_0} = -\sqrt{\left(\frac{V}{w_0} + \tan \alpha + \frac{\Delta u}{w_0}\right)^2 + \left(1 + \frac{\Delta w}{w_0}\right)^2} \tag{6b}$$

At this point, it is convenient to define a reference velocity w_h, chosen to be the vertical component of induced velocity while hovering in free air; that is, $w_h = w_0$ when $V = \alpha = \Delta u = \Delta w = 0$. Substituting these values into equation (6) yields the result that $V_R = -w_h$. Now substitute that result into equation (1) and solve for w_h to obtain

$$w_h = -\sqrt{\frac{L}{2\rho\pi R^2}} \tag{7}$$

Observe that the negative value of the square root is chosen in equation (7) since, with the present sign convention, equation (1) requires a negative induced velocity to produce a positive lift. Now solve equation (1) for w_0, and divide the resulting equation by equation (7) squared, to yield

$$\frac{w_0}{w_h}^2 = \frac{\frac{-L}{2\rho\pi R^2 V_R}}{\frac{L}{2\rho\pi R^2}} = \frac{-1}{V_R} \tag{8}$$

Then multiply both sides of equation (8) by w_0 to obtain the general result that

$$\left(\frac{w_0}{w_h}\right)^2 = -\frac{w_0}{V_R} \tag{9}$$

For the specific problem of the rotor in ground effect, substitute equations (6) into equation (9), and square both sides of the equations to obtain the momentum quartic as

$$\left(\frac{w_0}{w_h}\right)^4 = \frac{1}{\left(\frac{V}{w_0} + \frac{u_0}{w_0} + \frac{\Delta u}{w_0}\right)^2 + \left(1 + \frac{\Delta w}{w_0}\right)^2} \tag{10a}$$

$$\left(\frac{w_0}{w_h}\right)^4 = \frac{1}{\left(\frac{V}{w_0} + \tan\alpha + \frac{\Delta u}{w_0}\right)^2 + \left(1 + \frac{\Delta w}{w_0}\right)^2} \tag{10b}$$

Wake skew angle. - The wake skew angle, the angle between the vertical axis and the wake centerline, is a major parameter of the current study. This angle may be obtained by inspection from figure 3, together with the use of equation (4), as

$$\tan\chi = -\frac{\frac{V}{w_0} + \tan\alpha + \frac{\Delta u}{w_0}}{1 + \frac{\Delta w}{w_0}} \tag{11}$$

In the present investigation, the skew angle χ must be used at the outset to determine Δu and Δw, and the angle of attack will be used as an input value. Under such conditions, it is often more convenient to solve equation (11) for V/w_0 to obtain

$$\frac{V}{w_0} = -\left(1 + \frac{\Delta w}{w_0}\right)\tan\chi - \tan\alpha - \frac{\Delta u}{w_0} \tag{12}$$

Reference 25 has shown that for level flight in free air, $\cos\chi = (w_0/w_h)^2$; however, as noted in reference 24, this relationship is more complicated when an additional vertical velocity, such as Δw, is present. Therefore, multiply by sides of equation (11) by $-(1 + \Delta w/w_0)$ to yield

$$-\tan\chi\left(1 + \frac{\Delta w}{w_0}\right) = \frac{V}{w_0} + \tan\alpha + \frac{\Delta u}{w_0} \tag{13}$$

Then substitute equation (13) into equation (10b) to obtain

$$\left(\frac{w_0}{w_h}\right)^4 = \frac{1}{\left(1 + \frac{\Delta w}{w_0}\right)^2\left(1 + \tan^2\chi\right)} \tag{14a}$$

$$\left(\frac{w_0}{w_h}\right)^2 = \frac{\cos\chi}{1 + \frac{\Delta w}{w_0}} \tag{14b}$$

Finally, solve equation (14b) for cos χ, to yield

$$\cos\chi = \left(\frac{w_0}{w_h}\right)^2 \left(1 + \frac{\Delta w}{w_0}\right) \tag{15a}$$

$$\cos\chi = \frac{w_0}{w_h} \left(\frac{w_0}{w_h} + \frac{\Delta w}{w_h}\right) \tag{15b}$$

Induced shaft power. - The induced power at the shaft is given by the scalar (or dot) product of the force and velocity vectors. Using the present sign convention, this power is

$$P_s = - \bar{F} \cdot \bar{V} \tag{16}$$

Substitute the force and velocity vectors from figure 3 into equation (16) and expand the scalar product to obtain

$$P_s = - D (V + u_0 + \Delta u) - L (w_0 + \Delta w) \tag{17}$$

The shaft power when hovering out of ground effect is a convenient reference power. For this condition, $w_0 = w_h$ and $V = D = \Delta u = \Delta w = 0$. Substitute the foregoing values into equation (17) to obtain

$$P_h = - L w_h \tag{18}$$

Now, nondimensionalize equation (17) by dividing it by equation (18), and use equation (4) to obtain

$$\frac{P_s}{P_h} = \left(\frac{V}{w_h} + \frac{\Delta u}{w_h}\right) \tan\alpha + \frac{w_0}{w_h} \sec^2\alpha + \frac{\Delta w}{w_h} \tag{19}$$

or, by rearranging terms

$$\frac{P_s}{P_h} = \frac{w_0}{w_h} \left[\left(\frac{V}{w_0} + \frac{\Delta u}{w_0}\right) \tan\alpha + \sec^2\alpha + \frac{\Delta w}{w_0}\right] \tag{20}$$

WAKE ROLL UP

Observed roll up. - The wake of a planar lifting system does not remain flat but rolls up shortly after passage of the aircraft. This roll up occurs very rapidly for low aspect-ratio systems such as rotors. Reference 27 shows clearly that the roll-up process is already well under way by the time that the wake reaches the trailing edge of the rotor. This effect is illustrated in figure 4 (from ref. 27) which presents the contours of vorticity measured almost immediately behind the trailing edge of a rotor disk. The intersection of the theoretical inclined-cylinder wake and the survey plane is indicated. In the absence of roll up, the contours of vorticity would be expected to lie on, or within, the elliptical intersection region. Instead, the measured vorticity lies above the outer extremities of the ellipse. The wake is already essentially completely rolled up, and it has descended only about half as far as would have been anticipated in the absence of roll up.

Simple wing wake. - The wake of a rotor has several gross similarities to the simpler wake of a wing. Consider the horseshoe vortex of a uniformly loaded wing (fig. 5). The center of this wing lies directly on the bound vortex which thus has no effect on the induced velocity at that point. Each of the semi-infinite vortexes trailing from the wing tips contributes $w_0/2$ to the total induced velocity at the center of the wing. The situation is altered in the far wake where the bound vortex is too distant to have any effect. At this location, each of the trailing vortexes is essentially doubly infinite; thus, each contributes an induced velocity of w_0 for a total induced velocity, as expected, of $2w_0$.

The vortexes themselves are convected by their own induced velocity field. Consider a point far downstream lying exactly on one of the trailing vortexes. Once more the bound vortex has no effect because of its distance. Under the assumption that the trailing vortexes are straight, the vortex upon which the point lies will also have no effect on the induced velocity at that vortex. Only the opposite vortex influences the velocity at the chosen point. Since the total distance between vortexes is twice that from either one to the center of the wake, the total velocity induced on the trailing vortex is only $w_0/2$. Thus, the final inclination of the vortexes to the main flow is only one-half the vortex inclination calculated at the center of the wing.

The foregoing analysis does not mean that the vortexes and the center of the wake follow totally different paths, for the greatest velocities throughout the wake will still occur somewhere between the trailing vortexes. However, the local angle of the flow between the vortexes will not be normal to the vortexes. At any cross-section normal to

the trailing vortexes, there will still be some flow in or out of the plane. Even at an infinite distance behind the wing, a true uniplanar (Treffetz plane) cross-flow can only be achieved for vanishingly small lifts for which it is permissible to ignore the wake deflection.

Choice of wake angle. - The choice of the wake skew angle will have a significant influence on many calculated results, and the foregoing discussion indicates a multiplicity of choices for the skew angle which should be used. Undoubtedly, it would be best to calculate the actual deformed wake shape rather than to idealize the wake so that it lies along a straight line. Such calculations have been performed for simple cases in free air (for example, ref. 34); however, the complexity and expense of similar calculations in ground effect does not appear to be worthwhile, even if all of the computational convergence problems could be overcome.

In practice, it is clear that the use of the skew angle obtained from momentum theory leads to reasonable results for performance calculations (ref. 35) and for calculating the induced flow over most of the rotor (ref. 27). Even in free air, however, reference 27 has shown that it is necessary to modify the momentum-theory skew angle to account for roll up when calculating the flow behind a rotor. More specifically, in examining the closely analogous case of wind-tunnel interference, reference 21 has demonstrated the need to use an effective wake skew angle, representing the skew angle of the rolled-up wake vorticity, when calculating the wall-induced interference velocities. A similar dual skew-angle approach will be used herein, with the momentum skew-angle χ being used to calculate induced performance, and an effective skew angle χ_e being used to calculate the ground-induced interference field.

Effective skew angle. - The use of an effective skew angle appeared with reference to helicopters in reference 27 where the half-deflection analogy to wings was used. A more elaborate analysis of the elliptically loaded wing has been made by Cone (ref. 36) who considered the motion of the center of gravity of the entire vortex system behind the wing. This analysis leads to a factor of $4/\pi^2$ rather than one-half.

The difficulty with wing analogies is that they are uniformly based on the assumption that the wake deflections are so small that the wake angles are directly proportional to the down-wash velocity. This assumption is an obvious contradiction under hovering conditions where both the momentum and effective wake skew angles must coincide at $\chi = \chi_e = 0^o$.

If the horizontal interference is neglected, the tangent of the wake deflection will be equal to w_0/V; so that the large-angle equivalent of Cone's analysis becomes

$$\tan\chi_e = \frac{\pi^2}{4} \tan\chi \qquad (21)$$

An equivalent equation could be written for the simple factor of one-half. Several of these approximations are compared in figure 6. It is evident that there is little significant difference unless χ is on the order of 30 degrees or less. Consequently, equation (21) will be used to define the effective skew angle in the present analysis.

COMPUTATIONAL PROCEDURE

The calculation begins with given values of rotor diameter, height above the ground, angle of attack with respect to the ground, and an assumed axisymmetric rotor load distribution. A value of the momentum skew angle χ is chosen, and the effective skew angle χ_e is calculated from equation (21).

The next step is to obtain the ground-induced interference velocity ratios $\Delta u/w_0$ and $\Delta w/w_0$. If either a single doublet string or a nest of doublet strings is used, the programs of reference 20 are directly applicable for any angle of attack when used in conjunction with equation (4). If vortex cylinders are used to represent the wake (in which case, the angle of attack must be zero), the program of Appendix C in reference 23 can be used provided that it is modified to obtain the average interference velocities over the entire rotor disk.

Once the interference velocity ratios are in hand, the rotor forward velocity ratio is obtained from equation (12). Then the induced velocity ratio is calculated using equation (10b). Finally, the shaft power ratio is obtained from equation (20), and V/w_h is obtained from the identity:

$$\frac{V}{w_h} = \frac{V}{w_0}\frac{w_0}{w_h} \tag{22}$$

It will be observed that the forward velocity is a product of the calculation and not an initial value. This procedure is required, since it is necessary to know the skew angle to calculate the interference velocities, which, in turn, influence the skew angle. The foregoing procedure eliminates the necessity to cycle iteratively through the entire calculation. It is simpler to perform the calculations for a range of skew angles and then to interpolate between the calculated results for the desired forward speed.

RESULTS AND DISCUSSION

DISTRIBUTION OF GROUND-INDUCED INTERFERENCE OVER THE ROTOR DISK

Hovering flight. - The distribution of the ground-induced interference velocities over the longitudinal axis of a hovering rotor is shown in figure 7. Obviously, an identical result would be obtained for any diameter of the rotor because of the symmetry of rotor and wake when hovering.

The vertical interference velocity is symmetric about the center of the rotor and is nonuniformly distributed over the rotor disk (fig. 7a). The nonuniformity is particularly obvious for the triangular disk load distribution where it results from the zero load at the rotor center. Because the disk load distribution of real rotors must always be zero at the center (ref. 27), a similar distribution will always be present in practice.

The longitudinal induced velocity over this axis is really a radial flow, generally inward, which is axisymmetric over the disk. The antisymmetry indicated in figure 7b results from the presentation in terms of a streamwise velocity rather than a radial velocity. Regardless of load distribution, this component of interference is nonuniform, being greatest at the rotor tips and decreasing to the symmetry-forced value of zero at the center of the rotor. The nonuniformity is greatest for the triangular disk load distribution, where, in close proximity to the ground, the flow is outward near the center of the rotor.

Reference 13 examines the adequacy of the linearized vortex theory in hovering flight near the ground, and it observes that the actual distortions of the wake from the assumed cylindrical shape can significantly affect the accuracy of calculated results. Nevertheless, reasonable qualitative results can be obtained. For example, reference 12 has computed the flow field near a triangularly loaded rotor in ground effect and has shown (fig. 8) that the calculation indicates a large region of net upwash below and extending upward through the rotor. This region was evident in the balsa-dust flow pictures of reference 9 (fig. 9).

Forward flight. - Figures 10 and 11 show the distribution of the vertical and longitudinal ground-induced interference velocities over the longitudinal axis of the rotor for several skew angles representative of forward flight. A similar presentation for the lateral axis is given in figures 12 and 13.

The ground-induced interference velocities are evidently very nonuniformly distributed over the rotor disk. The longitudinal growth of vertical interference (fig. 10) is particularly significant. The analysis of reference 16, which was limited by the relatively slow computational speed of the computers available at that time, assumed that the value of interference at the rotor center was a suitable average of the interference over the rotor. Examination of figure 10 indicates that this assumption was not completely adequate, particularly when nonuniform load distributions were considered.

It is clear from figures 10 to 13 that the ground-induced interference velocities can attain values sufficiently great to alter the load distribution over the rotor. Ideally, the interference should be cycled into the rotor performance equations to obtain a new load distribution, eventually iterating to a load distribution compatible with ground interference. Unfortunately, the wake models used for the ground interference have been simplified to the point where time-dependence has been lost. As pointed out in reference 12, the time-averaged velocities obtained by the present method are unsuitable for the calculation of blade loads, thus, the aforementioned interation would be invalid.

Since it is not possible to perform the calculations for the actual blade loading, and because the idealized wake is significantly deformed in practice (refs. 13, 22, 23), exact correlation between experiment and theory is too much to expect. Instead, somewhat qualitative results must be anticipated. Numerical utilization of the theoretical results depends upon correlation with controlled experiments. Irrespective of the absolute numerical accuracy, it should be possible to increase the overall understanding of the problem by a qualitative comparison of theory and experimental observations.

HOVERING PERFORMANCE IN GROUND EFFECT

Ground-induced interference velocities. - In hovering, the axial symmetry of the flow requires that the average value of the streamwise interference velocity must be zero. The average vertical interference velocity ratio $\Delta w/w_0$ is shown as a function of height above the ground in figure 14. This average interference is always an upwash, and it increases rapidly as the rotor approaches the ground. There is a significant difference in the average interference velocity as the rotor disk load distribution is changed, particularly in the range of heights of primary interest ($0.3 < H/R < 2$). Figure 15 gives a similar presentation of the interference velocity at the center of the rotor. Comparison of

figure 15 with figure 14 shows that the single value at the center of the rotor with the triangular disk load distribution has no relationship to the corresponding average value. Significant differences exist for the uniformly loaded rotor as well; for example, at H/R = 1, the average value is $\Delta w/w_0 = -0.37$, whereas the value at the center of the rotor is $\Delta w/w_0 = -0.48$.

Rotor induced velocity. - The ground-induced interference velocities shown in figure 14 are relatively large compared to the rotor's own induced velocity, and, in the absence of any free stream velocity, the interference results in a major decrease in the mass flow through the rotor (equation (6)). Because of the reduced mass flow, the average rotor induced velocity must be increased to maintain constant lift (equation (10)). The required ratio of rotor induced velocity in ground effect to that out of ground effect w_0/w_h is shown in figure 16. The increase in rotor induced velocity is rapid as the ground is approached; it must increase by about 20 percent at H/R = 1.0, about 50-percent at H/R = 0.5, and about 100-percent at H/R = 0.3.

The required increase in rotor induced velocity is obtained by increasing the average angle of attack of the blades; however, this increased angle of attack does not necessarily imply any significant alteration of the collective pitch setting. The ground-induced upwash itself causes an increased angle of attack on the blades which may be sufficiently great to create large regions of blade stall when operating very close to the ground. This upwash, in terms of w_h, is shown in figure 17.

Rotor shaft power. - The values of w_0/w_h and w/w_h from figures 16 and 17 are sufficient to calculate the rotor induced shaft power from equation (19). The result of this calculation is shown in figure 18. These induced shaft power ratios agree closely with those given in reference 37, as they should, since the presentation in reference 37 stems basically from the analysis of Knight and Hefner in reference 11. The differences in hover between the present work and reference 11 are minor, depending only on the addition of calculations for triangular loading in the present paper. Reference 37 also collects comparisons of the theory and both model (ref. 11) and flight test (ref. 8) data. These comparisons indicate that the theoretical treatment yields reasonably adequate numerical results in hovering provided that the rotor is not too close to the ground. At very low heights, significant areas of stall were found on the rotor models of reference 11. The possibility of such stall because of the large ground-induced upwash has already been noted.

FORWARD FLIGHT PERFORMANCE IN GROUND EFFECT

Character of Interference Velocities. - The concept of a vanishingly small rotor in ground effect contains obvious inconsistencies since, proceeding in a formal manner, the ratio H/R must be infinite. Nonetheless, the use of this artifice does allow the ground-induced interference velocities to be expressed in a closed form which provides some insight into the general character of ground interference. The derivation of these closed forms is provided by Appendix A of Reference 18, which, together with the appropriate conversions for ground effect given in reference 16, leads to the following equations:

$$\frac{\Delta w}{w_0} = \frac{\pi}{4}\left(\frac{R}{H}\right)^2 \left(\delta_{w,L} + \delta_{w,D} \tan\alpha\right) \tag{23a}$$

$$\frac{\Delta u}{w_0} = \frac{\pi}{4}\left(\frac{R}{H}\right)^2 \left(\delta_{u,L} + \delta_{u,D} \tan\alpha\right) \tag{23b}$$

where

$$\delta_{w,L} = -\frac{1}{\pi}\left(3\cos^4\chi + \frac{1}{2}\right) \tag{24a}$$

$$\delta_{u,L} = \frac{1}{\pi}\left(3\sin\chi\cos^3\chi + \sin\chi\cos\chi + \frac{1}{2}\tan\frac{\chi}{2}\right) \tag{24b}$$

$$\delta_{w,D} = \frac{1}{\pi}\left(2\sin\chi\cos^3\chi - \sin^3\chi\cos\chi - 4\cos^3\chi - \frac{1}{2}\tan\frac{\chi}{2}\right) \tag{24c}$$

$$\delta_{u,D} = \frac{1}{\pi}\left(4\sin\chi\cos^2\chi - 3\sin^2\chi\cos^2\chi + \frac{1}{2}\frac{\cos\chi}{1+\cos\chi}\right) \tag{24d}$$

Equations (24) are derived on the assumption that the path of the wake is downward to an intersection with the ground. These equations are valid for $-90^\circ < \chi \leq 90^\circ$. Although such conditions are not treated specifically in the present paper, rapid descent toward the ground will leave the wake above the rotor so that it never does intersect the ground. In such cases ($\chi > 90^\circ$), the appropriate interference factors, replacing equations (24), are

$$\delta_{w,L} = -\frac{1}{2\pi} \tag{25a}$$

$$\delta_{u,L} = \frac{1}{2\pi} \cot \frac{\chi}{2} \tag{25b}$$

$$\delta_{w,D} = -\frac{1}{2\pi} \cot \frac{\chi}{2} \tag{25d}$$

$$\delta_{u,D} = \frac{1}{2} \frac{\cos\chi}{(1 - \cos\chi)} \tag{25d}$$

The interference factors defined by equations (24) and (25) are presented as a function of wake skew angle in figure 19. The region of primary interest herein is that for steady level flight; that is, skew angles between 0^o and 90^o. The interference factors related to the vertical interference velocity ($\delta_{w,L}$ and $\delta_{w,D}$) display closely analogous behavior within this range. Both factors are negative. Either positive lift or positive drag will produce an upwash ($\Delta w/w_0 < 0$) which will oppose the rotor induced vertical velocity. The magnitudes of these factors are greatest near hovering flight ($\chi = 0^o$) and their magnitudes decrease rapidly as the forward speed (or χ) increases. The factors $\delta_{u,L}$ and $\delta_{u,D}$, which determine the longitudinal, or streamwise, interference velocity are similar to each other throughout the range of skew angles between 0^o and 90^o. Both of these factors are positive. Either positive lift or positive drag will result in an interference velocity which opposes, and effectively reduces, the free-stream velocity. This streamwise interference is small both in hover ($\chi = 0^o$) and at high speed (χ approahing 90^o). The maximum streamwise interference will be encountered at a relatively low forward speed with a value of χ on the order of 30^o.

It will be shown subsequently that the streamwise interference plays a significant role in determining rotary wing ground effect; however, certain conclusions can be drawn from a first-order analysis of the vertical interference velocities. Under the assumption that $\alpha = 0^o$, the vertical interference depends only on $\delta_{w,L}$ (eq. (23)). As the forward speed is increased (χ increased), the vertical ground-induced interference velocity decreases as rapidly as $\cos^4\chi$ (eq. (24a) and fig 19). In contrast, in the absence of ground effect, the normal reduction of w_0 with forward speed is much slower, at a rate of $\sqrt{\cos\chi}$ (eq. (15a) with $\Delta w/w_0 = 0$). This disparancy in rates is magnified further by the need to employ the momentum skew angle in determining $\sqrt{\cos\chi}$, and the more rapidly changing (fig. 6) effective skew angle for $\cos^4\chi$. Thus, if the rotor is sufficiently close to the ground to have a large favorable ground effect, it is likely that the ground

effect will decrease more rapidly than the intrinsic rotor efficiency increases as the forward speed is increased. The net result is that, in ground effect, the required rotor power will increase, rather than decrease, as forward speed is increased within the transition range.

A second observation can be made immediately from figure 19. Since the two vertical interference factors are almost identical, and the two streamwise interference factors also display almost identical behavior, it is evident (eq (23)) that an increase in D/L (or α) will increase ground effect. Indeed, an angle of attack of 45^{o} (which results in D/L = 1.0 (eq 4)) will essentially double the ground effect at a given skew angle. Conversely, an angle of attack of -45^{o} (D/L = -1) at the same skew angle will essentially negate ground effect. Note however, that the constant skew angles will result in different forward speeds (eq (12) and (22)). At constant forward speed, negative angle of attack increases the wake skew angle and further decreases ground effect. Conversely, positive angle of attack decreases the wake skew angle with a further increase in ground effect. Thus, angle of attack excursions significantly smaller than 45^{o} may produce effects of the magnitude described.

Interaction of ground effect and rotor performance. - Figure 20 shows several of the factors influencing the induced power in ground effect and illustrates the interactions that lead to the required induced power. This figure was prepared using cylindrical vortex sheets to compute the ground-induced interference. The rotor angle of attack is zero, and both uniform and triangular disk load distributions are considered. Calculated results are presented for flight in free air as well as at a rotor height of one radius.

As noted earlier, in free air, the rotor induced velocity decreases as $\sqrt{\cos \chi}$ when the speed increases, and equation (19) shows that the shaft power ratio P_s/P_h is identical to w_0/w_h under the assumed conditions ($\alpha = \Delta w = 0$). Thus, the dashed lines in figure 20 show both ratios in free air.

In ground effect, the mass flow through the rotor is diminished by the presence of the indicated interference velocities (eq. (6)). To maintain the same lift with the reduced mass flow, the rotor must work harder with an increase in w_0 (eq. (10)). Thus, as indicated in figure 20, w_0/w_h in ground effect is as much as 25-percent greater than in free air. Finally, the shaft power ratio in ground effect is obtained from equation (19). Ground effect at this rotor height represents a saving of about 20-percent of the induced power when hovering. The saving vanishes rapidly as forward speed is increased. Figure 20 shows almost immeasureable ground effect when

the forward speed is only about three-quarters of the hovering induced velocity w_h. Furthermore, the maximum induced power no longer occurs when hovering; it now occurs at some significant forward speed. This possibility was discussed in connection with figure 19, was noted in the more cursory analysis of reference 16, and is in distinct contrast to the results of reference 15. The nature of the present result is confirmed by the experimental measurements of references 4 and 5.

Choice of wake model.- Once the general character of the ground effect has been established, the adequacy of the various wake models must be assessed before proceeding to examine fully the effects of height above the ground. Figure 21 presents the induced shaft power in ground effect as calculated using three of the wake models discussed earlier. In comparing these calculated results with each other, it would be anticipated that the vortex-cylinder wake model should produce the most nearly correct results since it most nearly represents the character of a real rotor wake. This presumption is supported further by the previously noted fact that powers computed for hovering using this wake model agree reasonably well with the measured power in ground effect.

The single doublet string wake model has been shown to indicate the correct trends for power as a function of speed in ground effect. Figure 21 shows clearly that this model is hopelessly inadequate for quantitative calculations of ground effect. The result should be anticipated. This wake model represents only a vanishingly small rotor. The calculated results are no more than the extrapolation to small ground clearances of nondimensionalized results obtained from a limiting case in which the height of the rotor above the ground is infinite.

The multiple doublet string model of the wake is a reasonable approximation to a cylindrical wake provided that the point of interest is somewhat removed (perhaps several tenths of a radius) from the wake. In this application, the portions of the wake which generate the interference are either at ground level or in the image system below the ground. As a result, this model should be reasonably adequate provided that H/R has a value of several tenths. Inspection of figure 21 shows that the anticipated result is obtained. The multiple doublet string wake yields results close to those of the vortex cylinder wake at H/R = 0.5 and the two sets of results diverge at H/R =0.3.

For very low heights above the ground, only the vortex cylinder model is adequate, and even its adequacy could be questioned because of sparse verification experiments below H/R = 0.4. Unfortunately, this model cannot be used unless $\alpha = 0^{o}$. For other angles of attack, the multiple doublet string model can be used provided that the rotor is sufficiently far above the ground.

Forward flight in ground effect at $\alpha = 0^{o}$. - A series of calculations similar to those of figure 20 have been made for a wide range of rotor heights. The resulting shaft powers for both uniform and triangular load distributions are presented in figure 22. The corresponding momentum theory values of wake skew angle are also shown on the figure.

Figure 22 shows that the initial trend with forward speed of induced shaft power in ground effect is an increase in required power. The magnitude of the increase is greater as the ground is approached. The speed for maximum power also increases as the ground is approached; it increases from about 0.4 $|w_h|$ at H/R = 2 to about 1.6 $|w_h|$ at H/R = 0.1. The influence of the ground-induced interference velocities on the momentum skew angle is large. The increase in skew angle with forward speed is slower initially than in free air. At the speed for maximum induced power, the wake angle rapidly increases, and, at higher forward speeds, the increase of skew angle with speed is more rapid than in free air. At the lowest heights above the ground, the change from an almost vertical wake to an almost flat wake occurs in a sudden jump near the speed for maximum power. This rapid change in wake angle has already been noted in reference 5. Indeed, reference 38, which examined experimentally the analogous problem of the interaction of the rotor wake with the floor of a wind tunnel, specifically refers to the rapid change in wake angle as having a "snap through" action.

The lowest rotor heights in figure 22 are below those of most helicopters even when resting on the ground. Nevertheless, an examination of the indicated nonlinearities and multiple values of power is enlightening. Obviously, the forward speed of the helicopter will not increase and decrease to follow the curves of figure 22. Instead, the wake will pop up to a high skew angle and the power will change in an essentially discontinuous manner.

The appearance of multivalued powers generally indicates the existence of a vortex-ring mode of rotor operation (as in ref. 24). That is not the case in figure 22 since the wake skew angles are such that the wake is always passing downward from, and not upward through, the rotor.

Now the forward velocity V is the velocity with which the rotor is passing through the entire air mass; in the absence of winds, it is the ground speed of the helicopter. It is not the effective aerodynamic speed of the rotor because the aerodynamic speed is really the sum of the forward velocity V and the ground-induced streamwise interference velocity Δu. If the results of figure 22 are replotted against the effective aerodynamic velocity $V + \Delta u$, the presentation of

figure 23 is obtained. It will be observed that the nonlinearities in power and wake angle are totally absent in figure 23. The induced power curves are smooth and continuous.

The momentum skew angle curves in figure 23 are a series of radial lines through the origin. This result should be expected since, from equation (12) with $\alpha = 0^{o}$,

$$\frac{w_0 + \Delta w}{w_0} = - \frac{(V + \Delta u)}{w_0} \cot \chi \qquad (26)$$

Multiply both sides of equation (26) by w_0/w_h to obtain

$$\frac{w_0 + \Delta w}{w_h} = - \frac{V + \Delta u}{w_h} \cot \chi \qquad (27)$$

But from equation (19) with $\alpha = 0^{o}$

$$\frac{P_s}{P_h} = \frac{w_0 + \Delta w}{w_h} \qquad (28)$$

Now substitute equation (27) into equation (28) to yield

$$\frac{P_s}{P_h} = \cot \chi \left[- \frac{(V + \Delta u)}{w_h} \right] \qquad (29)$$

Equation (29) is obviously the equation of a series of radial lines, with slope determined solely by χ, when plotted in the coordinates of figure 23.

It is clear when figure 22 is compared with figure 23 that the streamwise interference velocity Δu plays a major role in determining the performance of the rotor when flying forward in ground effect. Its

omission, as in references 15 and 16, can lead to significant errors when the rotor is close to the ground. The magnitude of the streamwise interference increases along the wake below the rotor and leads to severe gross distortions of the wake. These distortions, which have resulted in operational difficulties with several helicopters, can also be calculated qualitatively by the theory (refs. 22, 23), and they have been the subject of numerous recent experimental studies (refs. 4-7).

Forward flight in ground effect with $\alpha \neq 0^{o}$. - When the rotor angle of attack is other than zero, the less accurate multiple-doublet wake must be used for the calculation of ground effect. The induced shaft power has been calculated and is shown for several angles of attack in figures 24 (uniform disk load distribution) and 25 (triangular disk load distribution). The minimum height above the ground shown in figures 24 and 25 is 0.7R when $|\alpha| = 20^{o}$, because the angle of attack locally reduces the ground clearance at one edge of the rotor. In examining these figures, it should be observed that equations (19) and (20) include the effect on shaft power of producing the horizontal component of force; that is, the propulsive thrust when $\alpha < 0^{o}$, and the rotor drag when $\alpha > 0$.

Qualitatively, figures 24 and 25 display the trends with angle of attack that were noted in the discussion of figure 19; that is, negative angle of attack significantly reduces ground effect and positive ground effect significantly increases ground effect. These effects are large because of the additive effects of angle of attack on both the ground interference and the wake skew angle.

The power curves for $H/R = 0.7$ when $\alpha = 20^{o}$ are of interest because of their multivalued nature near $V/w_h = -1.4$. The mass flow through the rotor is severely reduced by the ground-induced interference velocities; the reduction in mass flow is so great that the power is increased rather than reduced, for speeds on the order of $0.9 < |V/w_h| < 1.5$. The combination of the interference velocities and angle of attack is such that the resultant flow direction is upward with respect to the rotor. Effectively, the rotor experiences a brief excursion into the vortex ring state since it is really descending at a rate of Δw with a forward speed reduced by Δu.

Operational aspects of ground effect in transition. - The primary benefit of ground effect is that it allows the helicopter to take off with gross weights in excess of those allowable for hovering in free air. Under such conditions, the helicopter is extremely underpowered and it is sensitive to relatively small changes in power required. Because of this sensitivity, the interaction between angle of attack and ground effect assumes some operational significance. These operational

aspects will be discussed with the aid of figure 26 which shows the required induced shaft power for several angles of attack in free air and in ground effect at a rotor height of one radius.

Consider the case of a helicopter overloaded to the point where it can hover with only a small power margin at a height of one radius. This overload condition is allowable in hover only because the induced power is reduced by about 20 percent in ground effect. Longitudinal cyclic pitch is applied to tilt the rotor forward, thus initiating forward flight. This attitude change has a greater effect on power in ground effect than in free air. Figure 26 shows that for an extreme case of a 20-degree rotor tilt, the induced power in ground effect would increase by about 20 percent rather than about 9 percent in free air. Indeed, at $\alpha = -20^{o}$, the induced power in ground effect is essentially equal to that at $\alpha = 0^{o}$ when hovering out of ground effect. Under such conditions, the helicopter must sink as it accelerates, and some altitude margin must be allowed if ground contact is to be avoided. Fortunately, the sink rate leads to an increased ground effect which tends to limit the total loss of altitude.

It is noted that this portion of the takeoff is omitted in the optimization analyses presented in references 1 and 2, which merely assume a uniform acceleration rate of 0.2 g during this initial portion of the takeoff maneuver. This acceleration implies that $\alpha \approx -11^{o}$, which is a more modest rotor tilt than that of figure 26. Even so, interpolation of figure 26 implies that some settling is required, and the recommendation of reference 2 in favor of a 1.37 m (4.5 ft) skid height provides an allowance for settling. In any event, it is clear from figure 26 that the initial acceleration should be mild whenever the terrain allows a slight increase in distance over the nearest obstacle. This caution need not be a major penalty; halving the acceleration rate to 0.1 g would require less than an additional 30 m (100 ft) of space for the sample case of reference 1.

The optimum climbout profile of references 1 and 2 calls for nose-up rotation and climbout once the helicopter has reached a forward speed of about $0.7\ |w_h|$. The trends shown in figures 24 and 25 indicate that this rotation will increase ground effect and briefly add an initial boost to the climb over that attainable with the ground-effect routines used in the reference papers.

Landing in ground effect is generally in a decelerating mode with rearward rotor tilts on the same order as that shown in figure 26. It is observed that as the helicopter slows down the initial appearance of ground effect is adverse at $\alpha = 20^{o}$. The rotor efficiency is reduced so much by decreased mass flow that the required power is greater in ground effect than in free air, despite the ground-induced upwash.

As noted earlier, if the rotor is sufficiently close to the ground, the rotor is forced prematurely into the vortex-ring, or power-settling, state because of the reduced mass flow. This effect does not carry the same connotations of danger in ground effect as in free air (ref. 24) for several reasons. First, there is insufficient altitude to build up to dangerous vertical descent velocities. Second, the pilot is planning to descend in any event and is prepared to settle. Finally, the maneuver is generally transient and of brief duration. Rather than presenting a danger, the only effect is a pronounced shuddering and a briefly increased vibration level.

Finally, as the helicopter speed decreases to a value less than $|w_h|$, favorable ground effect increases rapidly and attains values significantly greater than at $\alpha = 0^o$. As the helicopter approaches hover, the final leveling of the rotor causes no perceptible change in power at $H/R = 1$ (fig. 26), although some increase in power may be noted at lower heights (figs. 24, 25).

Obviously, if the helicopter forward speed could be held to zero as the rotor was tilted, the flow patterns for positive and negative angles of attack would be mirror images of each other. In this case, the shaft power would be independent of the direction of rotor tilt. That this result is not attained in the present calculation is due to the assumed wake in ground effect (fig. 2). The assumed wake is always required to flow off in the downstream direction. In reality, if the rotor was not leveled as zero speed was approached, the wake would snap forward along the ground at some very low speed, and the power required at $\alpha = 20^o$ would increase rapidly to that required at $\alpha = -20^o$. In practice, the helicopter is retrimmed to $\alpha = 0^o$ as hovering is approached and this inconsistency is of little consequence.

COMPARISON WITH EXPERIMENT

Reference 5 presents wind-tunnel measurements of the power required in ground effect for a rotor 0.71 R above the ground. Power measurements were not presented for the out-of-ground-effect case in that paper; thus, the present comparison is referenced to the theoretical in-ground-effect hovering power $P_{s,h}$ rather than P_h. It was assumed that 80 percent of the hovering shaft power was induced power.

The measurements of reference 5 are compared to the theoretical calculations for uniform and triangular disk-load distributions in figure 27. Considering that the actual load distribution is unknown and not axisymmetric, and that the large wake deformations at low speed are known to affect the results of the linearized vortex theory (ref. 13), the theoretical values must be

considered to be reasonably close to the measured powers. In particular, the overall initial increase in induced power as the rotor forward speed is increased from hover is present in both the calculated and measured powers.

WAKE DEFORMATION IN GROUND EFFECT

The effect of wake deformations on the performance and the flow-field of hovering rotors has been discussed in reference 13 and will not be considered further herein. The wake deformations in ground effect at low speed are of interest because of recent operational problems ascribed to such deformations (refs. 4-7). Since these effects were first encountered as a result of studies of wind-tunnel interference (refs. 22, 23, 38, 39), the implications with respect to helicopter operational problems did not become fully evident until the studies of references 4 and 5. Because of the importance of wake deformation, particularly with respect to tail-rotor operation, a brief discussion of these deformations is included at this point.

Calculated flow. - Figure 28 (from ref. 23) compares the flow field of a rotor in ground effect with the corresponding field in free air. The vectors indicate the direction and relative magnitude of the local flow at a point defined by the base of the vector. The flow is shown for the plane of symmetry of the rotor and for a plane at the location of the ground 2.6 rotor radii below the rotor. At this height above the ground, the previously presented results indicate that ground effect has essentially no effect on the rotor performance. The location of the rotor disk and the intersections of the rotor wake with the vector planes are shown.

In free air, the air approaching the rotor from about its own vertical height is accelerated and inclined upward to spill over the leading-edge of the rotor and then down through the wake. Well below the level of the rotor, the fluid passes smoothly around the wake with a slight downwash. Behind the rotor, the flow is retarded and redirected downward. These trends are magnified as the forward velocity is decreased from that corresponding to $\chi = 70^{\circ}$ (fig. 28(a)) to the velocity for $\chi = 10^{\circ}$ (fig. 28(g)) where the net flow velocity behind the rotor maybe opposite to the free-stream direction.

The entire flow pattern is altered to some extent by the presence of the ground; however, the deformations of primary interest herein occur near the intersection of the wake and the ground. Here the flow is severely retarded immediately ahead of the wake and accelerated behind it. At $\chi = 60^{\circ}$ (fig. 28(b)) the flow on the ground ahead of the wake is essentially stagnant. At $\chi = 50^{\circ}$ (fig. 28(c)), the flow at this location is opposite to the free stream. The magnitude of the reversed flow, and the

region which it occupies, grow as the wake angle is depressed further (fig. 28(d) to 28(g)). The vortex-like character of this flow is evident, particularly for $\chi \leq 30^{o}$ (fig. 28(e) to 28(g)). This effect first achieves significant prominence at the skew angles which correspond to the region of rapid wake-angle change and power-curve inflection noted earlier in the discussion of figure 22. The cause of those nonlinearities was shown to be the large streamwise ground-induced interference velocities. The cause of the flow reversal of figure 28 is the same streamwise-interference velocity which grows to unmanageable proportions near the lowest portions of the wake.

In the presence of such powerful flows, the wake deforms from the simple inclined cylinder used for the present calculations. References 22 and 23 demonstrate qualitatively that the wake deformation itself should augment the calculated effects, and these references also confirm the qualitative analysis by comparing the calculated flow with the flow observed in reference 40 (see fig. 29). The actual flow is much like that illustrated in figure 30. The wake streams forward along the ground and ahead of the rotor, and it rolls up into a large vortex which lies near the ground and assumes a horseshoe shape around and behind the main wake. Behind the rotor, the flow along the ground is accelerated and passes off smoothly.

Operational significance of wake distortion.- The significance of the wake distortion in ground effect has received prominence (refs. 4 to 7) recently because of directional control problems encountered in varying degrees by operational helicopters. The particular problem was a loss of directional control when hovering in ground effect with winds from the rear. In the present context, this condition corresponds to low-speed tail-first forward flight.

Wind-tunnel tests were conducted to examine the directional stability problem in detail (refs. 4, 5). A number of effects, largely additive, were found to have caused the problem. First, the power required by the main rotor increased with wind speed (fig. 22), and, thus, additional tail-rotor thrust was required to balance the main rotor torque. Second, in rearward flight, the fuselage moments were basically unstable, and this instability was worsened by the fin required for normal forward flight. Additional tail-rotor thrust was required to balance these unstable fin and fuselage moments. Finally, at some critical wind speed, the tail rotor became immersed in the rolled-up ground vortex. Since both the tail rotor and the ground vortex rotated in the same direction, the effective rotational speed of the tail rotor was reduced, reducing its maximum thrust capability. This reduction in available thrust occurred simultaneously with the increased thrust requirements required to offset the main rotor torque and the adverse fin and fuselage moments. The result, under unfavorable conditions, led to an uncontrolled yawing motion which could be stabilized only after the helicopter had almost completely reversed its heading.

The factors which led to this problem will generally always be present when hovering in ground effect with tail winds; however, the loss of control can be avoided by a judicious choice of tail rotor location and direction of rotation. Several possible solutions are explored experimentally in references 6 and 7. The overall phenomena involved do introduce the need to examine ground effect as one of the critical design factors for rotors in general and tail rotors in particular.

CONCLUSIONS

This study of rotors in forward flight within ground effect indicates the following conclusions:

1. Ground-induced interference has the character of an upwash and a streamwise interference velocity which opposes the free-stream velocity. Both interference velocities may be large, and both oppose the normal flow directions through the rotor with consequent large effects on the induced efficiency of the rotor.

2. In hovering at small heights above the ground, the ground-induced upwash produces large gains in efficiency; however, its effect on mass flow may result in significant amounts of blade stall.

3. In general, the induced shaft power of a rotor in ground effect increases, rather than decreases, as the forward speed is increased initially from hover.

4. At very low heights above the ground, the power requirements become decidedly nonlinear with speed primarily as a result of the action of the streamwise component of ground-induced interference velocity. This streamwise interference becomes greater along the wake as the wake approaches the ground. It produces a ground vortex which has been shown previously to be one cause of directional instabilities in near-hovering flight. The magnitude of the effects engendered by streamwise interference is so great that it cannot be ignored in the analysis.

5. Rotor angle of attack has a strong influence on ground effect in forward flight; forward tilt decreases ground effect and rearward tilt increases it. In the latter case, ground effect can become so great that it pushes the rotor into the vortex ring state of operation with a loss, rather than a gain, in rotor efficiency.

REFERENCES

1. Schmitz, Fredric H.: Optimal Takeoff Trajectories of a Heavily Loaded Helicopter. Jour. Aircraft, vol. 8, no. 9, Sept. 1971. pp. 717-723.

2. Schmitz, Fredric H.; and Vause, C. Rande: Near-Optimal Takeoff Policy for Heavily Loaded Helicopters Exiting from Confined Areas. Jour. Aircraft, vol. 13, no. 6, May 1976. pp. 343-348.

3. Lewis, Richard B., II: Army Helicopter Performance Trends. Jour. American Helicopter Soc., vol. 17, no. 2, April 1972. pp. 15-23.

4. Huston, Robert J.; and Morris, Charles E. K., Jr.: A Note on a Phenomenon Affecting Helicopter Directional Control in Rearward Flight. Journ. American Helicopter Soc., vol. 15, no. 4, Oct. 1970. pp. 38-45.

5. Huston, Robert J.; and Morris, Charles E. K., Jr.: A Wind-Tunnel Investigation of Helicopter Directional Control in Rearward Flight in Ground Effect. NASA TN D-6118, 1971.

6. Wiesner, Wayne; and Kohler, Gary: Tail Rotor Performance in Presence of Main Rotor, Ground, and Winds. Journ. American Helicopter Soc., vol. 19, no. 3, July 1974. pp. 2-9.

7. Empey, R. W.; and Ormiston, R. A.: Tail Rotor Thrust on a 5.5-Foot Helicopter Model in Ground Effect. American Helicopter Soc., Paper No. 802, 1974.

8. Zbrozek, J.: Ground Effect on the Lifting Rotor. R&M No. 2347, British A.R.C., 1950.

9. Taylor, Marion K.: A Balsa-Dust Technique for Airflow Visualization and its Application to Flow Through Model Helicopter Rotors in Static Thrust. NACA TN 2220, 1950.

10. Koo, Jiro; and Oka, Toichi: Experimental Study on the Ground Effect of a Model Rotor in Hovering. Report NAL-TR-113, National Aerospace Lab., Tokyo, Japan, 1966. (Available in English as NASA TT F-13,938, 1971.)

11. Knight, Montgomery; and Hefner, Ralph A.: Analysis of Ground Effect on the Lifting Airscrew. NACA TN 835, 1941.

12. Heyson, Harry H.: Induced Flow Near a Rotor and Its Application to Helicopter Problems. Proceed. 14th Ann. Nat'l Forum, American Helicopter Soc., April 16-19, 1958. (Also available as: Induced Flow Near a Helicopter Rotor. Aircraft Engineering, vol. 31, no. 360, Feb. 1959. pp. 40-44.)

13. Heyson, Harry H.: Evaluation of Linearized Vortex Theory as Applied to Single and Multiple Rotors Hovering In and Out of Ground Effect. NASA TN D-43, 1959.

14. Greenberg, Michael D.; and Kaskel, Alvin L.: Inviscid Flow Field Induced by a Rotor in Ground Effect. NASA CR-1027, 1968.

15. Cheeseman, I. C.; and Bennett, W. E.: The Effect of the Ground on a Helicopter Rotor in Forward Flight. R & M No. 3021, British A.R.C., 1957.

16. Heyson, Harry H.: Ground Effect for Lifting Rotors in Forward Flight. NASA TN D-234, 1960.

17. Heyson, Harry H.: Jet-Boundary Corrections for Lifting Rotors Centered in Rectangular Wind tunnels. NASA TR R-71, 1960.

18. Heyson, Harry H.: Linearized Theory of Wind-Tunnel Jet-Boundary Corrections and Ground Effect for VTOL/STOL Aircraft. NASA TR R-124, 1962.

19. Heyson, Harry H.: Use of Superposition in Digital Computers to Obtain Wind-Tunnel Interference Factors for Arbitrary Configurations, with Particular Reference to V/STOL Models. NASA TR R-302, 1969.

20. Heyson, Harry H.: Fortran Programs for Calculating Wind-Tunnel Boundary Interference. NASA TM X-1740, 1969.

21. Heyson, Harry H.; and Grunwald, Kalman J.: Wind Tunnel Boundary Interference for V/STOL Testing. Conference on V/STOL and STOL Aircraft, NASA SP-116, 1966. pp. 409-434.

22. Heyson, Harry H.: The Flow Throughout a Wind Tunnel Containing a Rotor with a Sharply Deflected Wake. Proceed. Third CAL/AVLABS Symposium on Aerodynamics of Rotary Wing and V/STOL Aircraft, vol. 2, Buffalo, NY, June 18-20, 1969.

23. Heyson, Harry H.: Theoretical Study of Conditions Limiting V/STOL Testing in Wind Tunnels with Solid Floor. NASA TN D-5819, 1970.

24. Heyson, Harry H.: A Momentum Analysis of Helicopters and Autogyros in Inclined Descent, with Comments on Operational Restrictions. NASA TN D-7917, 1975.

25. Heyson, Harry H.: Nomographic Solution of the Momentum Equation for VTOL-STOL Aircraft. NASA TN D-814, 1961 (also available as: V/STOL Momentum Equation, Space/Aeron. Vol. 38, No. 2, July 1962. PP B-18 to B-20.)

26. Castles, Walter Jr,; and De Leeuw, Jacob Henri: The Normal Component of Induced Velocity in the Vicinity of a Lifting Rotor and Some Examples of its Application. NACA Rep. 1184, 1954. (Supersedes NACA TN 2912.)

27. Heyson, Harry H.; and Katzoff, S.: Induced Velocities Near a Lifting Rotor with Nonuniform Disk Loading. NASA Rep. 1319, 1957. (Supersedes NACA TN 3690 by Heyson and Katzoff and NACA TN 3691 by Heyson.)

28. Jewel, Joseph W., Jr.; and Heyson, Harry H.: Charts of the Induced Velocities Near a Lifting Rotor. NASA MEMO 4-15-59L, 1959.

29. Heyson, Harry H.: Equations for the Induced Velocities Near a Lifting Rotor with Nonuniform Azimuthwise Vorticity Distribution. NASA TN D-304, 1960.

30. Wald, Quentin: A Method for Rapid Estimation of Helicopter Performance. Jour. Aero. Sci., Vol. 10, No. 4, April 1943. pp 131-135.

31. Coleman, Robert P.; Feingold, Arnold M.: and Stempin, Carl W.: Evaluation of the Induced-Velocity Field of an Idealized Helicopter Rotor. NACA WR L-126, 1945. (Formerly NACA ARR L5E10.)

32. Glauert, H.: A General Theory of the Autogyro. R & M No. 1111, British A.R.C., 1926.

33. Heyson, Harry H.: A Note on the Mean Value of Induced Velocity for a Helicopter Rotor. NASA TN D-240, 1960.

34. Crimi, Peter: Prediction of Rotor Wake Flows. CAL/USAAVLABS Symposium on Aerodynamic Problems Associated with V/STOL Aircraft. Buffalo, NY, June 1966. Vol I.

35. Gessow, Alfred: Review of Information on Induced Flow of a Lifting Rotor. NACA TN 3238, 1954.

36. Cone, Clarence D.: A Theoretical Investigation of Vortex-Sheet Deformation Behind a Highly Loaded Wing and Its Effect on Lift. NASA TN D-657, 1961.

37. Gessow, Alfred; and Myers, Garry C., Jr.: Aerodynamics of the Helicopter. MacMillian Co., NY, 1952. pp 106-114.

38. Rae, William H., Jr.; and Shindo, Shojiro: Comments on V/STOL Wind Tunnel Data at Low Forward Speeds. Proceed. Third CAL/AVLABS Symposium on Aerodynamics of Rotary Wing and V/STOL Aircraft. Vol. 2, Buffalo, NY, June 18-20, 1969.

39. Rae, William H., Jr.: Limits on Minimum-Speed V/STOL Wind Tunnel Tests. Jour. Aircraft, Vol. 4, No. 3, May-June, 1967. pp 249-254.

40. Jenkins, Julian L., Jr.: Trim Requirements and Static-Stability Derivatives from a Wind-Tunnel Investigation of a Lifting Rotor in Transition. NASA TN D-2655, 1965.

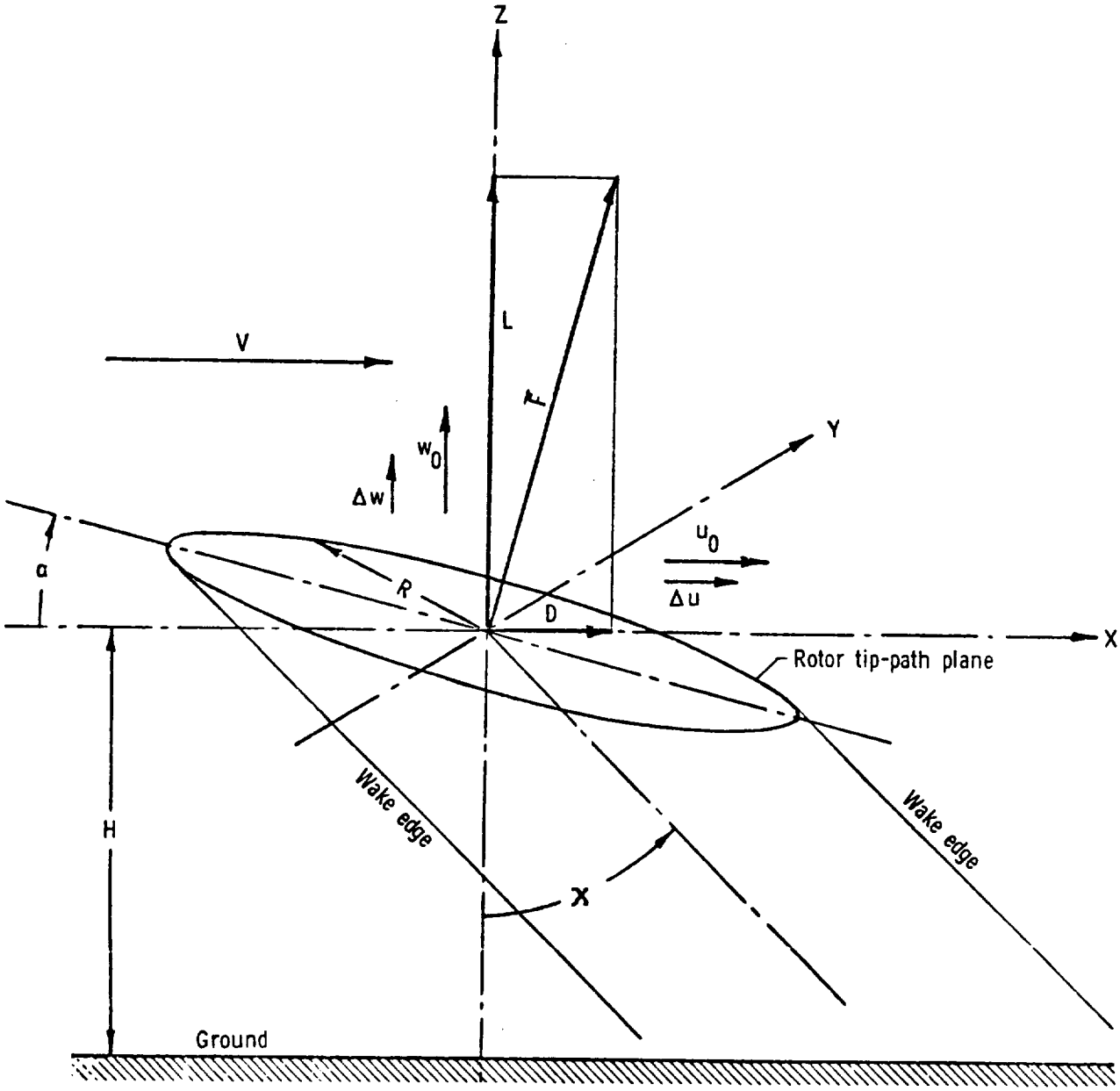

Figure 1. - Rotor and wake in ground effect.

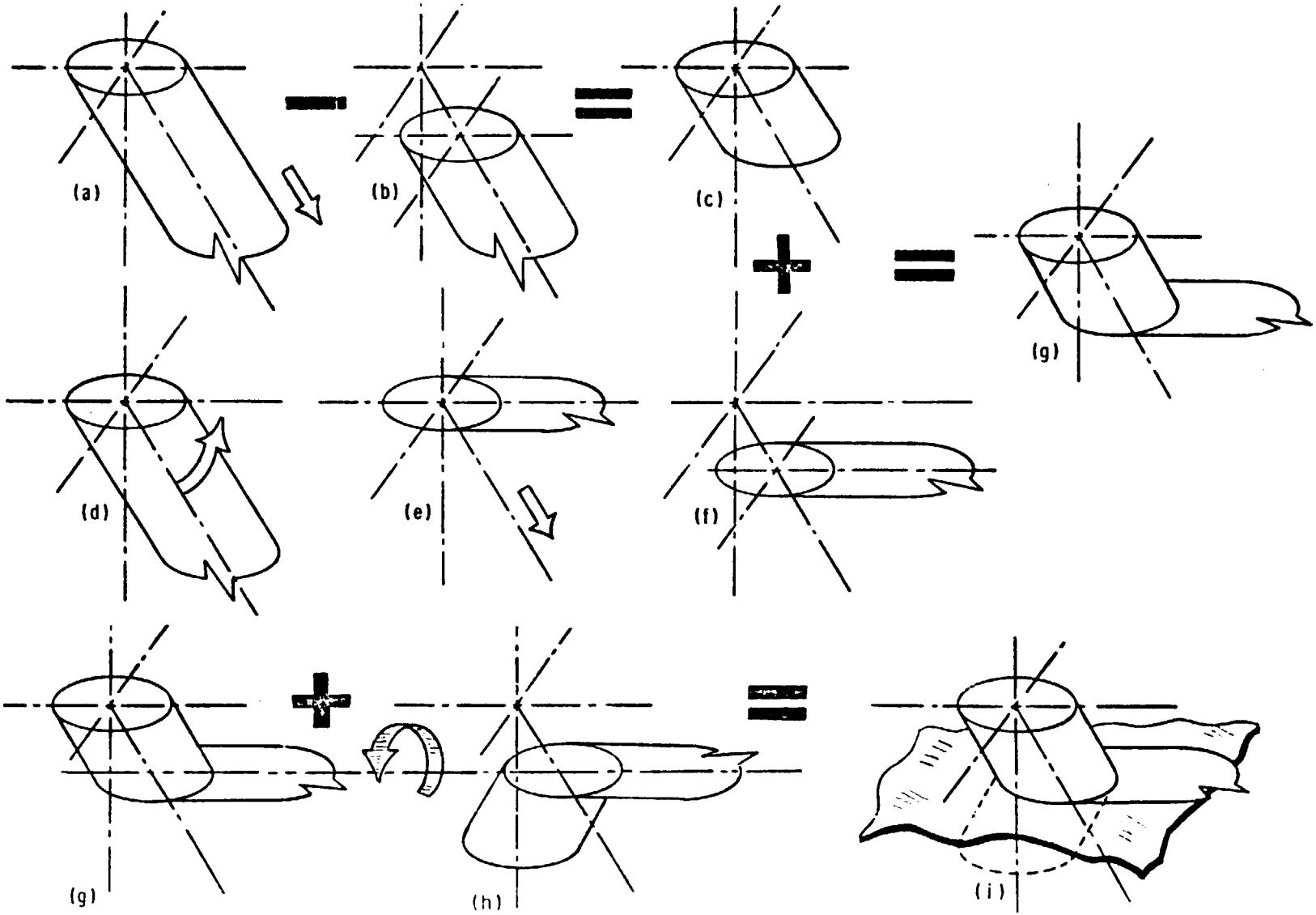

Figure 2. - Superpositions of the wake and its associated flow field used to obtain the wake and flow field in ground effect. Ground effect is the difference between the flow fields of (a) and (i).

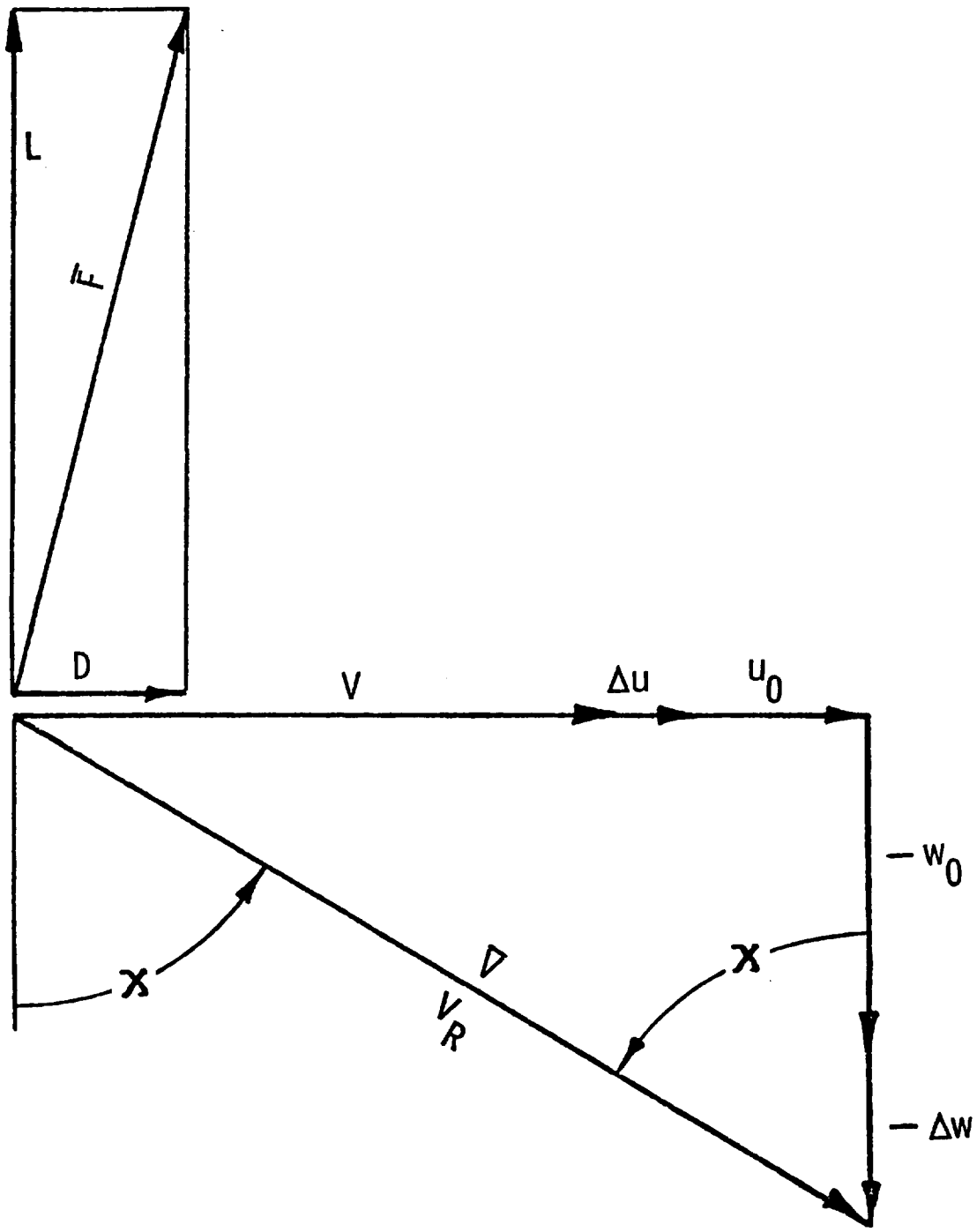

Figure 3. - Force and velocity vectors at the rotor.

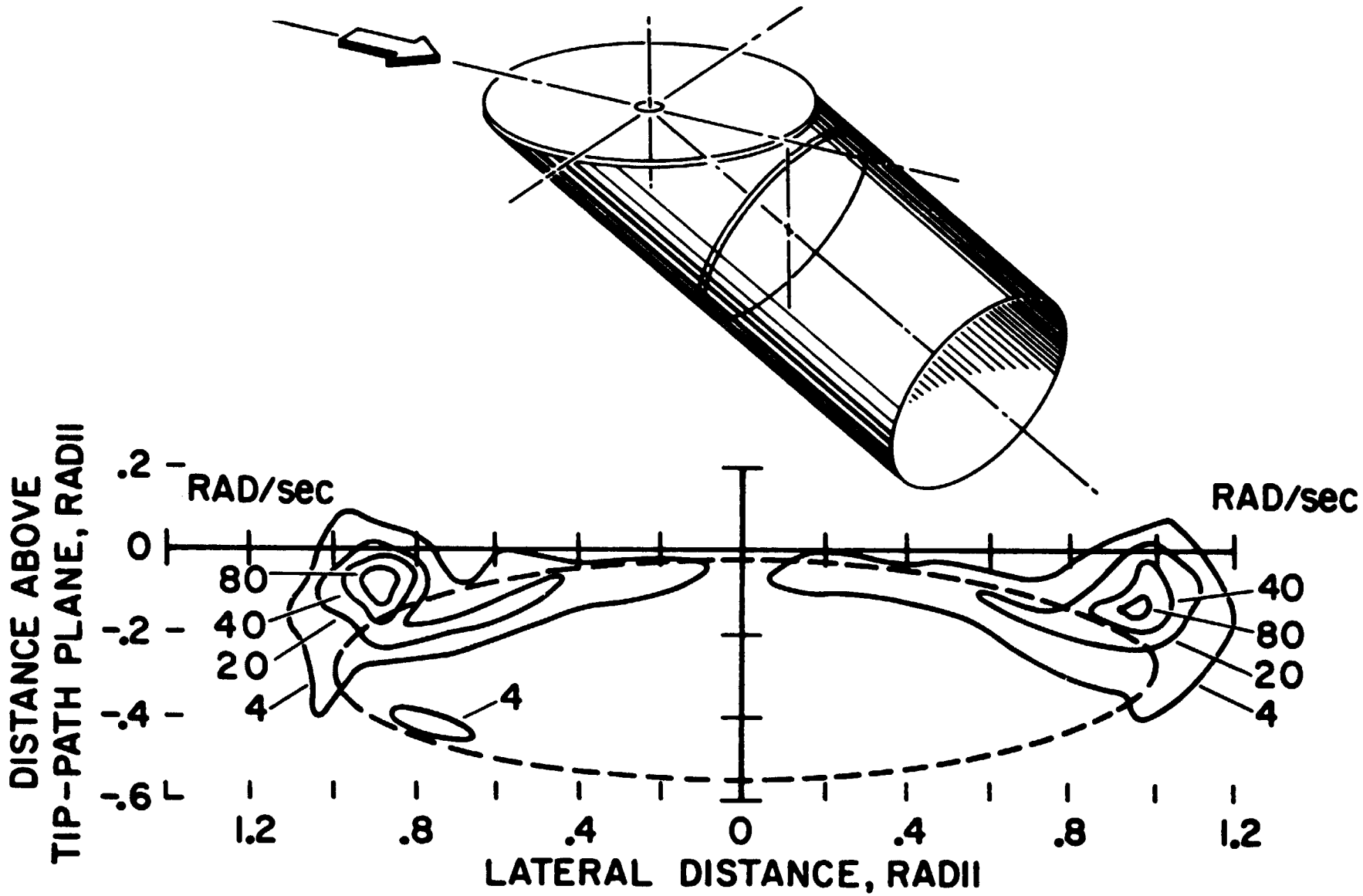

Figure 4. - Contours of equal vorticity measured 7-percent of a radius behind the trailing edge of a rotor. $\chi = 75^{o}$. (Data from reference 27.)

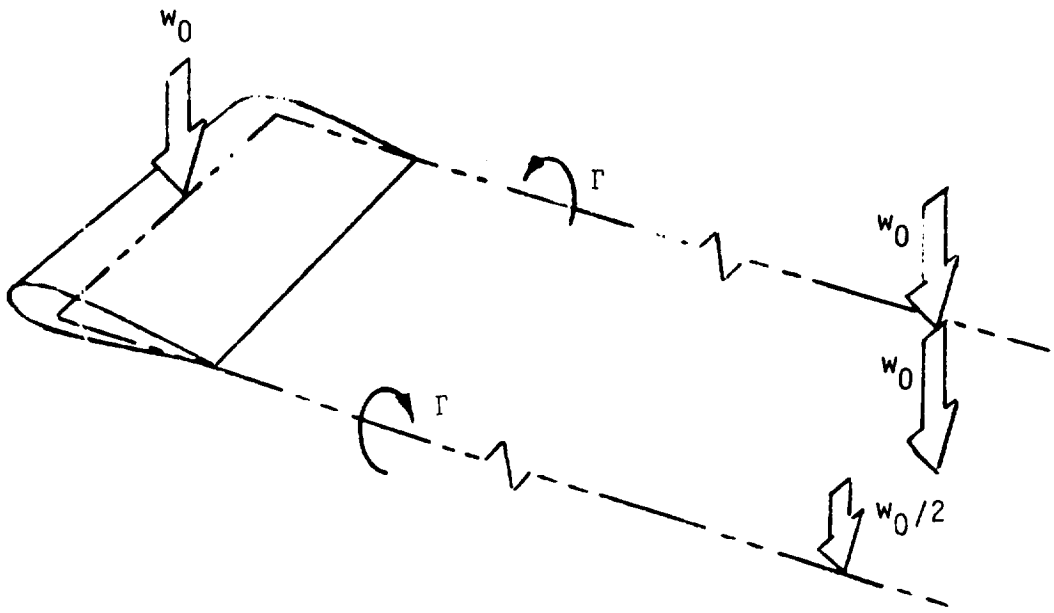

Figure 5. - Vorticity and induced velocities in the wake of a uniformly loaded wing.

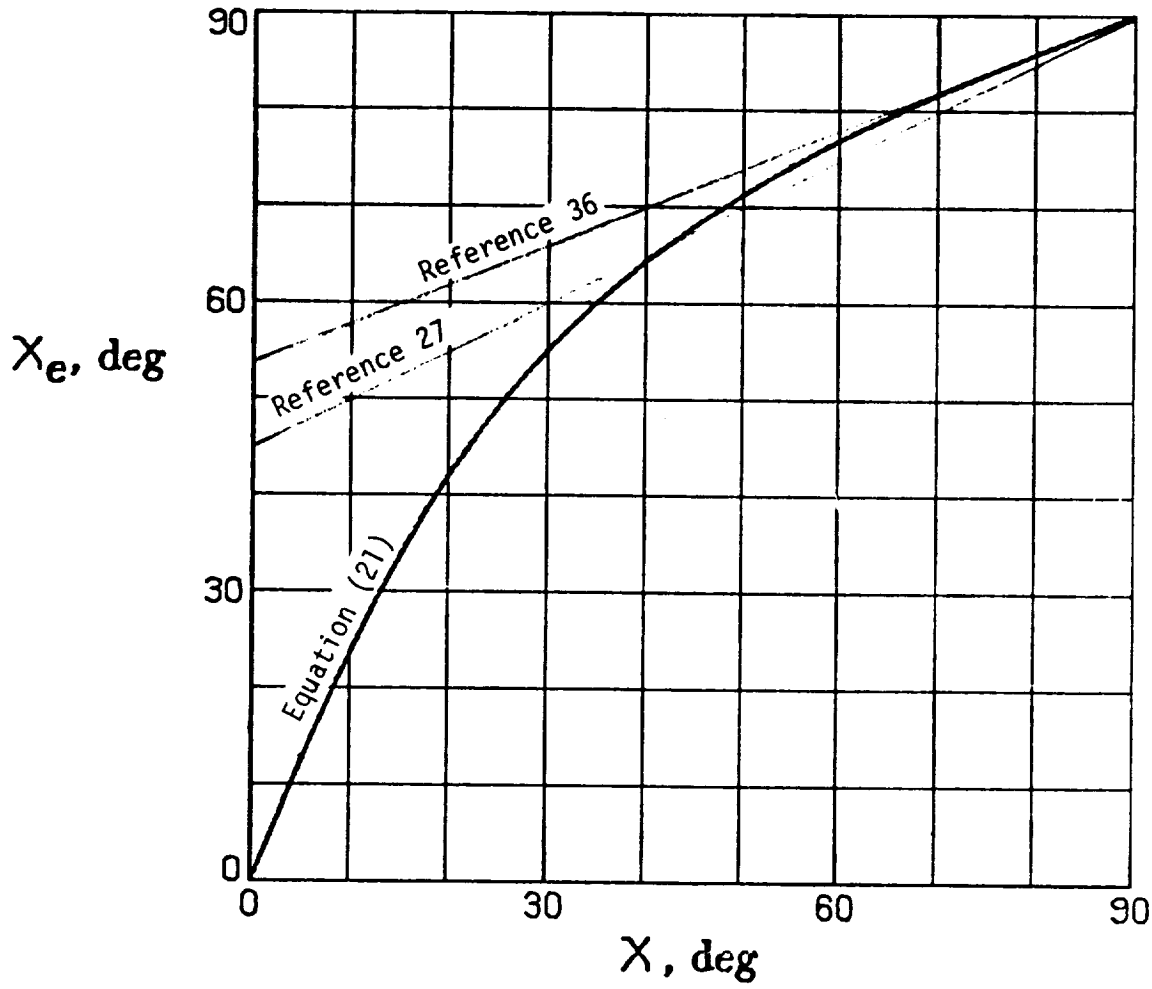

Figure 6. - Relationships between momentum skew angle and the effective skew angle χ_e of the rolled-up wake.

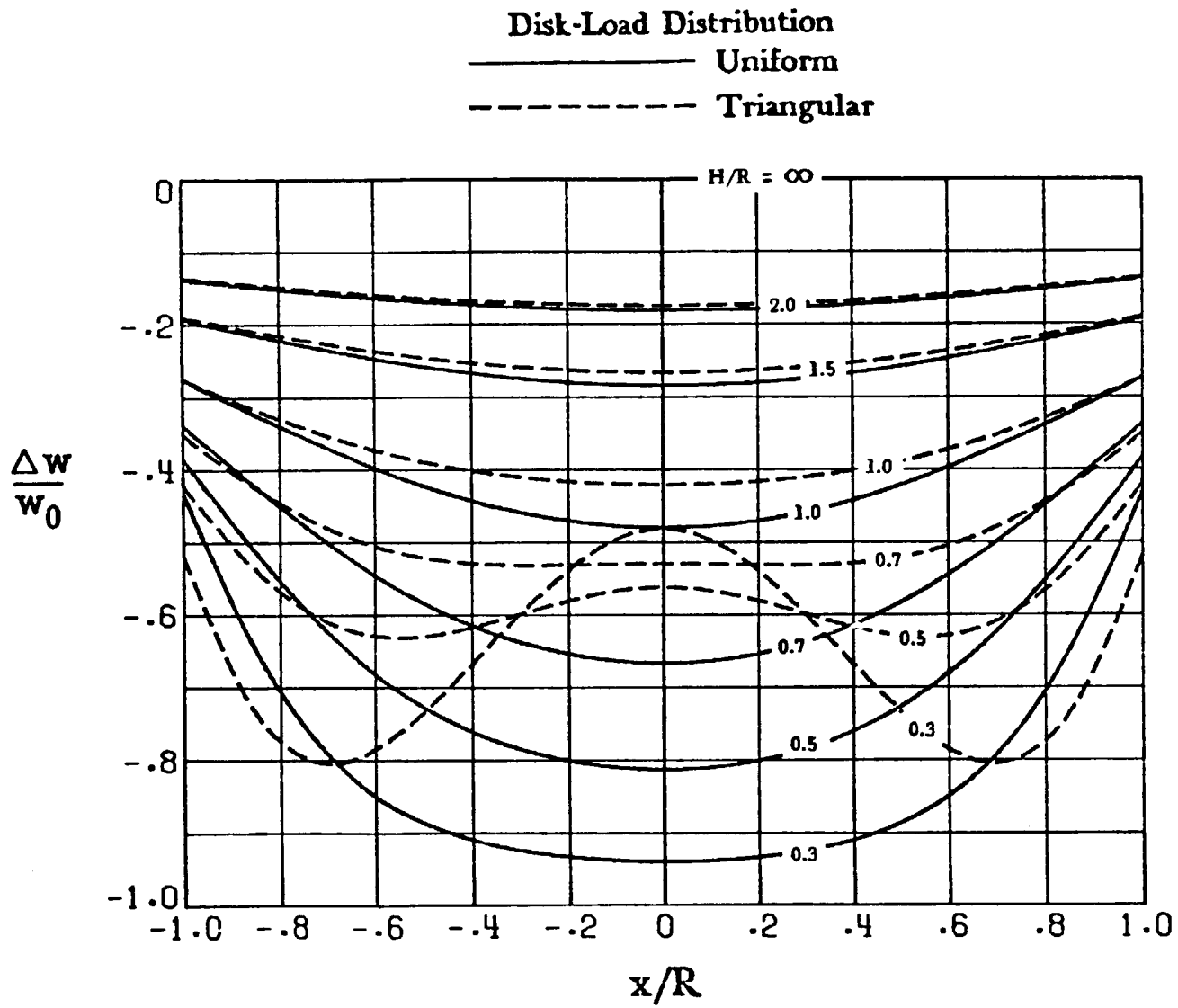

(a) Vertical component.

Figure 7. - Distribution of ground-induced interference velocities over the longitudinal axis of the rotor in hovering flight.

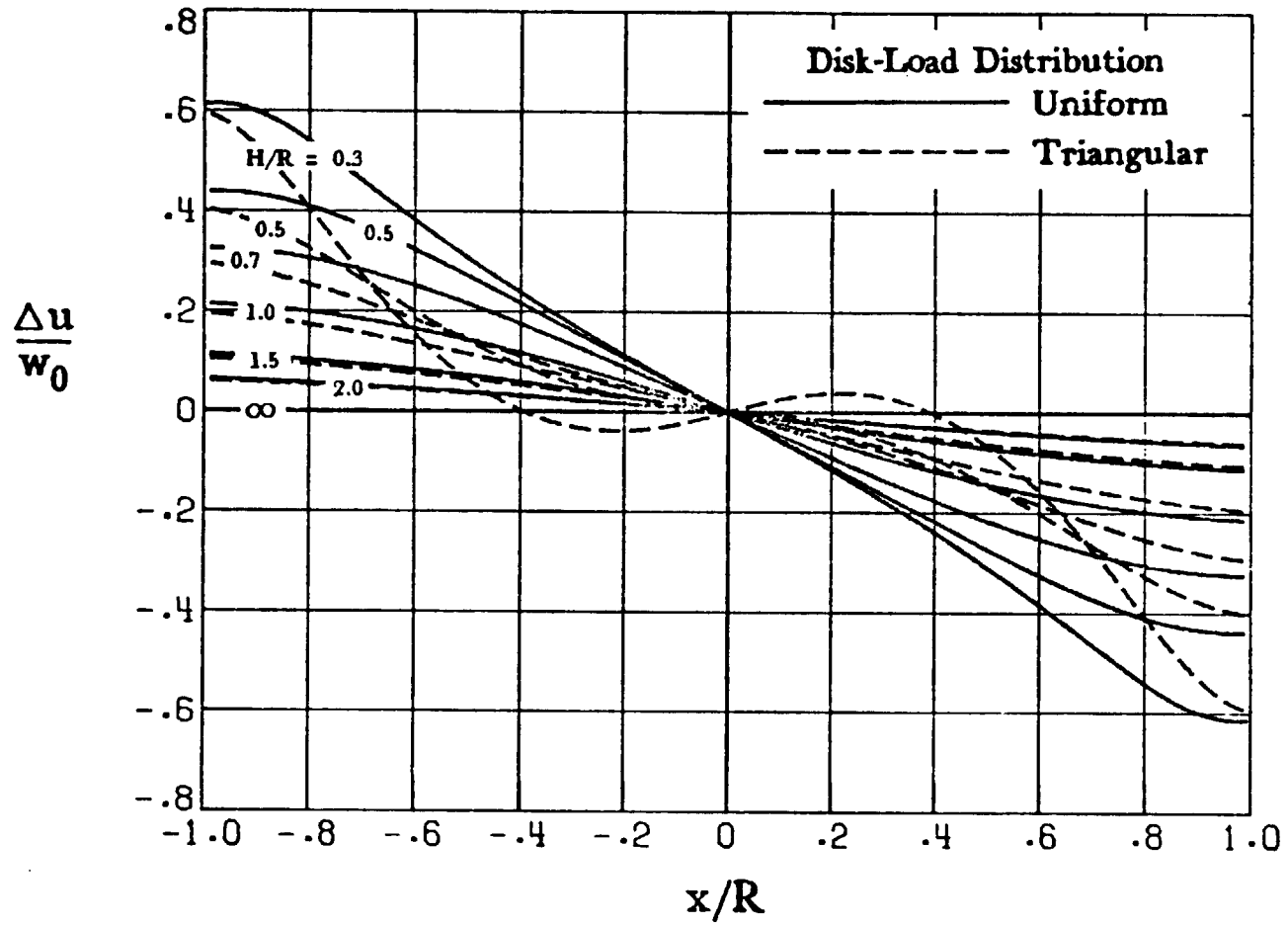

(b) Streamwise component.

Figure 7. - Concluded.

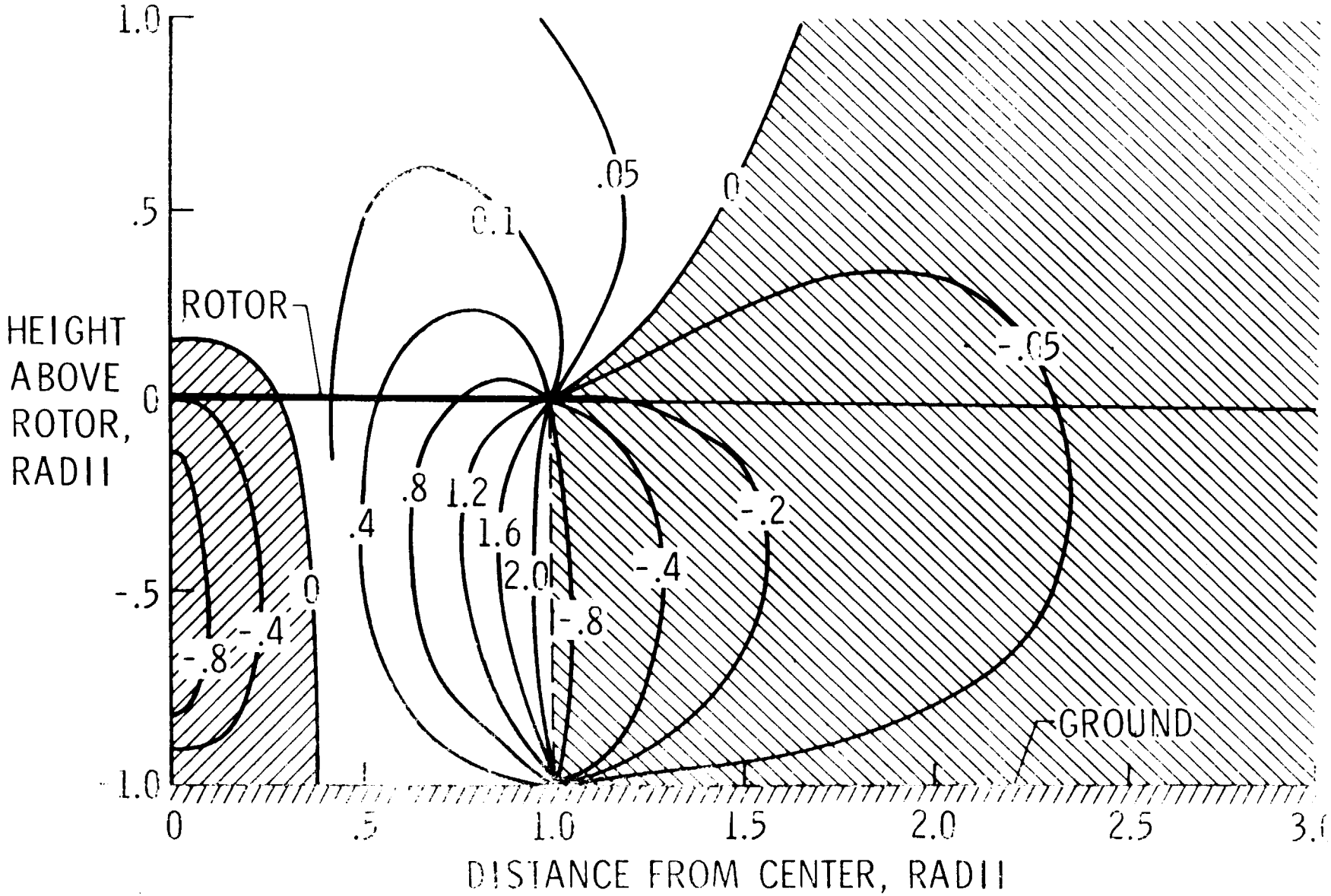

Figure 8. - Contours of equal local velocity w/w_0 in the vicinity of a rotor with a triangular disk load distribution when hovering one radius above the ground. The shaded areas represent regions of upwash. (References 12, 13)

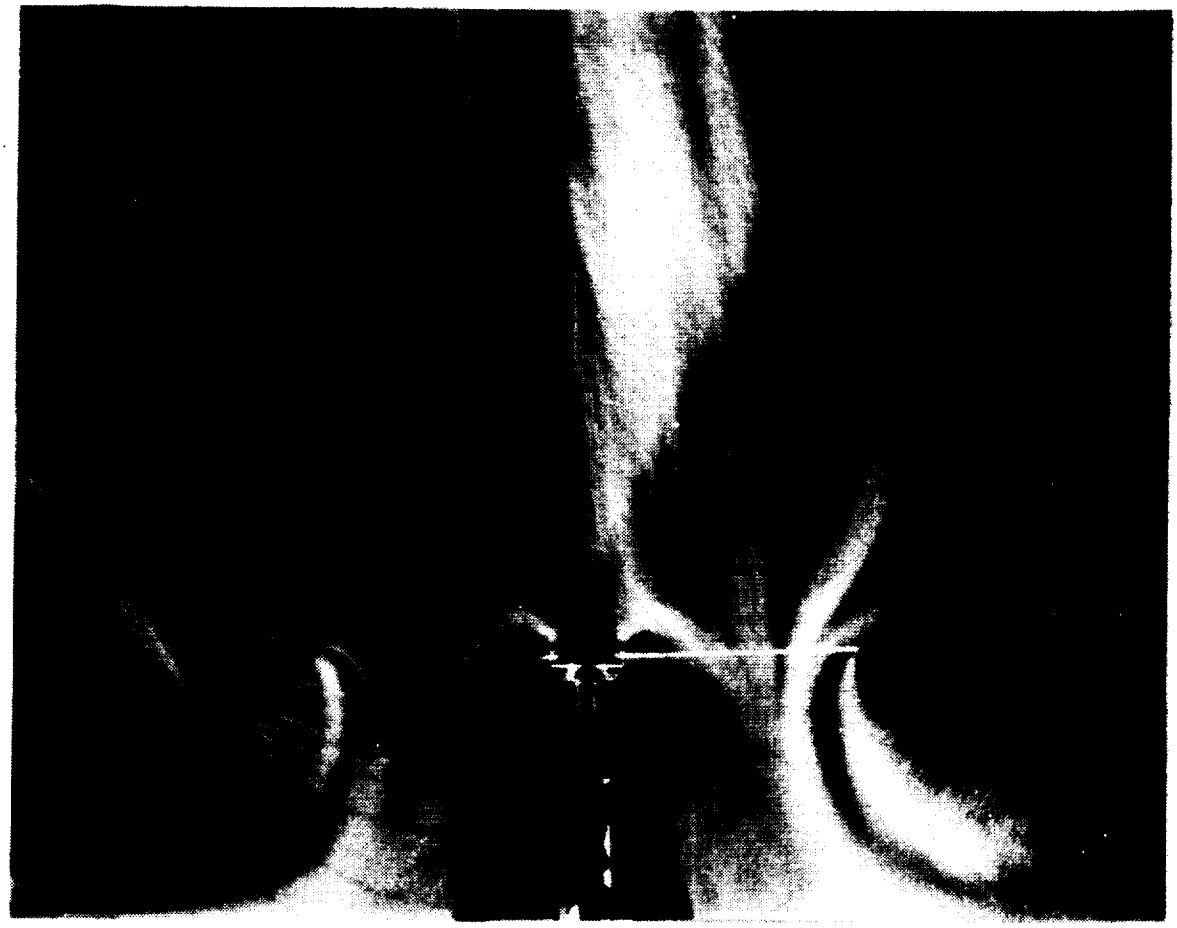

Figure 9. - Balsa dust visualization of the flow near a rotor hovering one radius above the ground (reference 9).

ORIGINAL
OF P

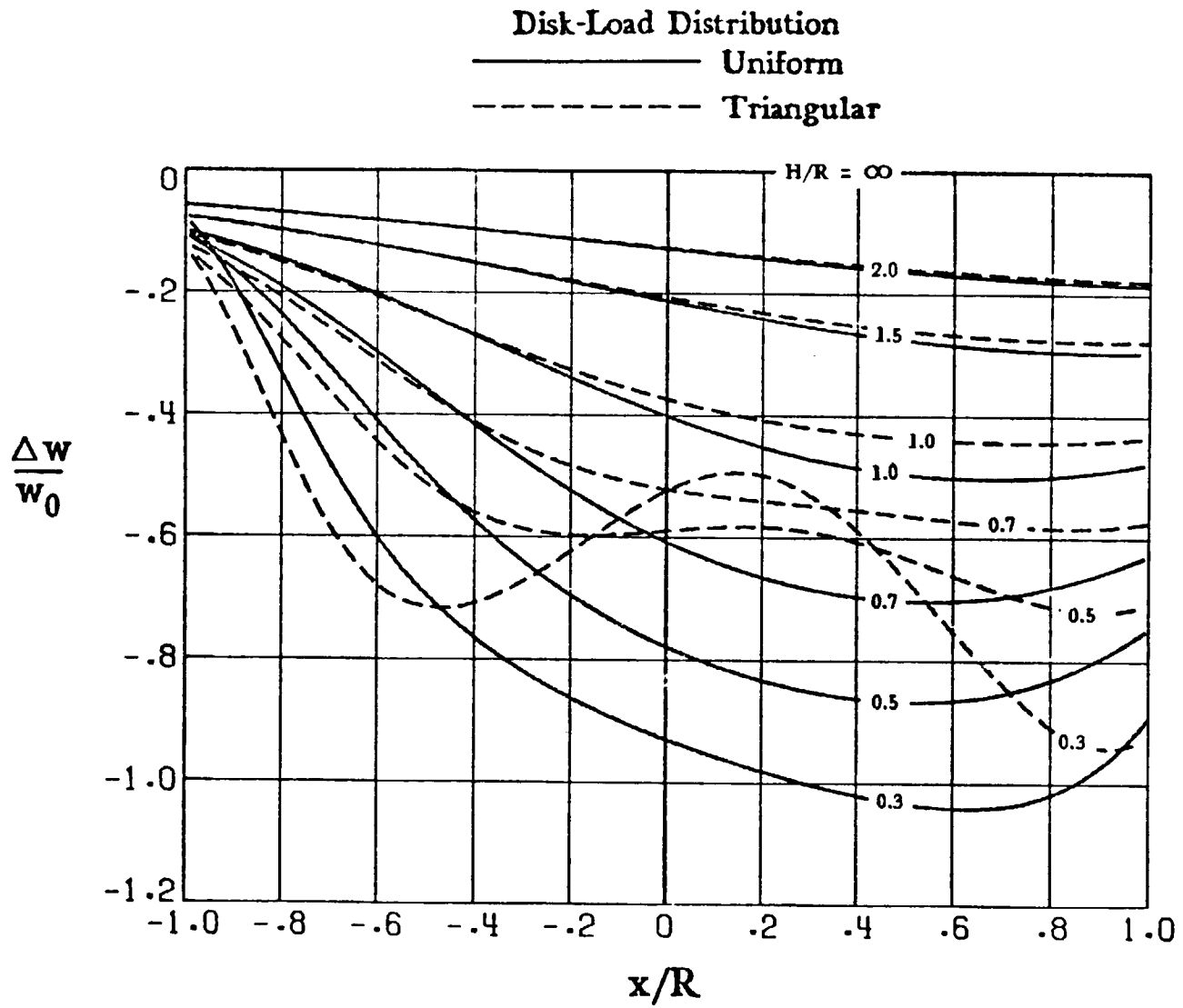

(a) $\chi_e = 30^0$.

Figure 10. - Distribution of the vertical component of ground-induced inteference inteference velocity over the longitudinal axis of a rotor in forward flight. $\alpha = 0^0$.

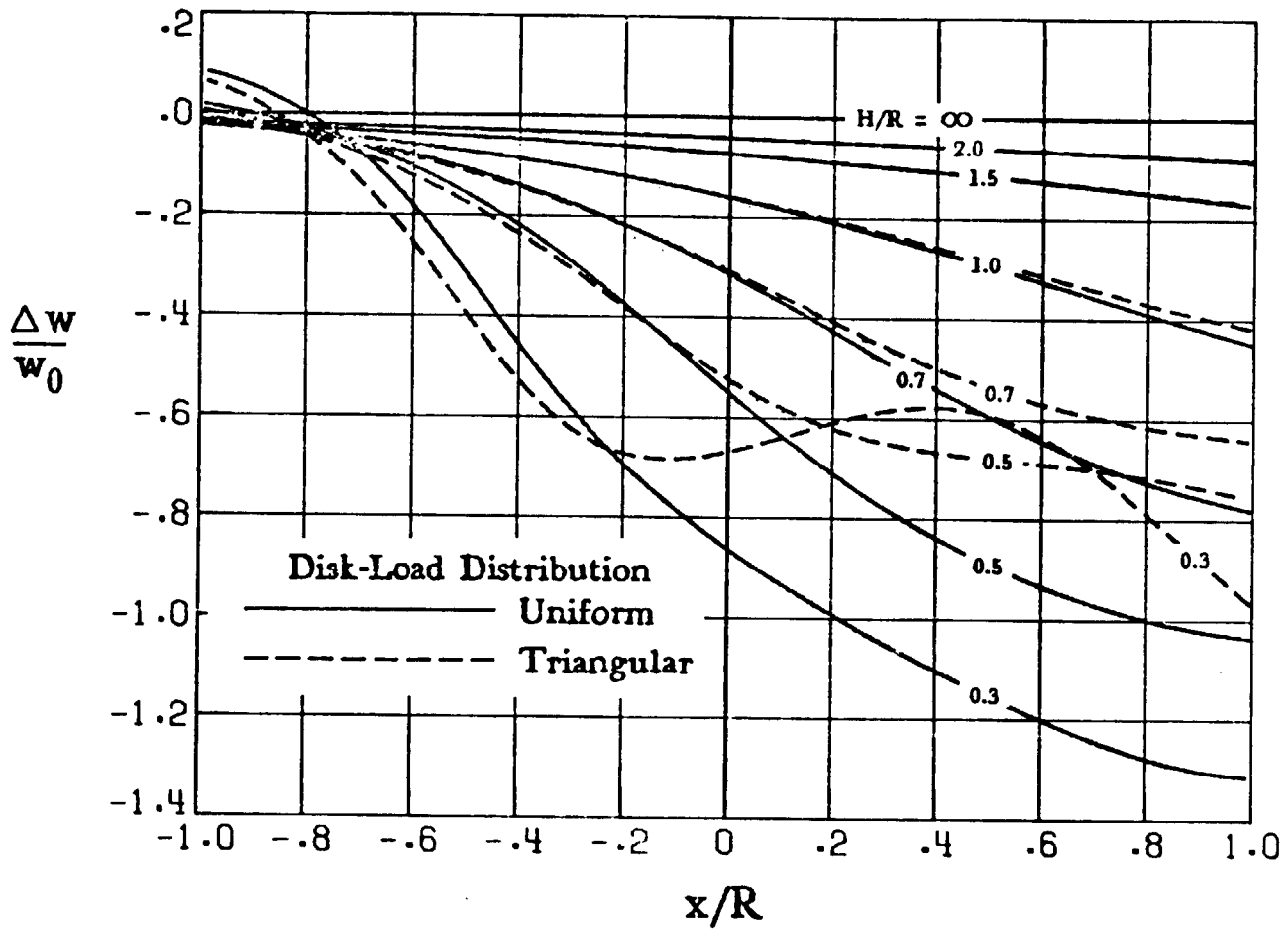

(b) $\chi_e = 60^o$.

Figure 10. - Continued.

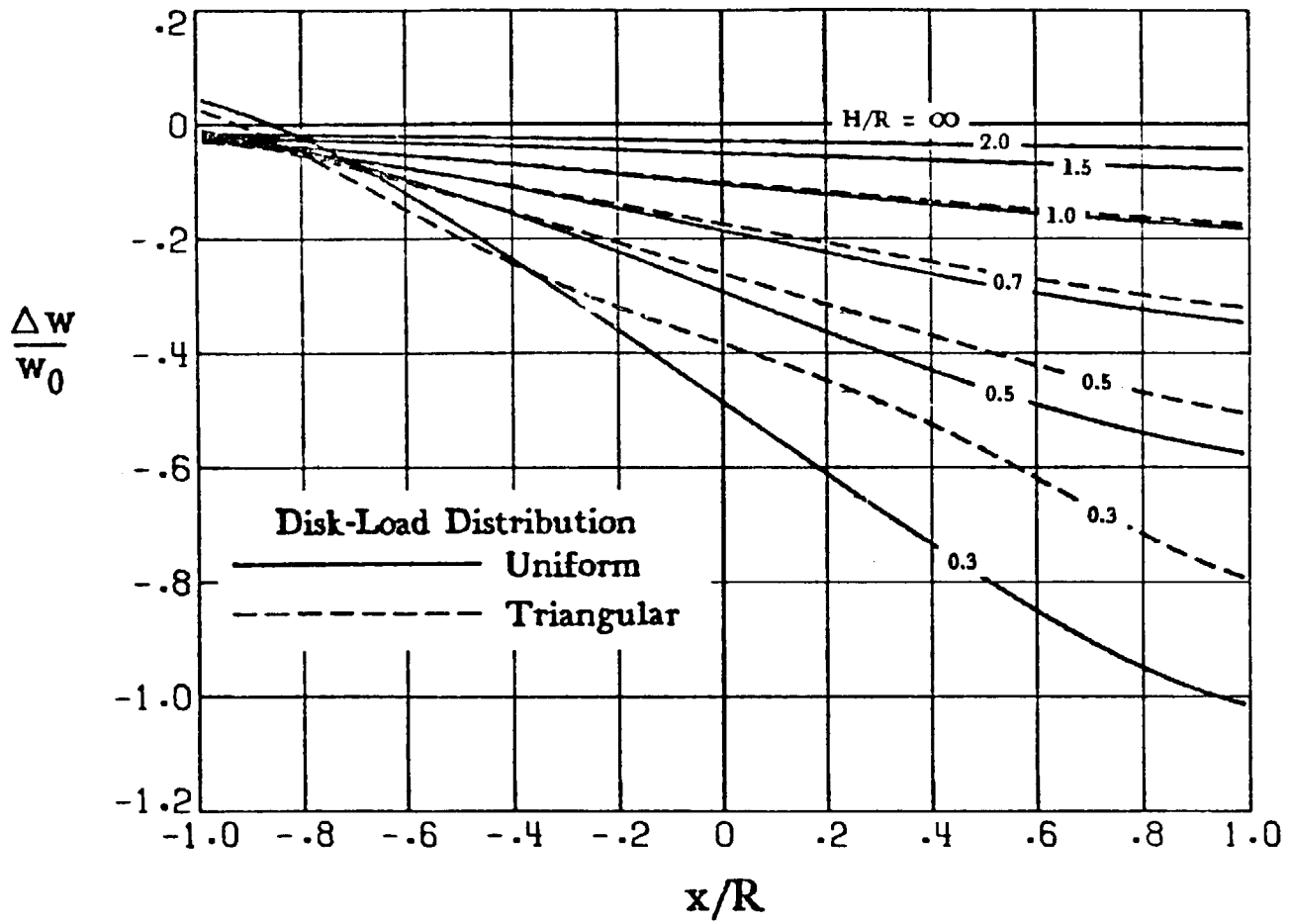

(c) $\chi_e = 90^o$.

Figure 10. - Concluded.

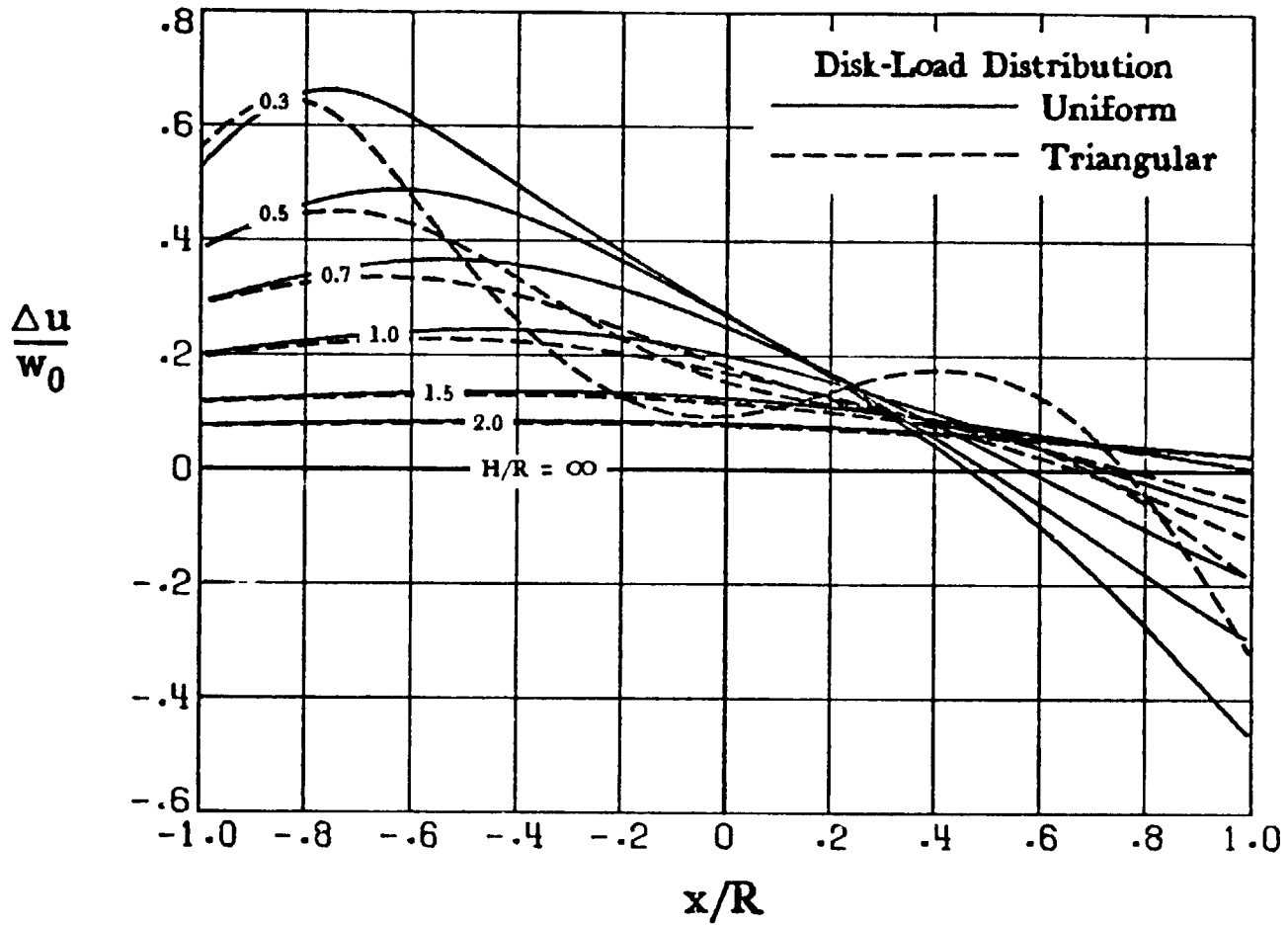

(a) $\chi_e = 30^o$.

Figure 11. - Distribution of the steamwise component of ground-induced interference velocity over the longitudinal axis of a rotor in forward flight. $\alpha = 0^o$.

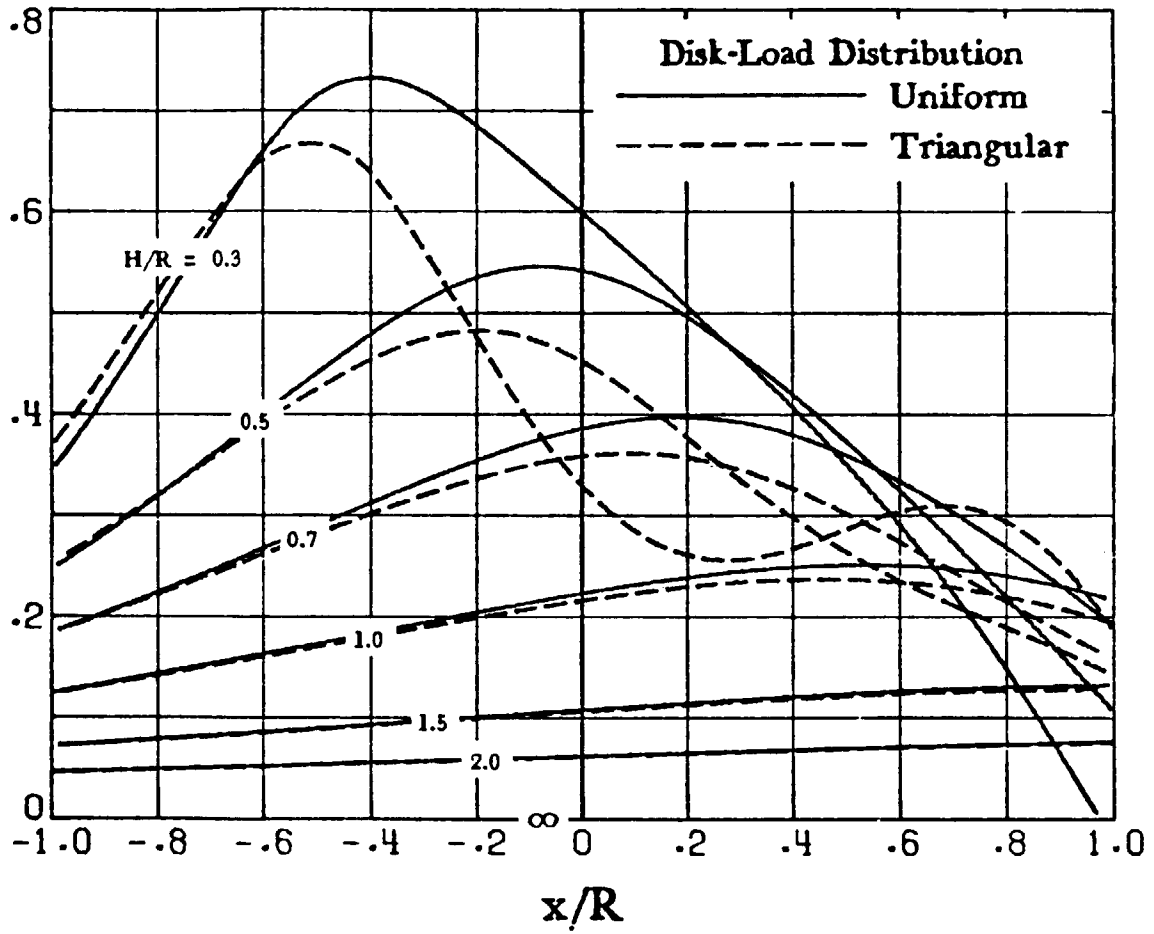

(b) $\chi_e = 60^o$.

Figure 11. - Continued.

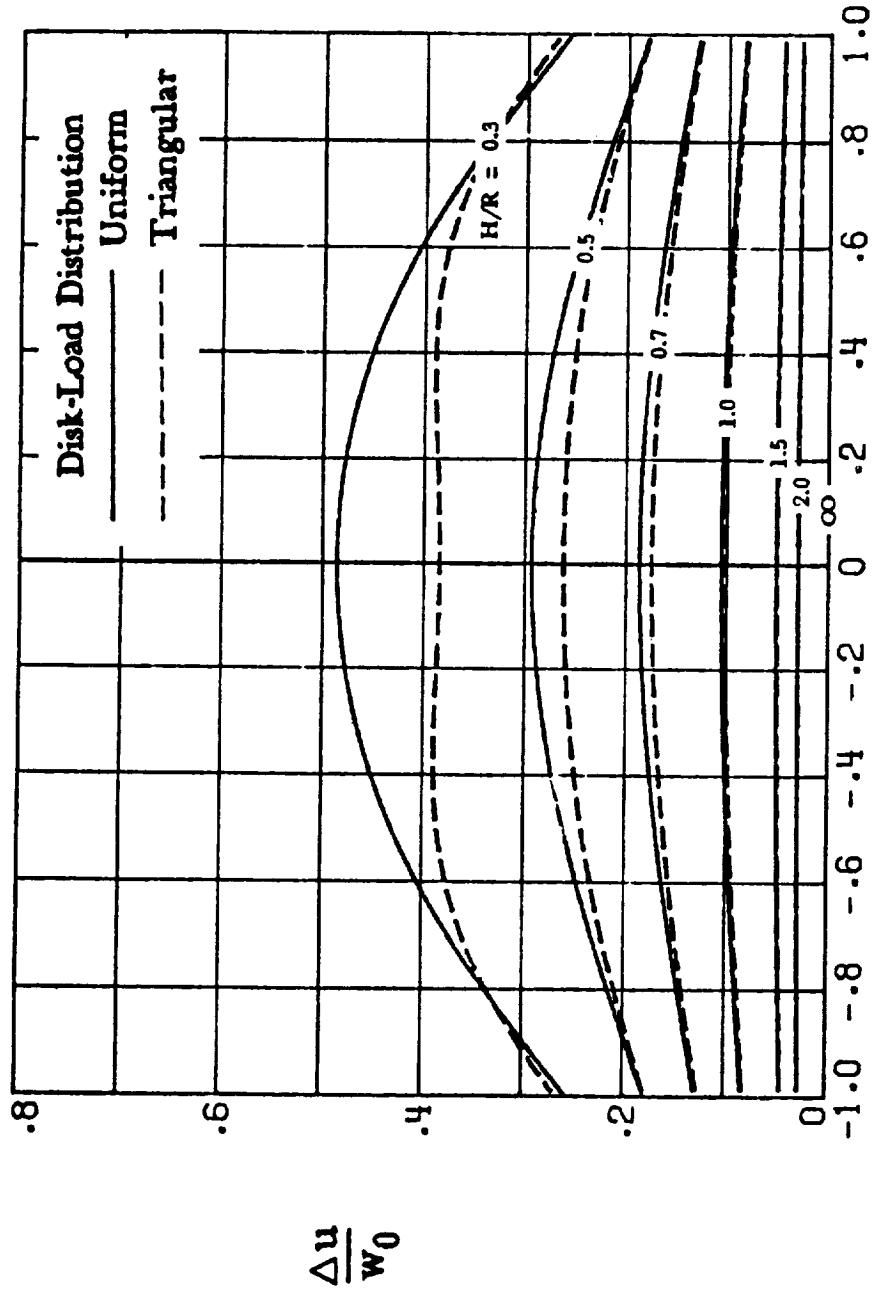

(c) $\chi_e = 90^o$.

Figure 11. - Concluded.

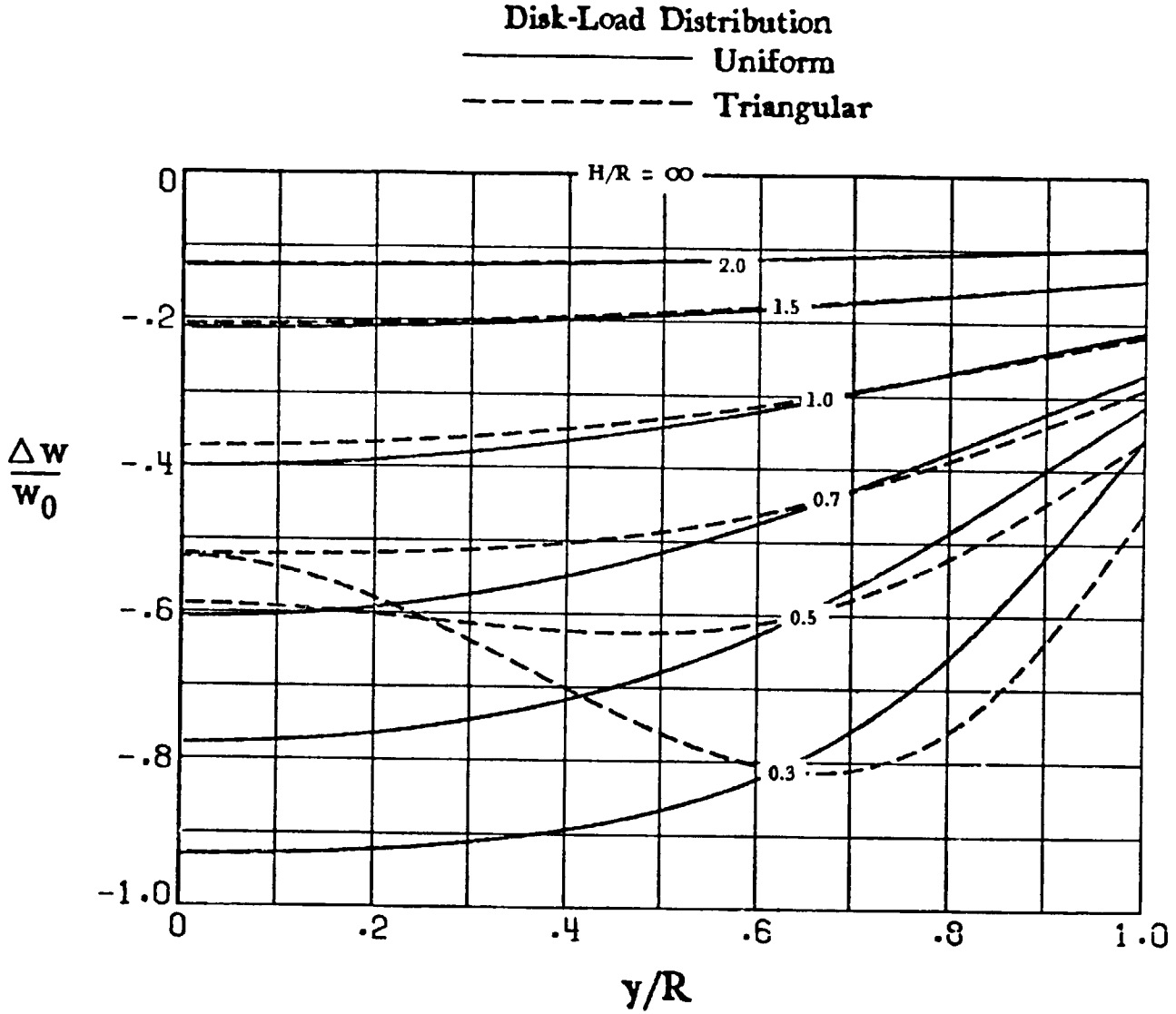

(a) $\chi_e = 30^0$.

Figure 12. - Distribution of the vertical component of ground-induced inteference velocity over the lateral axis of a rotor in forward flight. $\alpha = 0^0$.

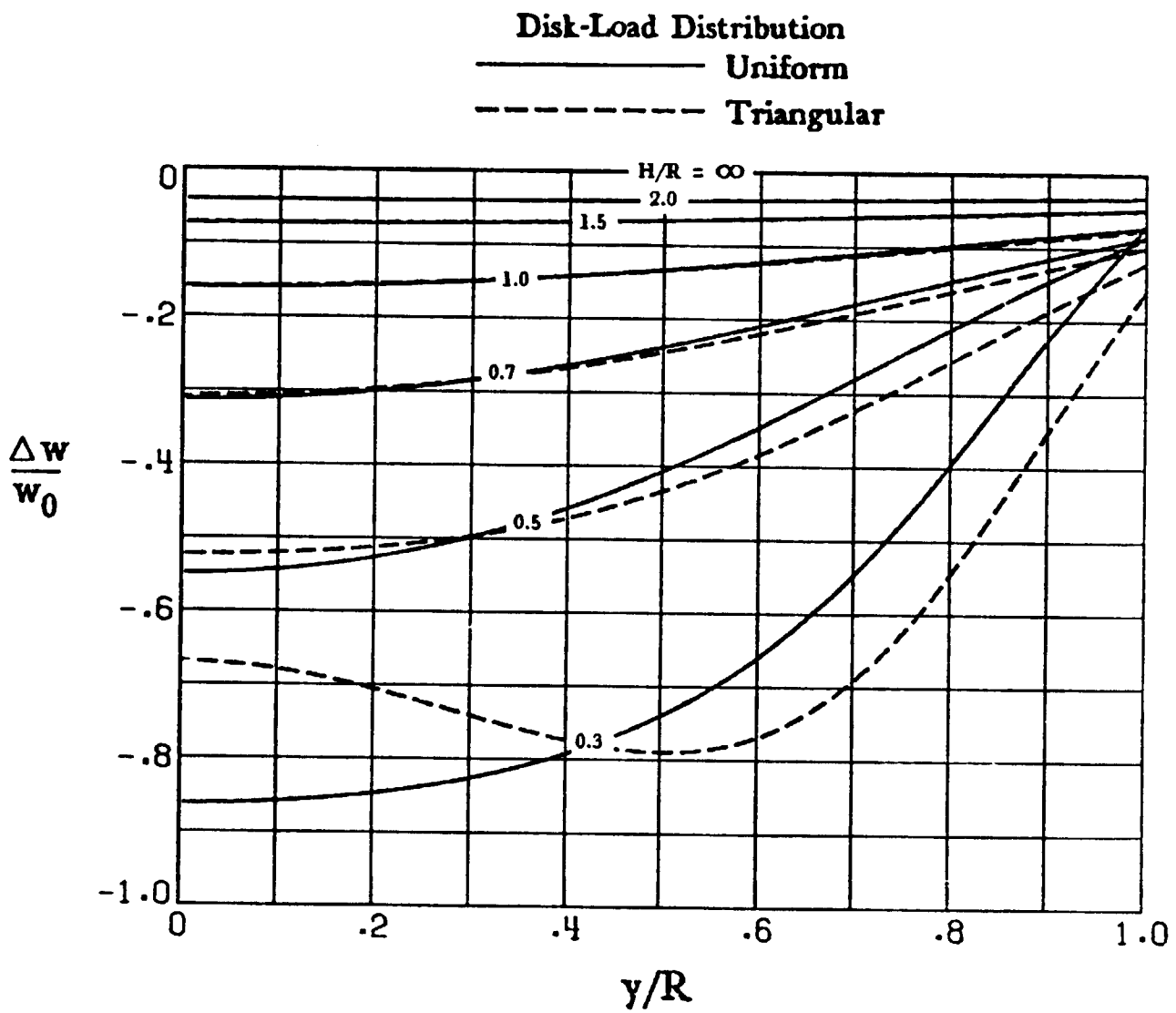

(b) $\chi_e = 60^o$.

Figure 12. - Continued.

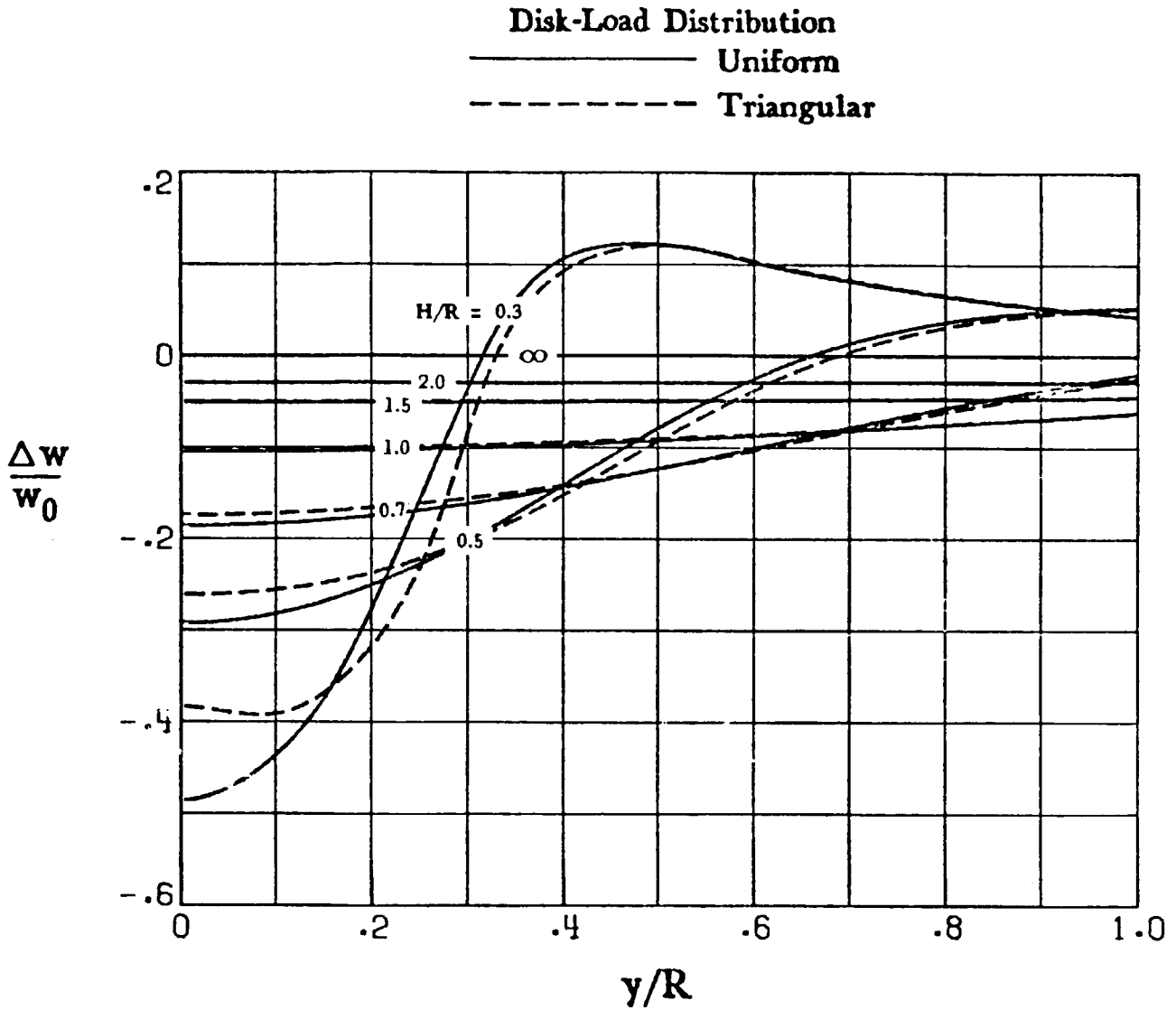

(c) $\chi_e = 90^o$.

Figure 12. - Concluded.

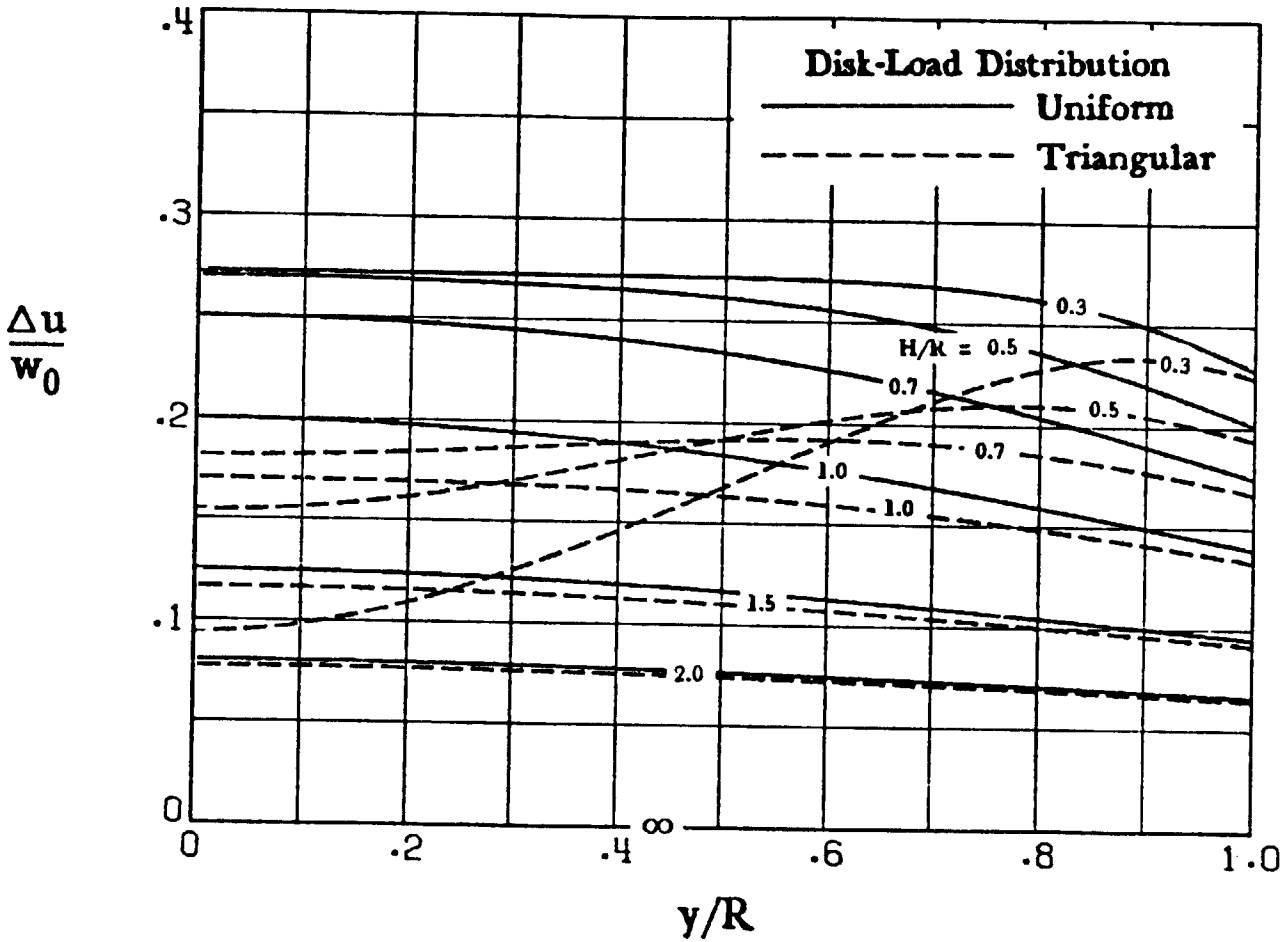

(a) $\chi_e = 30^0$.

Figure 13. - Distribution of the streamwise component of ground-induced inteference velocity over the lateral axis of a rotor in forward flight. $\alpha = 0^0$.

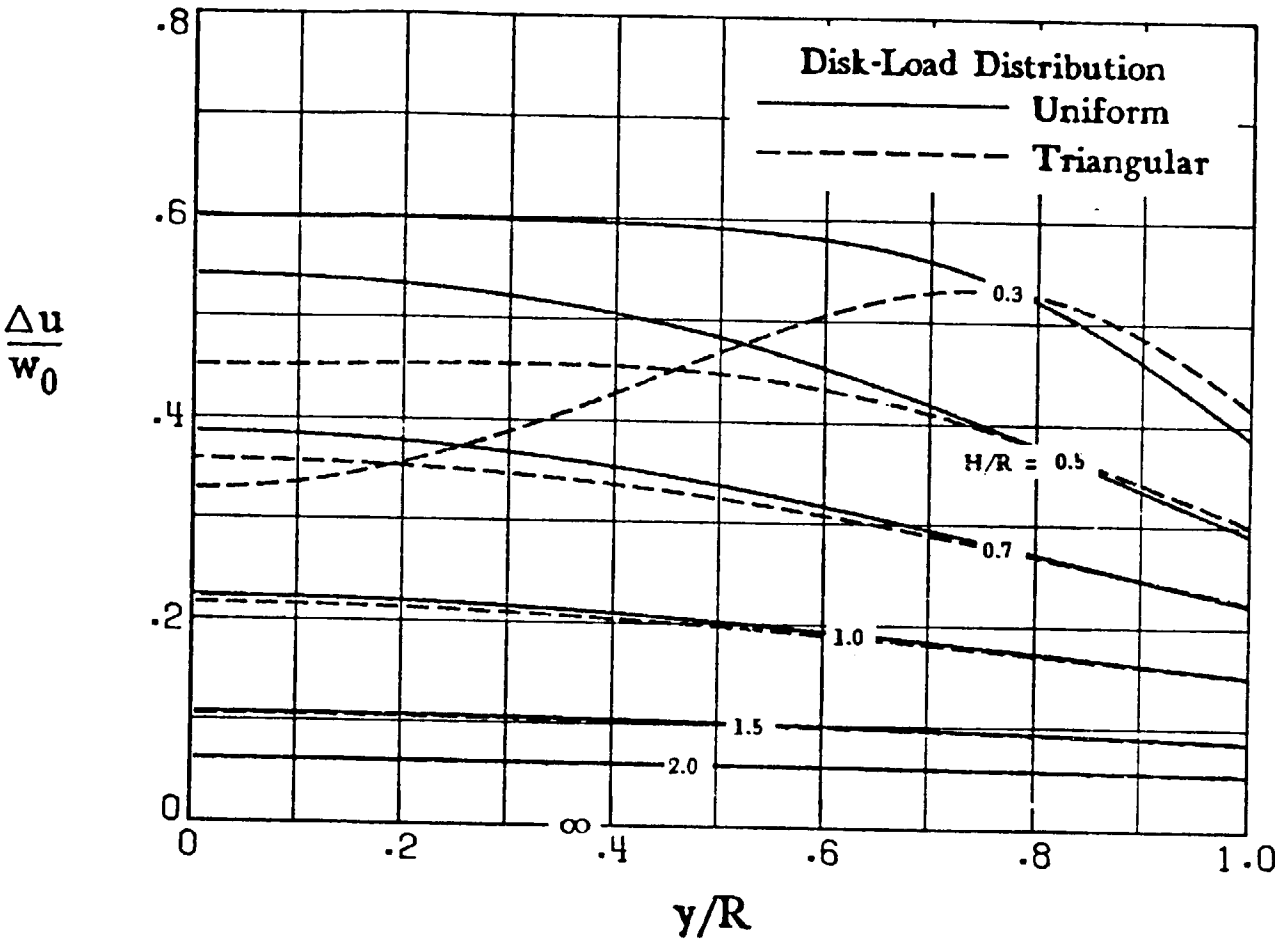

(b) $\chi_e = 60^o$.

Figure 13. - Continued.

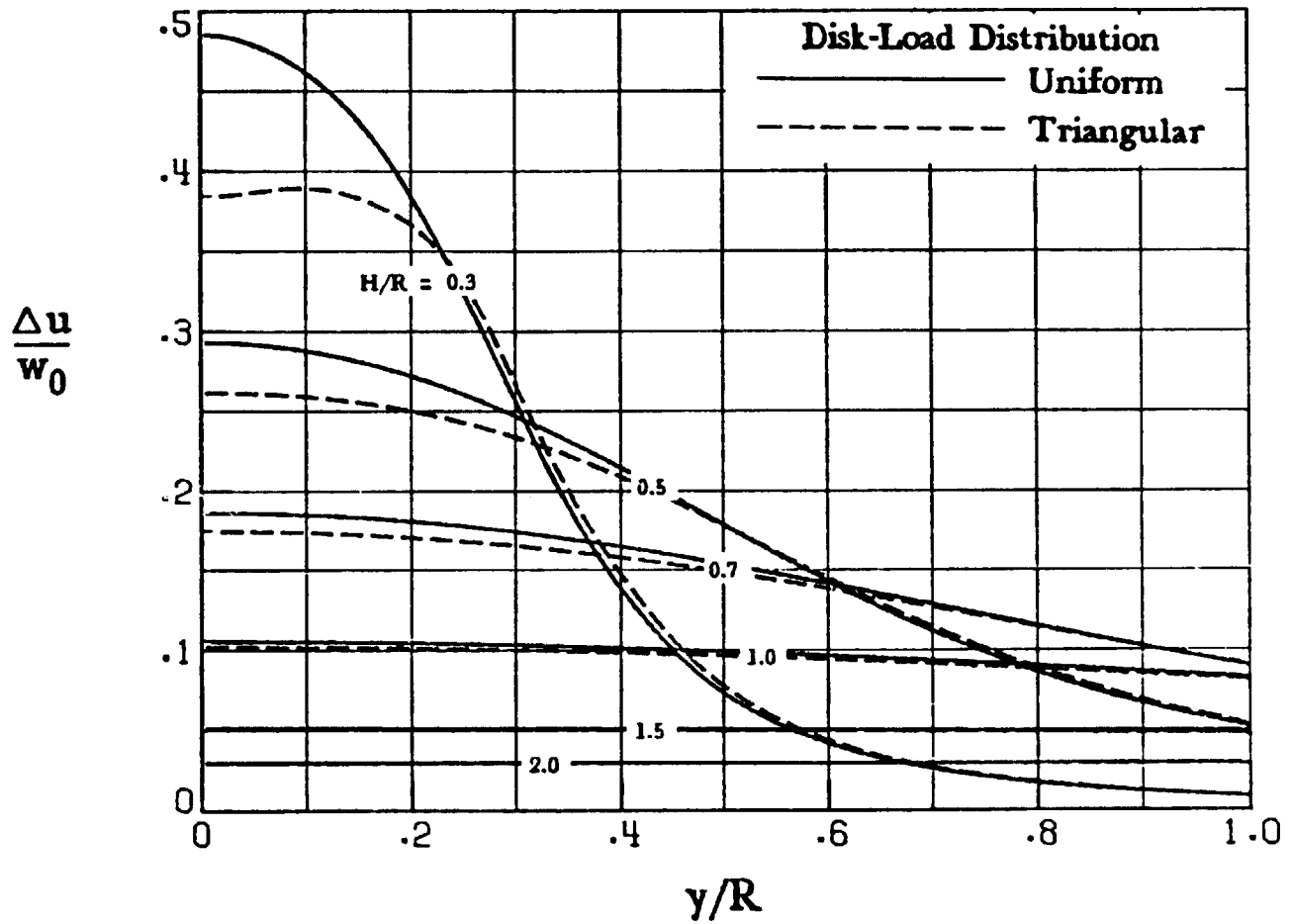

(c) $\chi_e = 90^o$.

Figure 13. - Concluded.

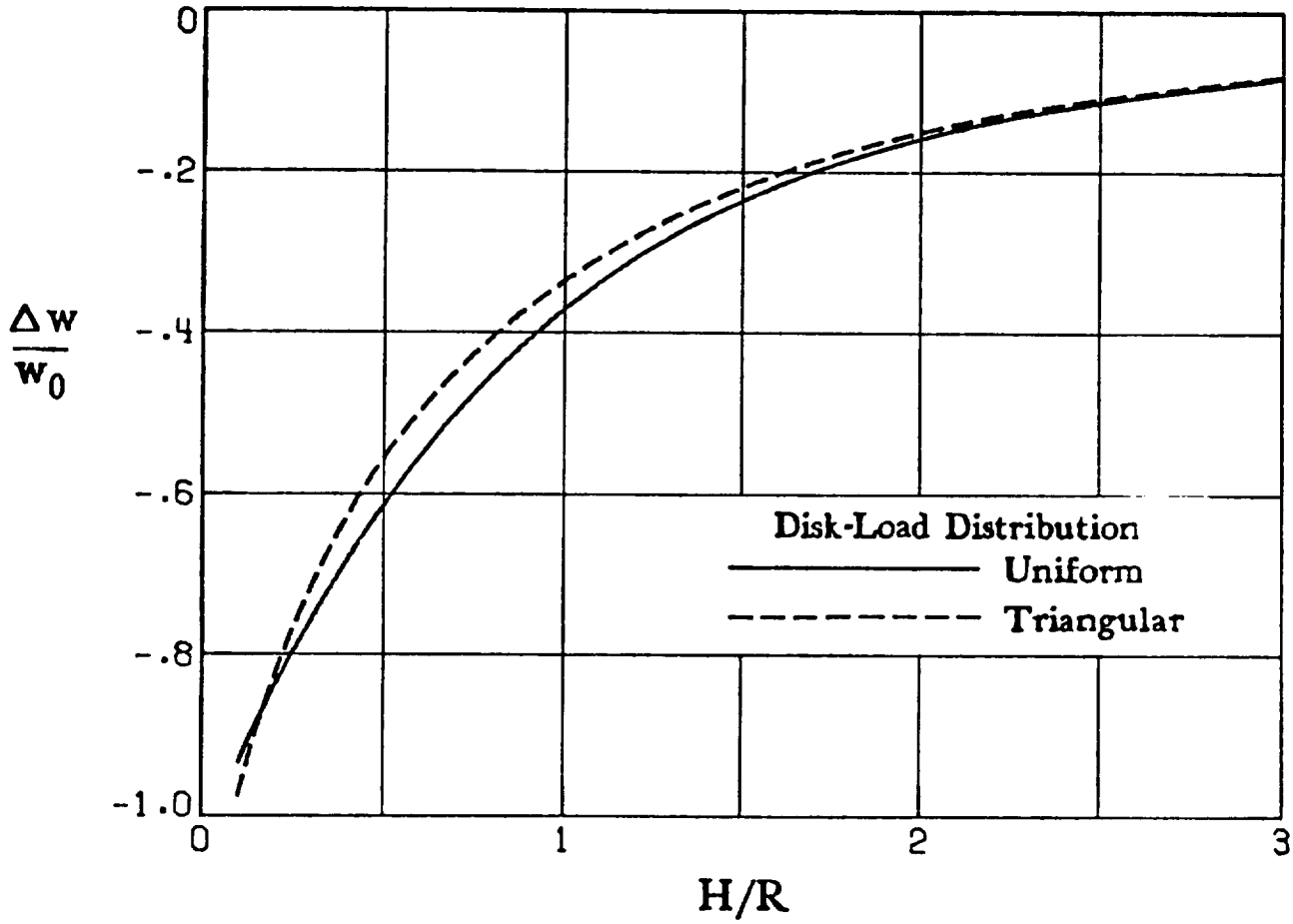

Figure 14. - Average vertical ground-induced interference velocity $\Delta w/w_0$ over the area of the rotor as a function of height above the ground. $\alpha = 0^o$.

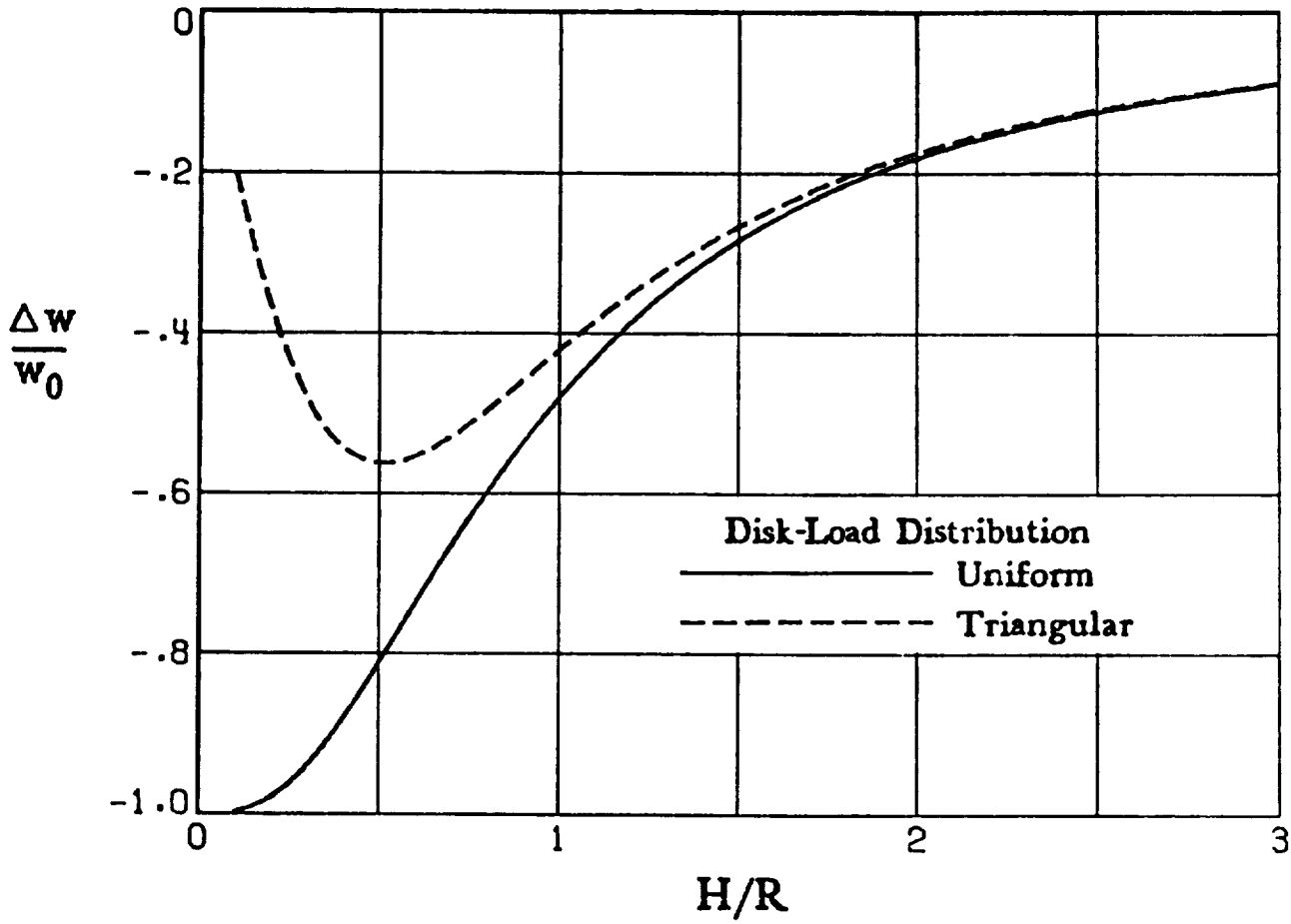

Figure 15. - Ground-induced vertical velocity at the center of the rotor as a function of height above the ground. $\alpha = 0^{o}$.

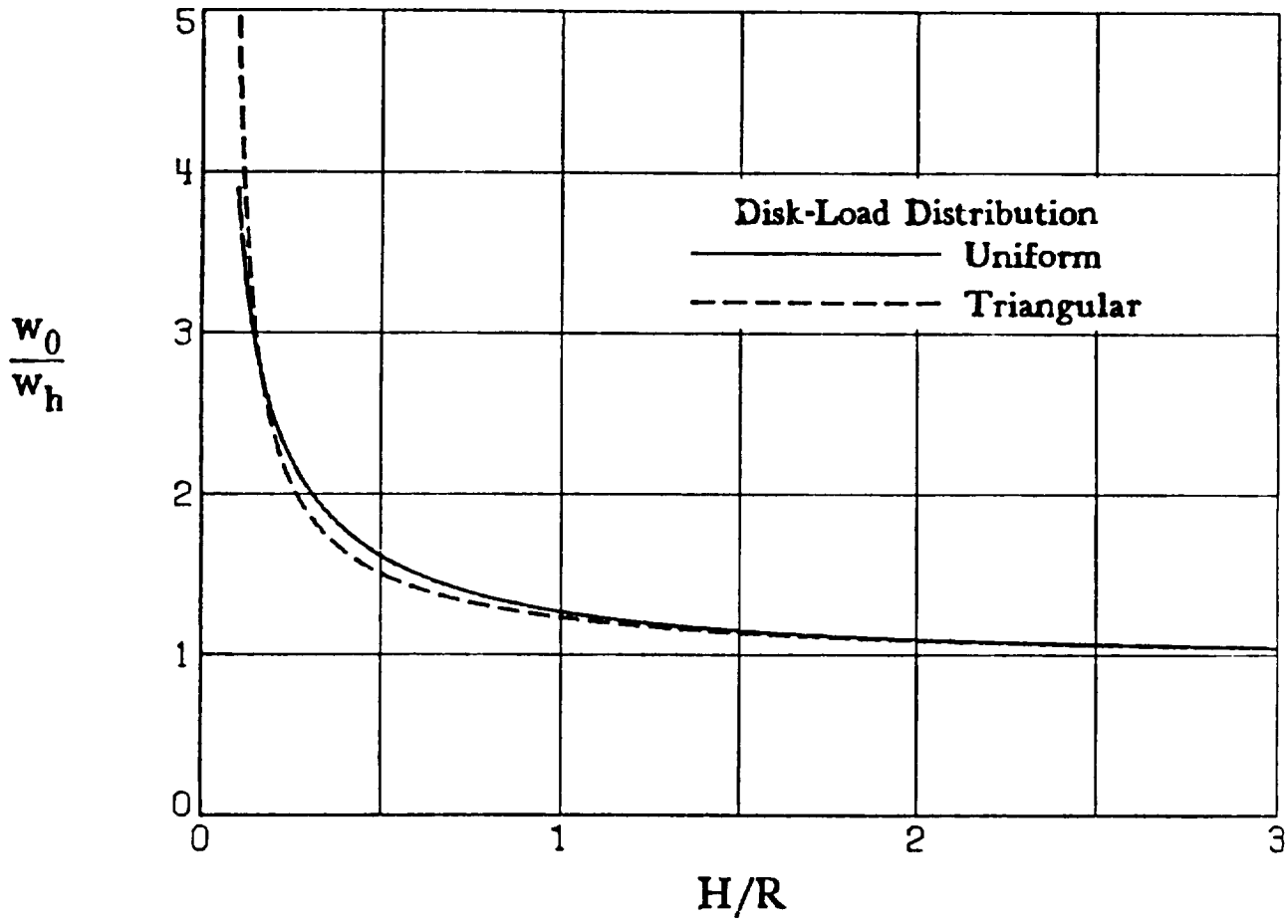

Figure 16. - Average rotor induced velocity w_0/w_h as a function of height above the ground. $\alpha = 0^o$.

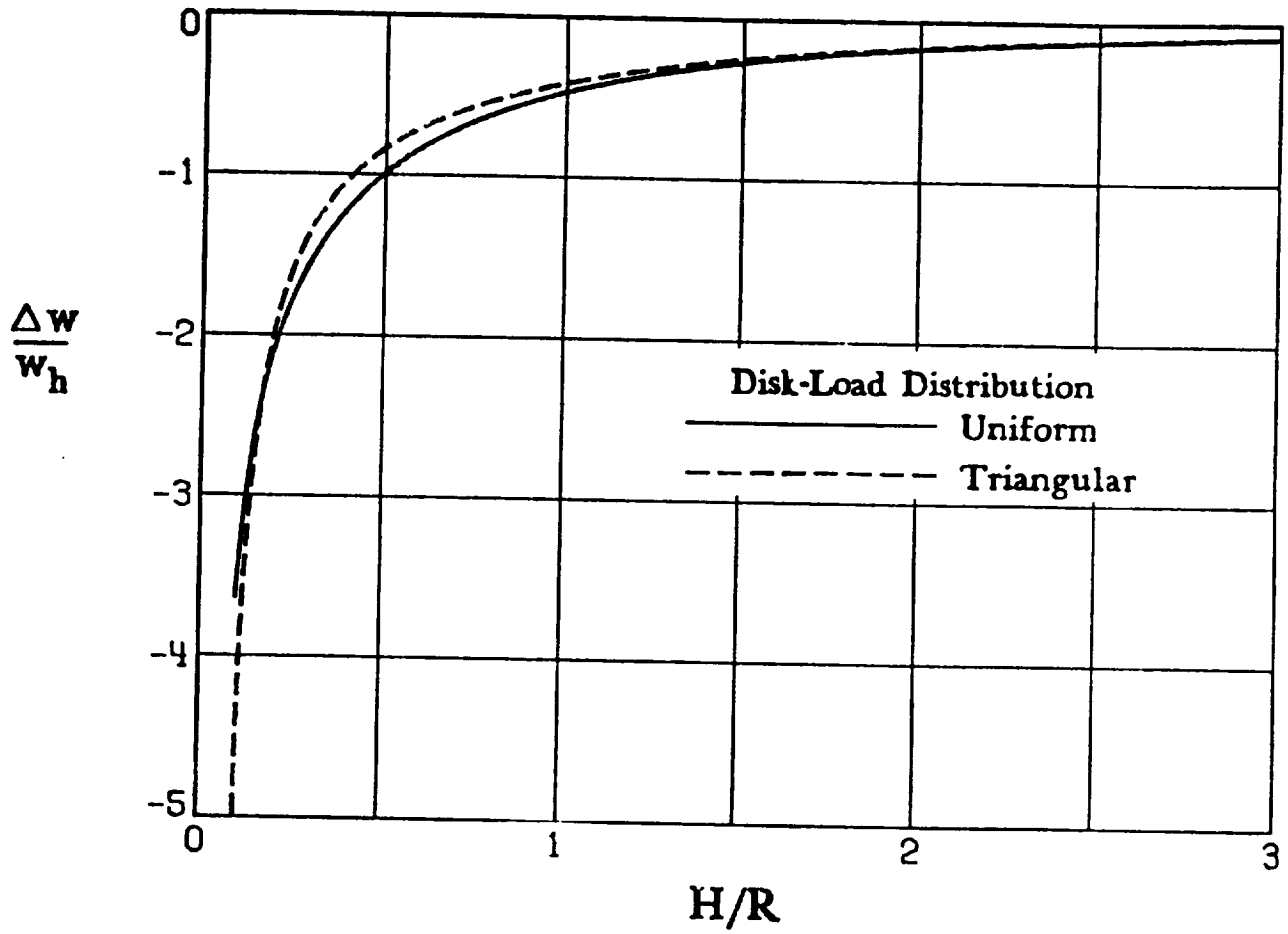

Figure 17. - Average vertical ground-induced interference velocity as a fraction of the induced velocity when hovering in free air. $\alpha = 0^{\circ}$

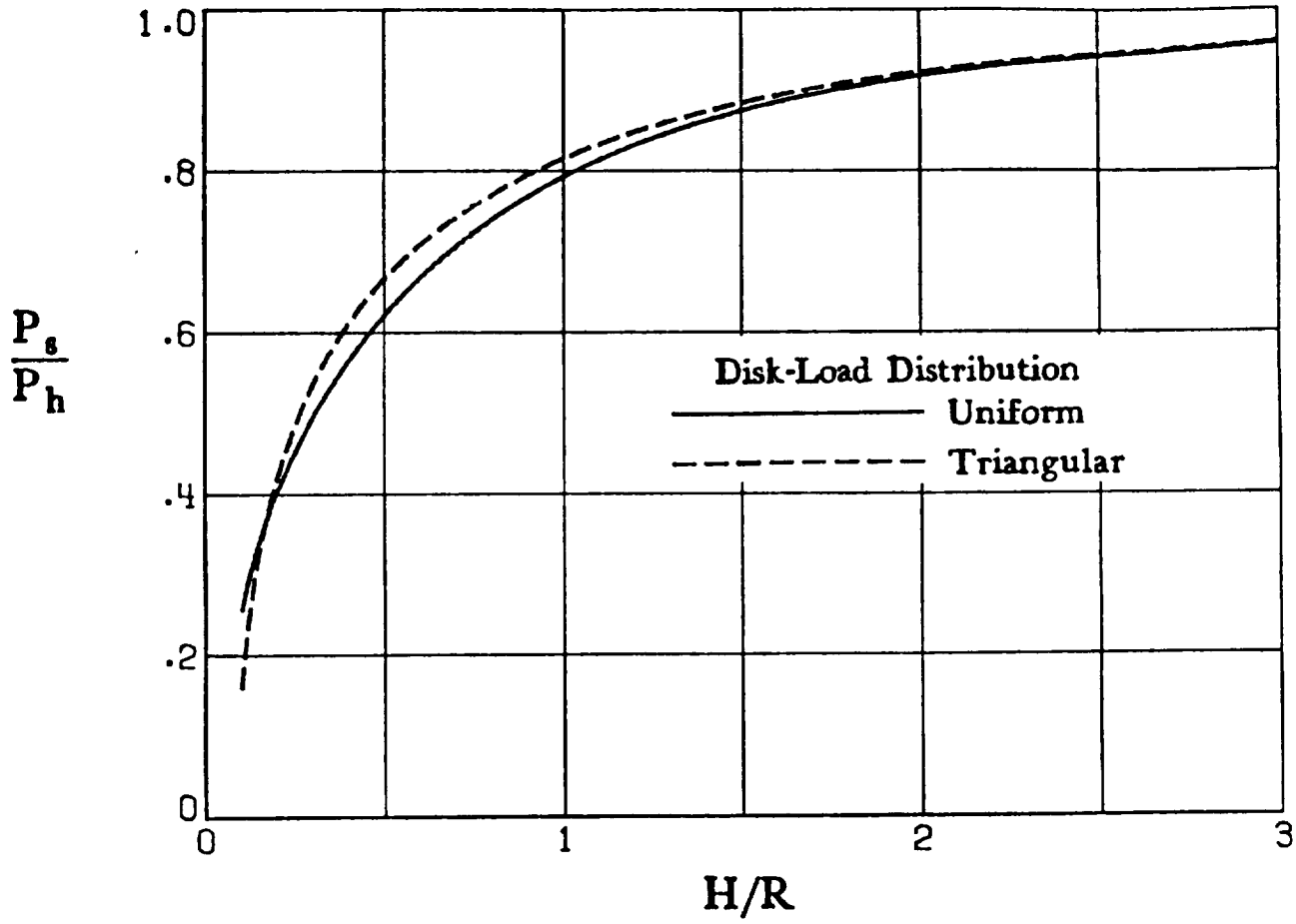

Figure 18. - Induced shaft power when hovering in ground effect. $\alpha = 0^{o}$.

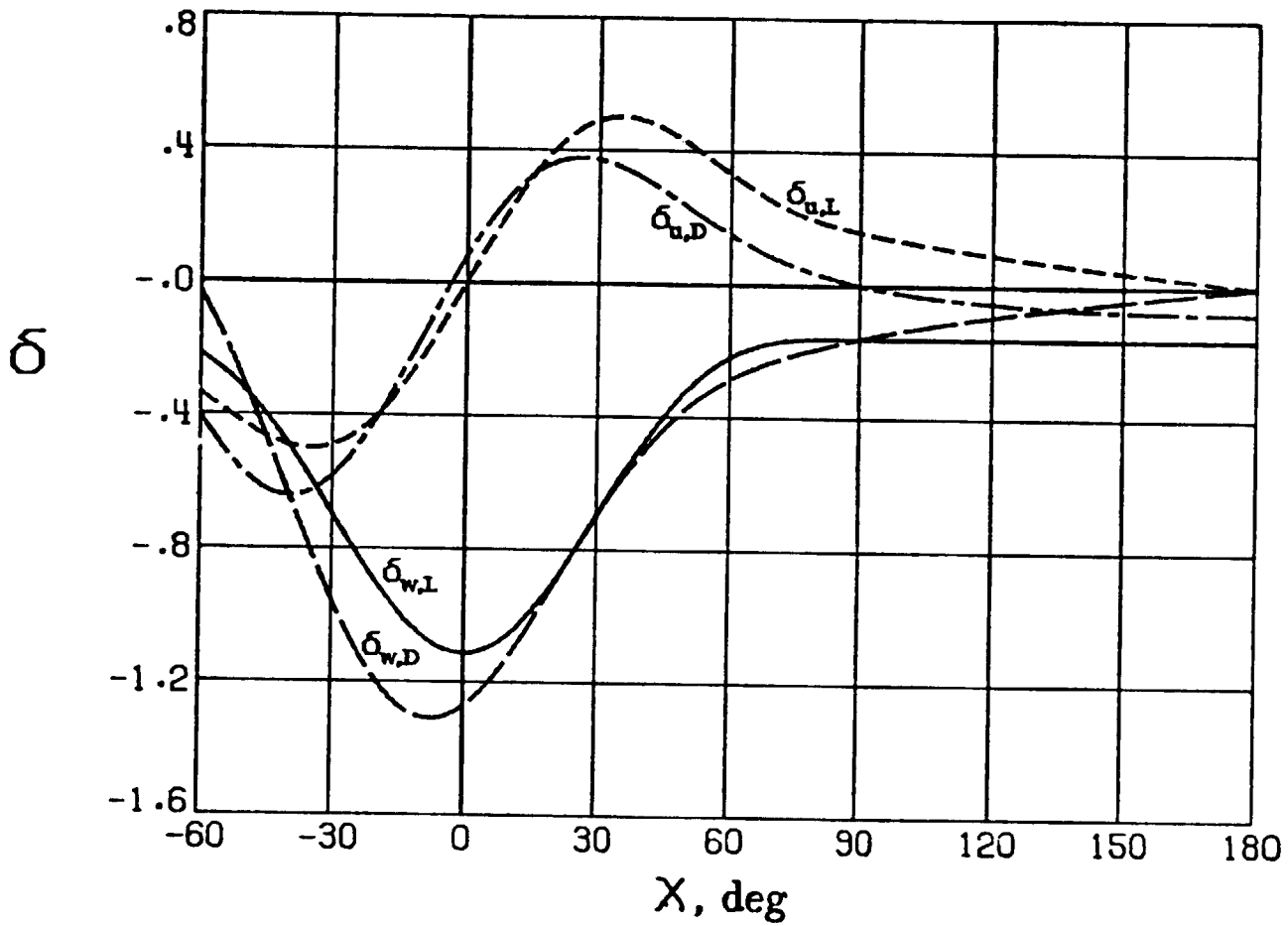

Figure 19. - Interference factors (equations (24) and (25)) proportional to the ground-induced interference velocities in forward flight for a vanishingly small rotor.

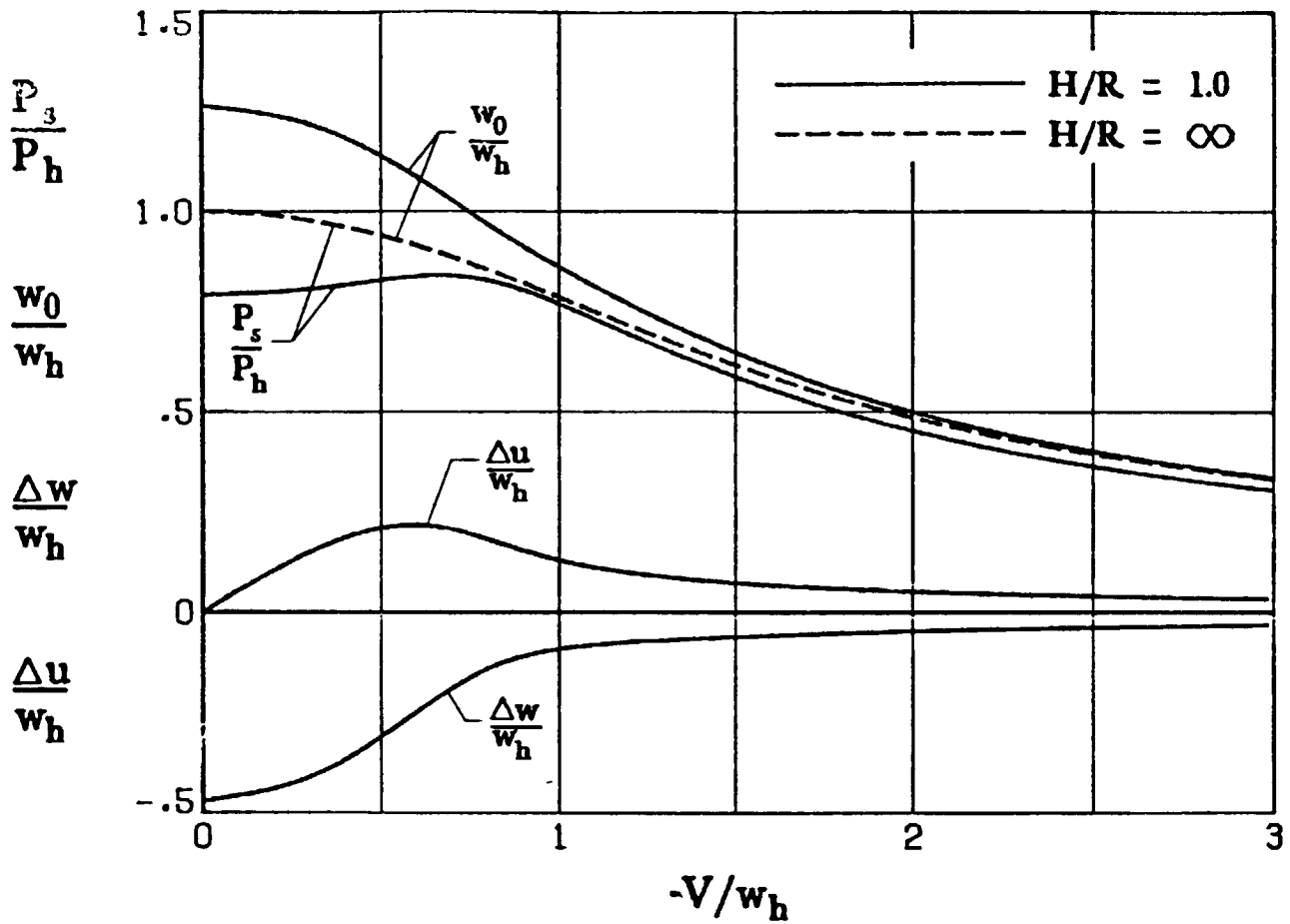

(a) Uniform disk-load distribution.

Figure 20. - Factors influencing rotor performance in forward flight near the ground. $\alpha = 0^o$.

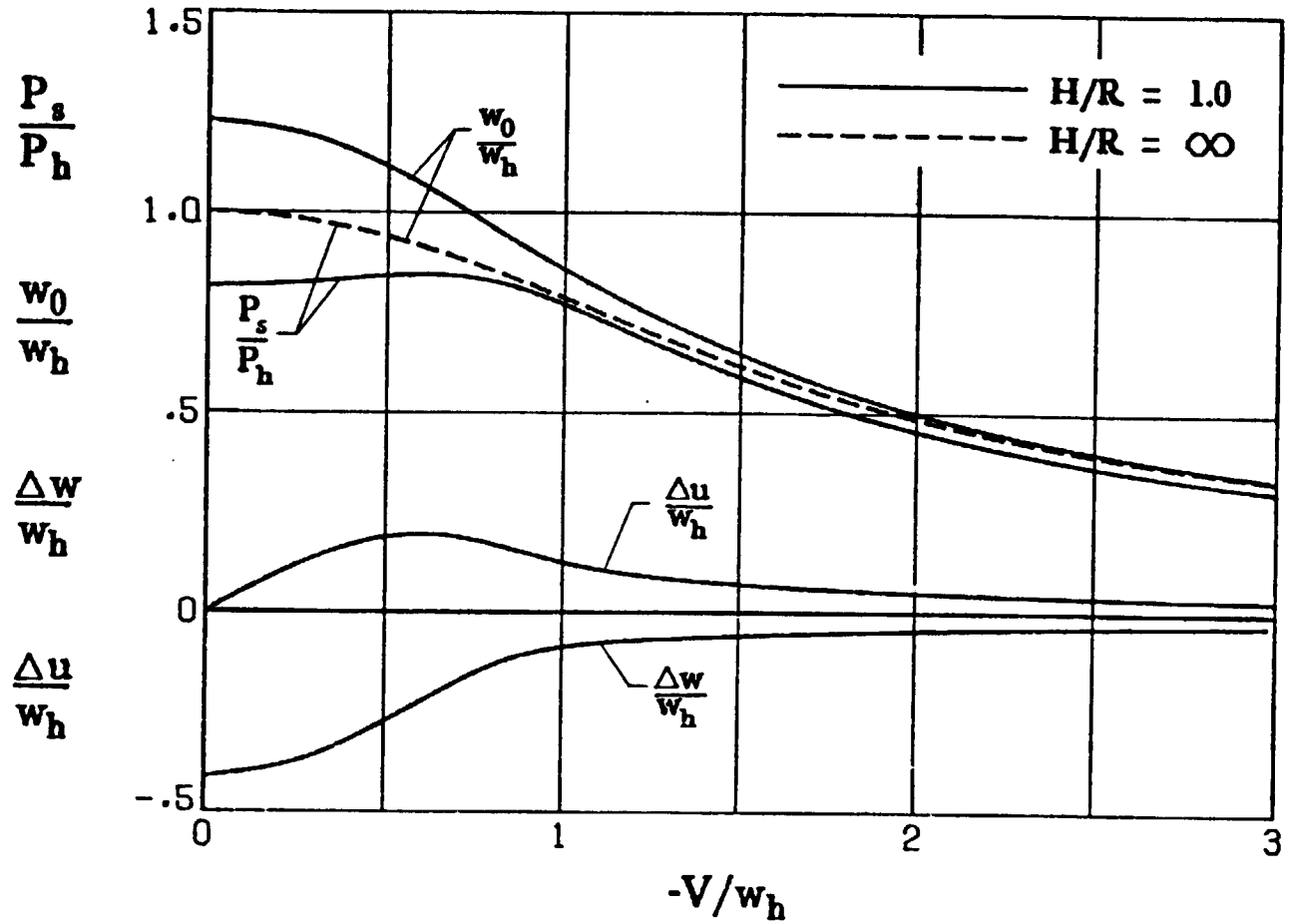

(b) Triangular disk-load distribution.

Figure 20. - Concluded.

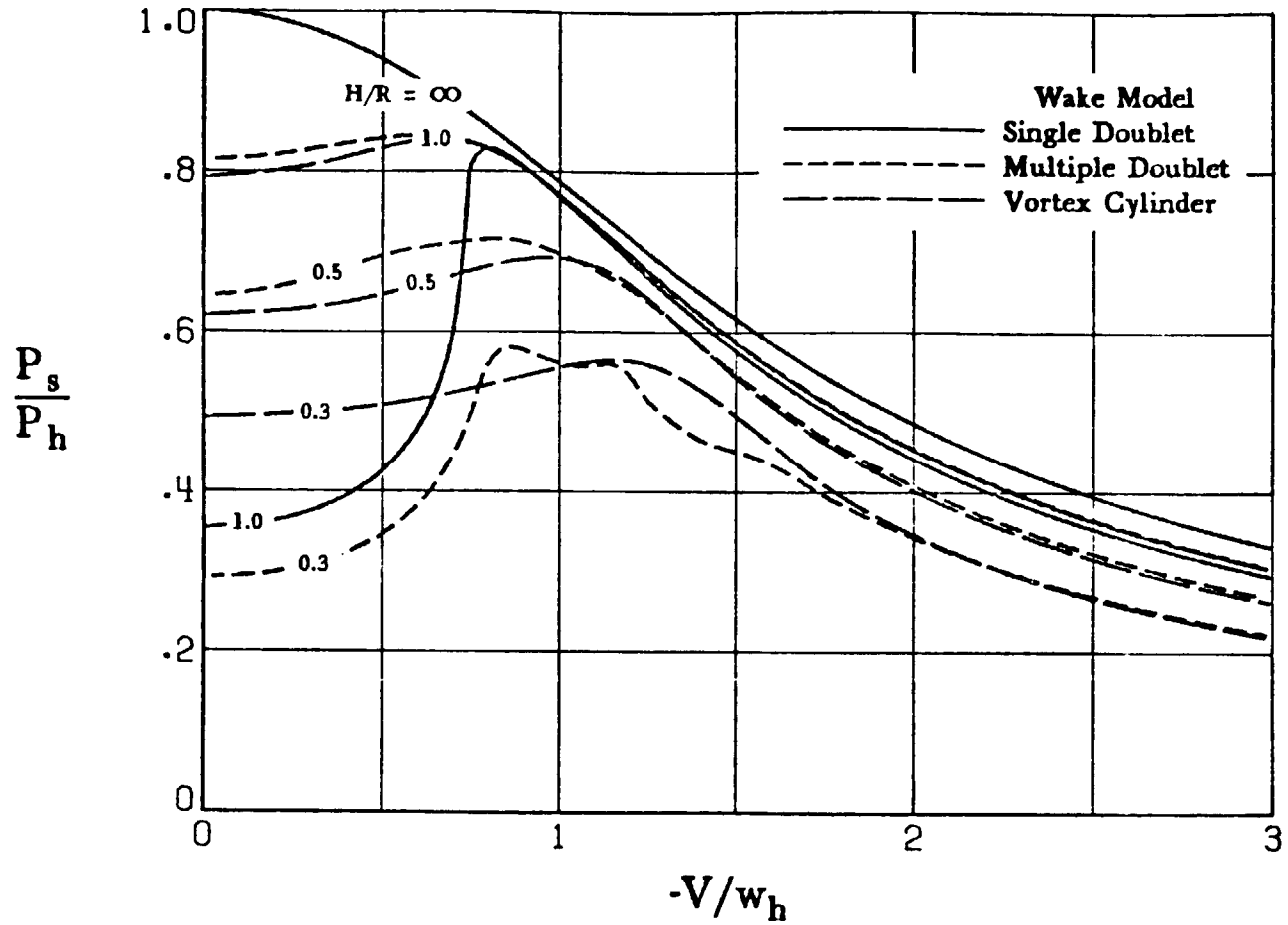

(a) Uniform disk-load distribution.

Figure 21. - Effect of chosen wake model on the calculated induced shaft power required for level flight ground effect. $\alpha = 0^0$.

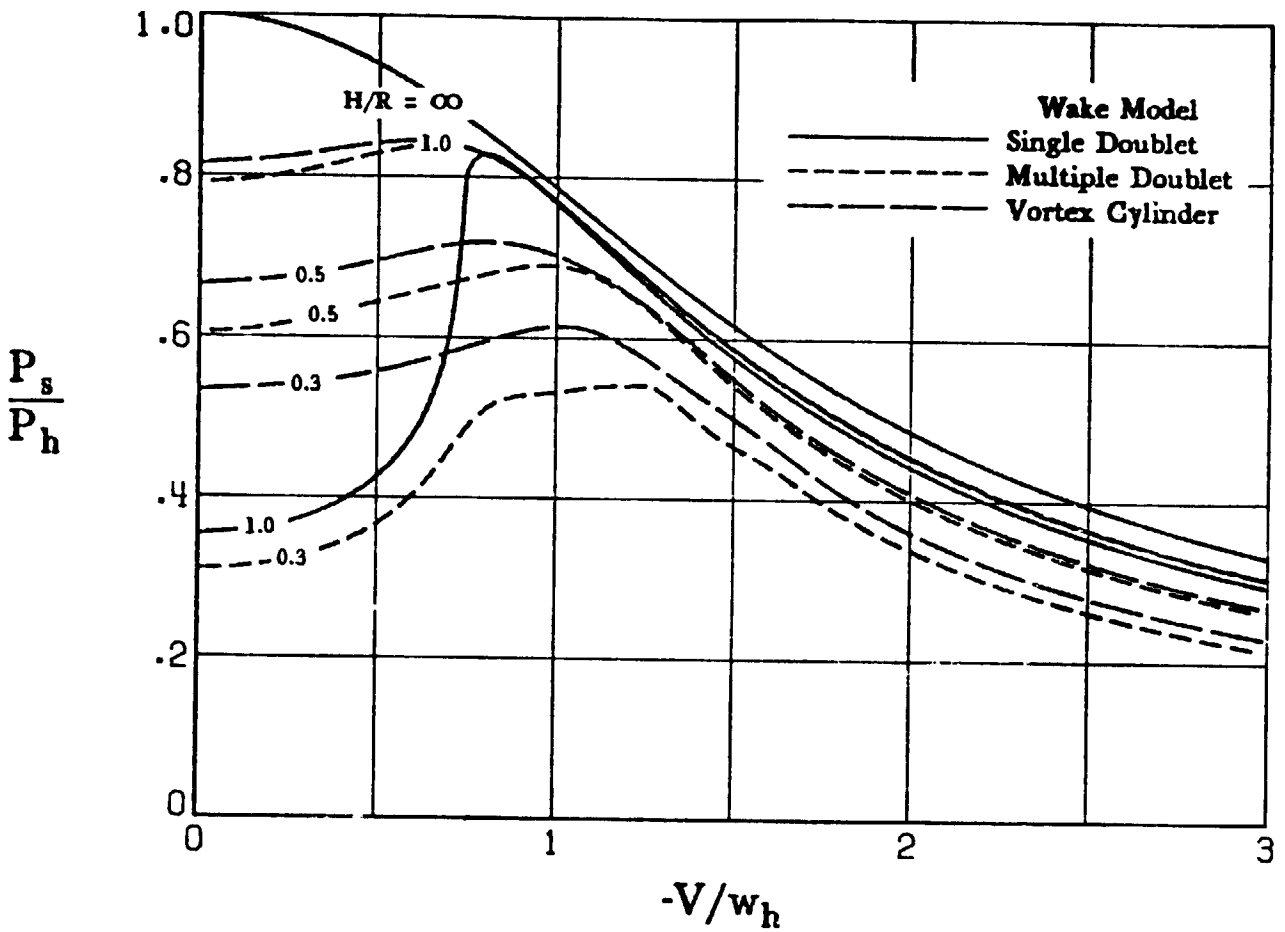

(b) Triangular disk-load distribution.

Figure 21. - Concluded.

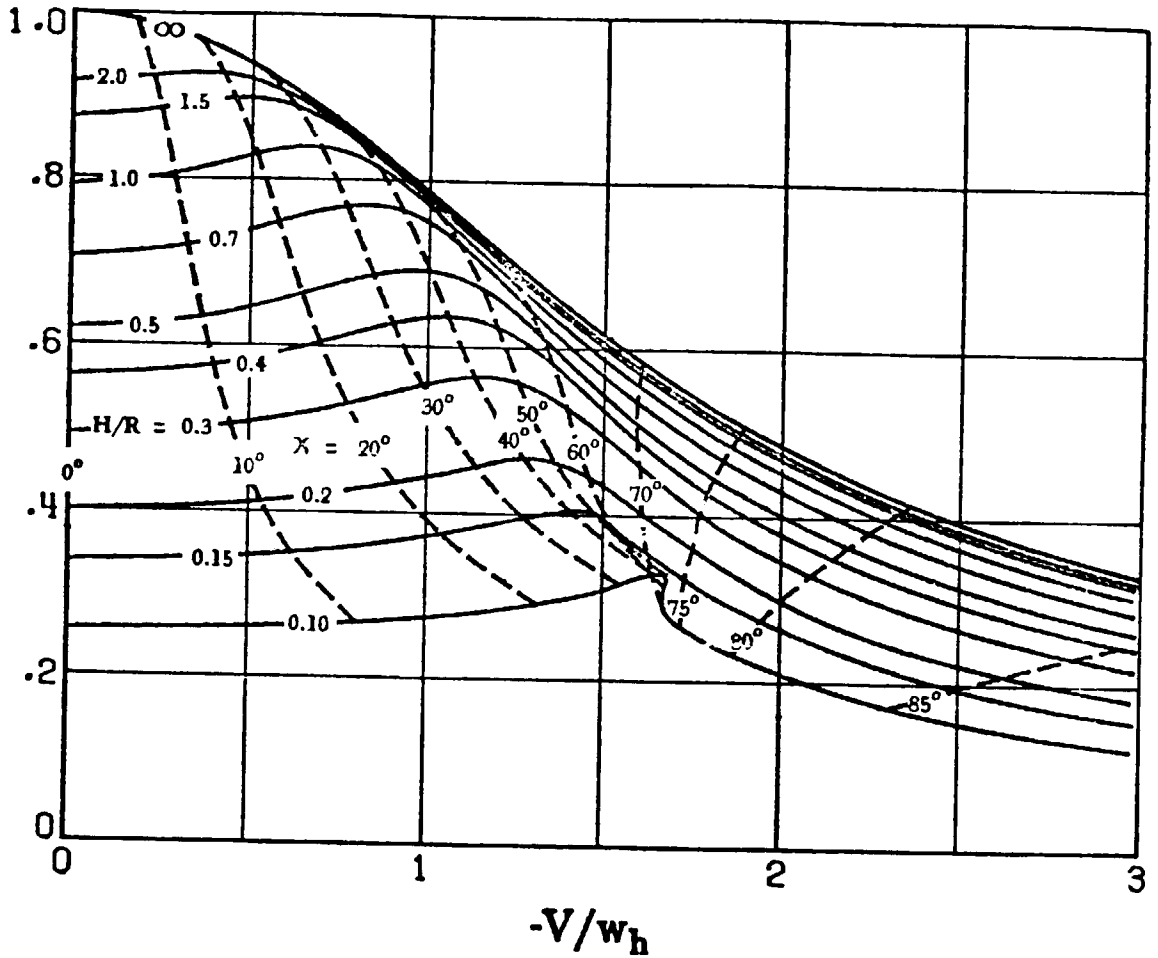

(a) Uniform disk-load distribution.

Figure 22. - Induced shaft power and momentum skew angle as a function of forward velocity in ground effect. $\alpha = 0^{o}$.

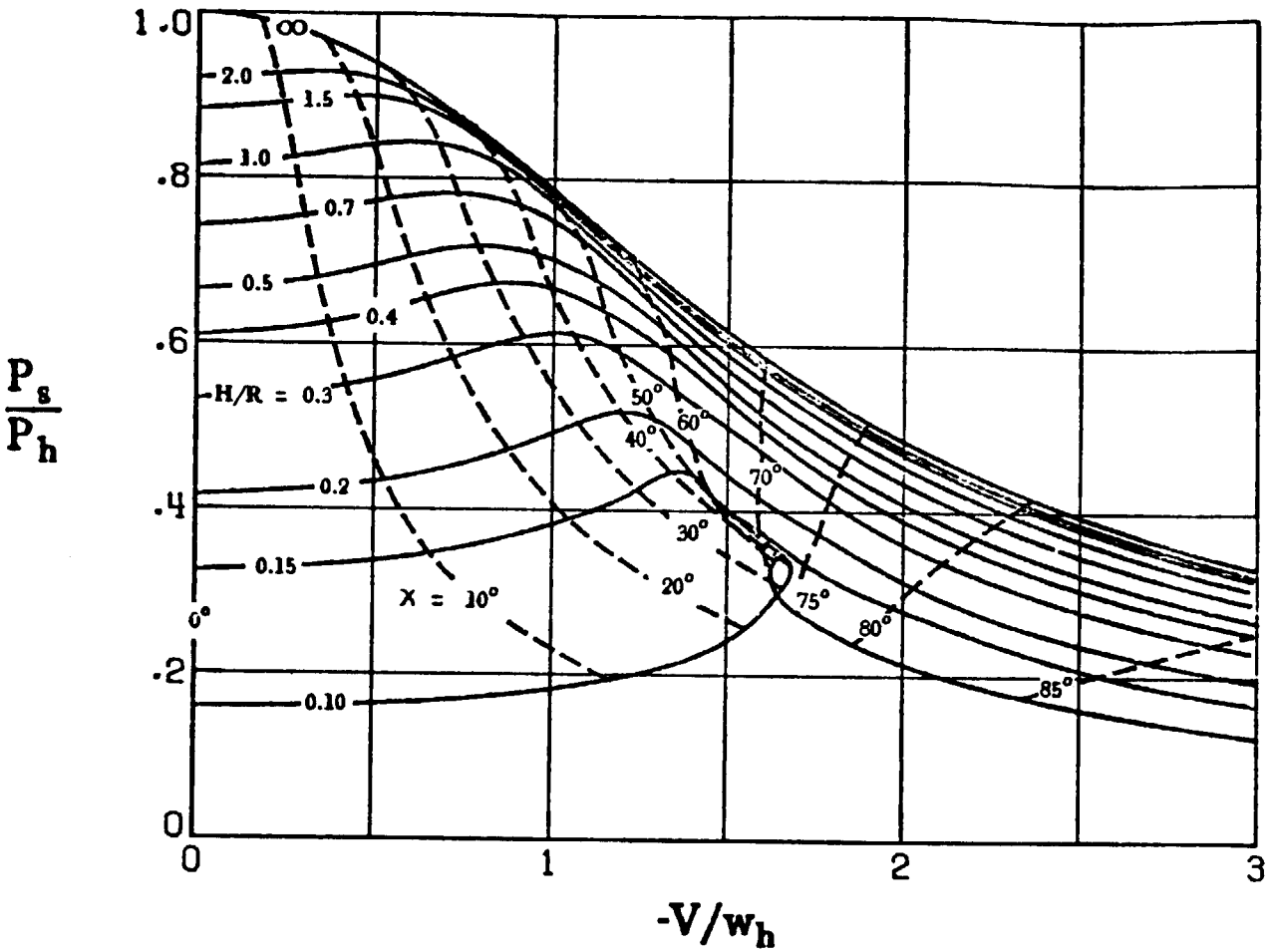

(b) Triangular disk-load distribution.

Figure 22. - Concluded.

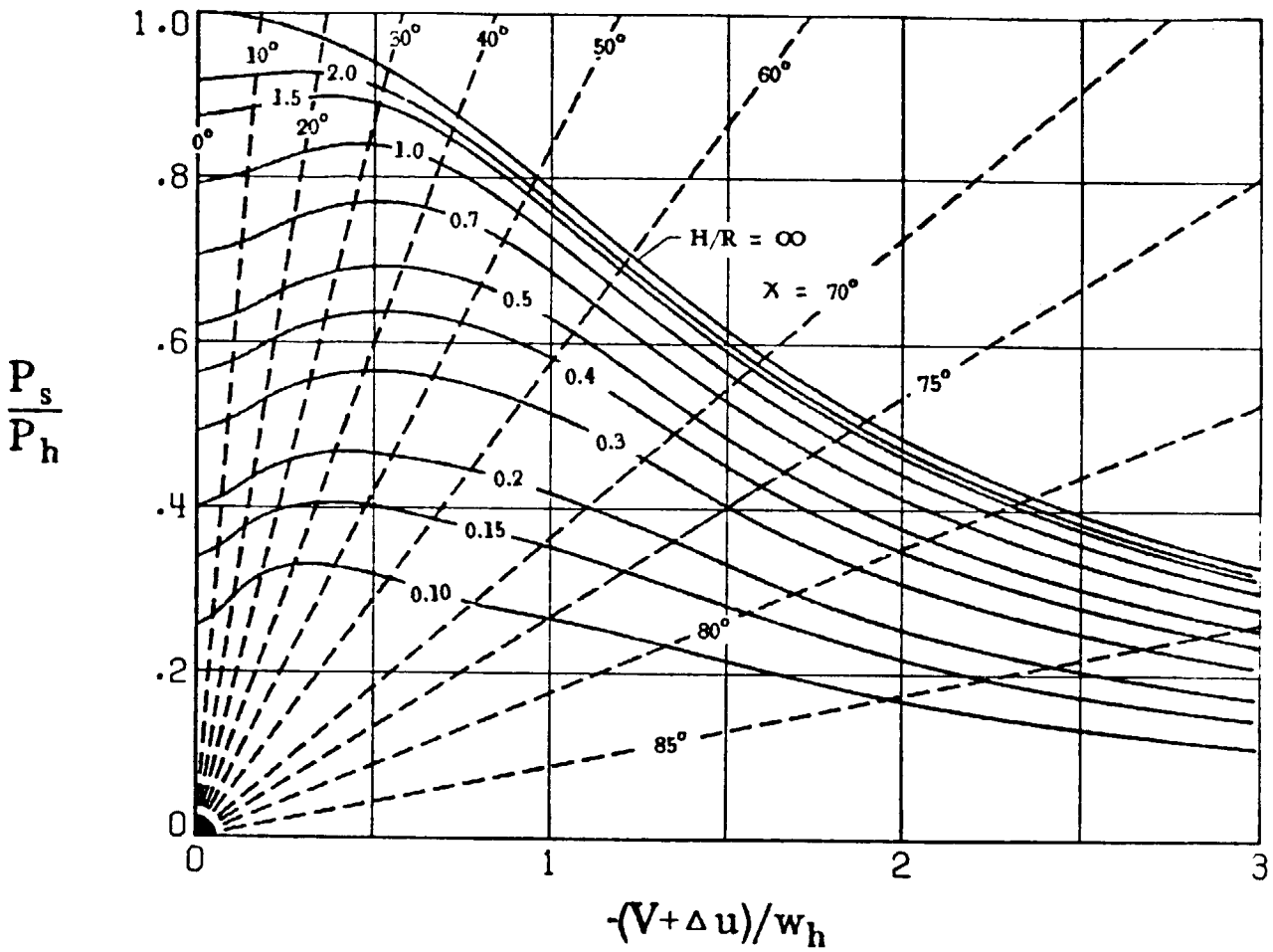

(a) Uniform disk-load distribution.

Figure 23. - Induced shaft power and momentum skew angle as a function of the aerodynamic speed ($V + \Delta u$) in ground effect. $\alpha = 0^{o}$.

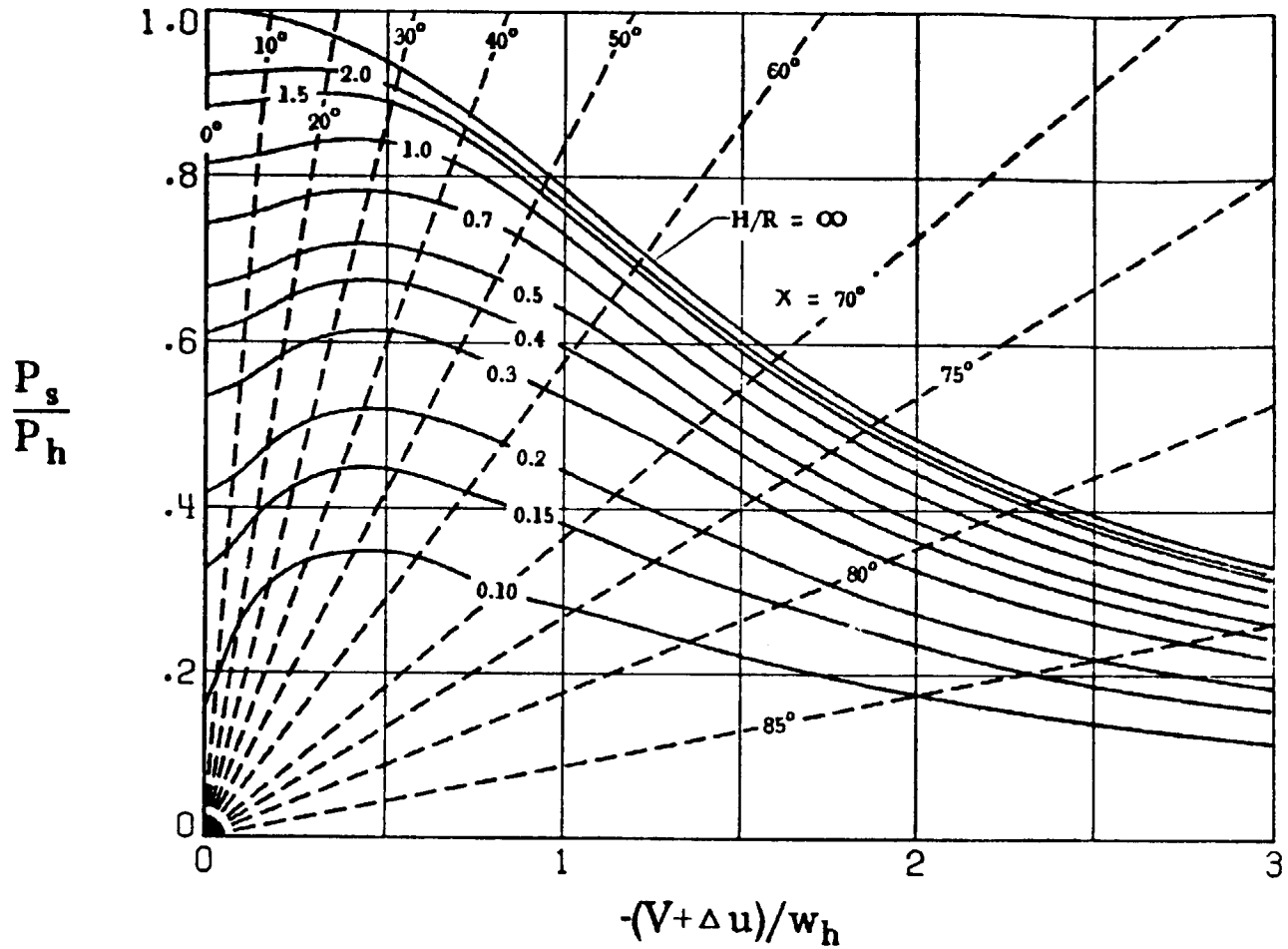

(b) Triangular disk-load distribution.

Figure 23. - Concluded.

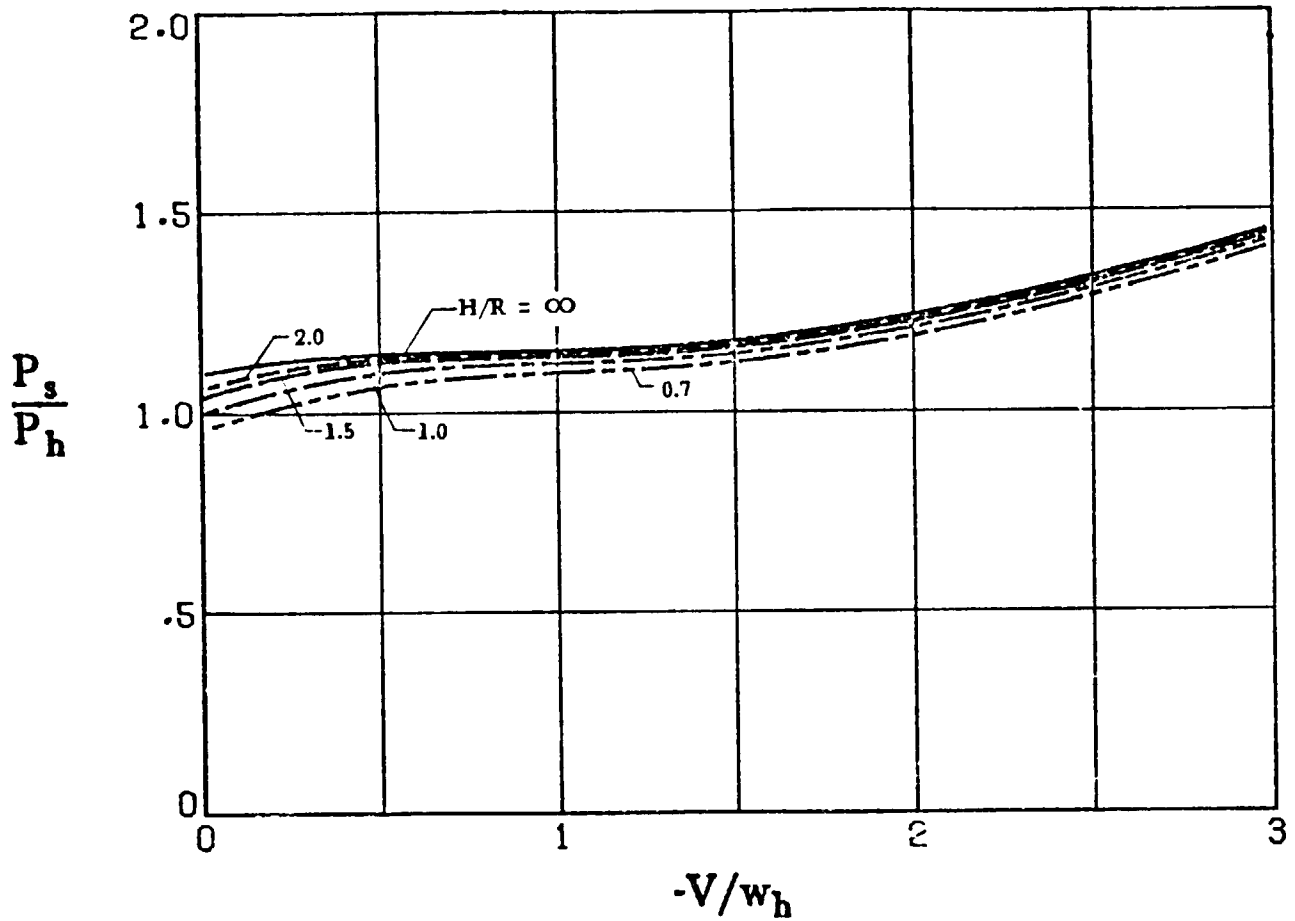

(a) $\alpha = -20^{o}$.

Figure 24. - Effect of angle of attack on the induced shaft power for a rotor with uniform disk-load distribution in ground effect.

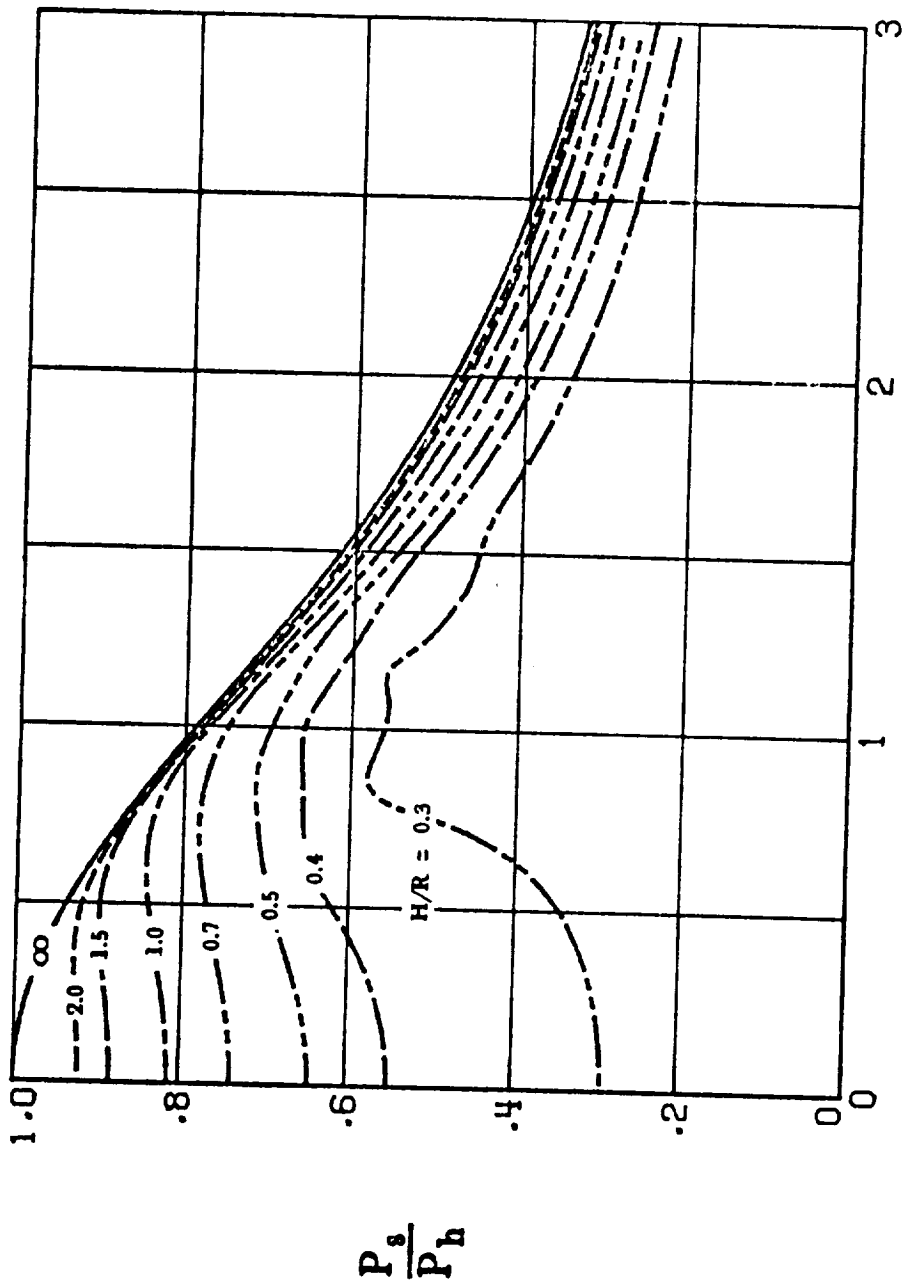

(b) $\alpha = 0^{o}$.

Figure 24. - Continued.

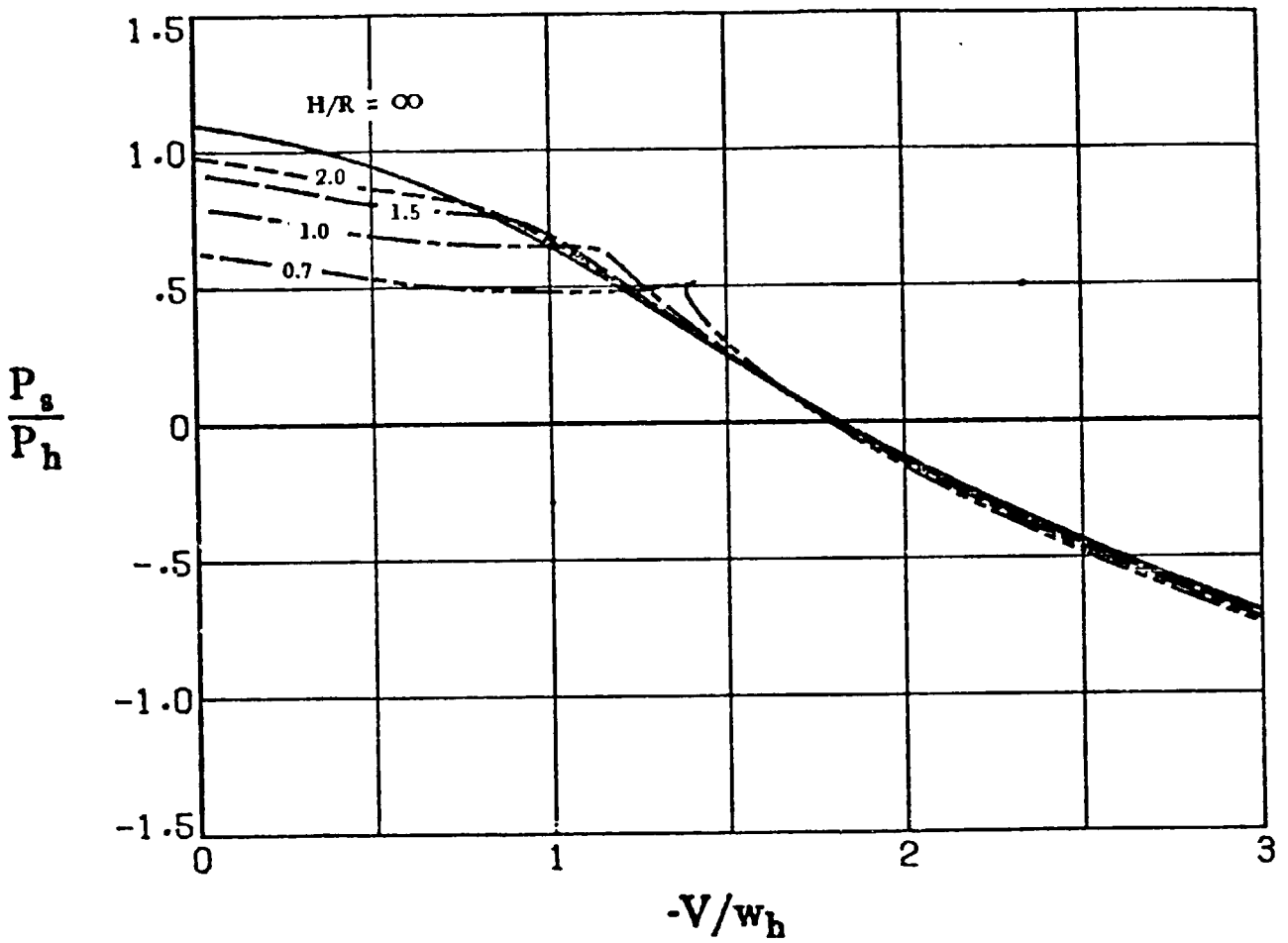

(c) $\alpha = 20^0$.

Figure 24. - Concluded.

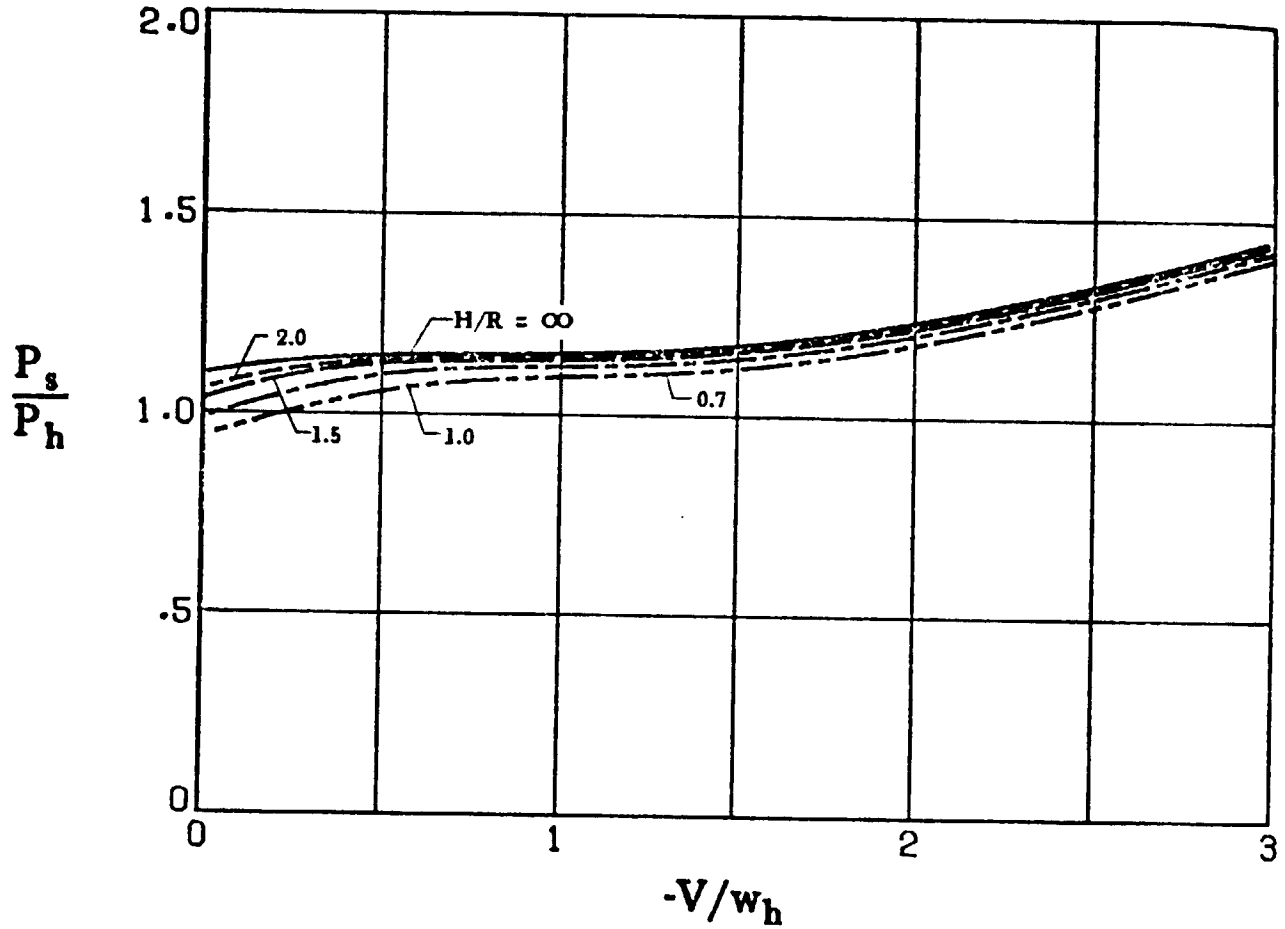

(a) $\alpha = -20^{0}$.

Figure 25. - Effect of angle of attack on the induced shaft power for a rotor with triangular disk-load distribution in ground effect.

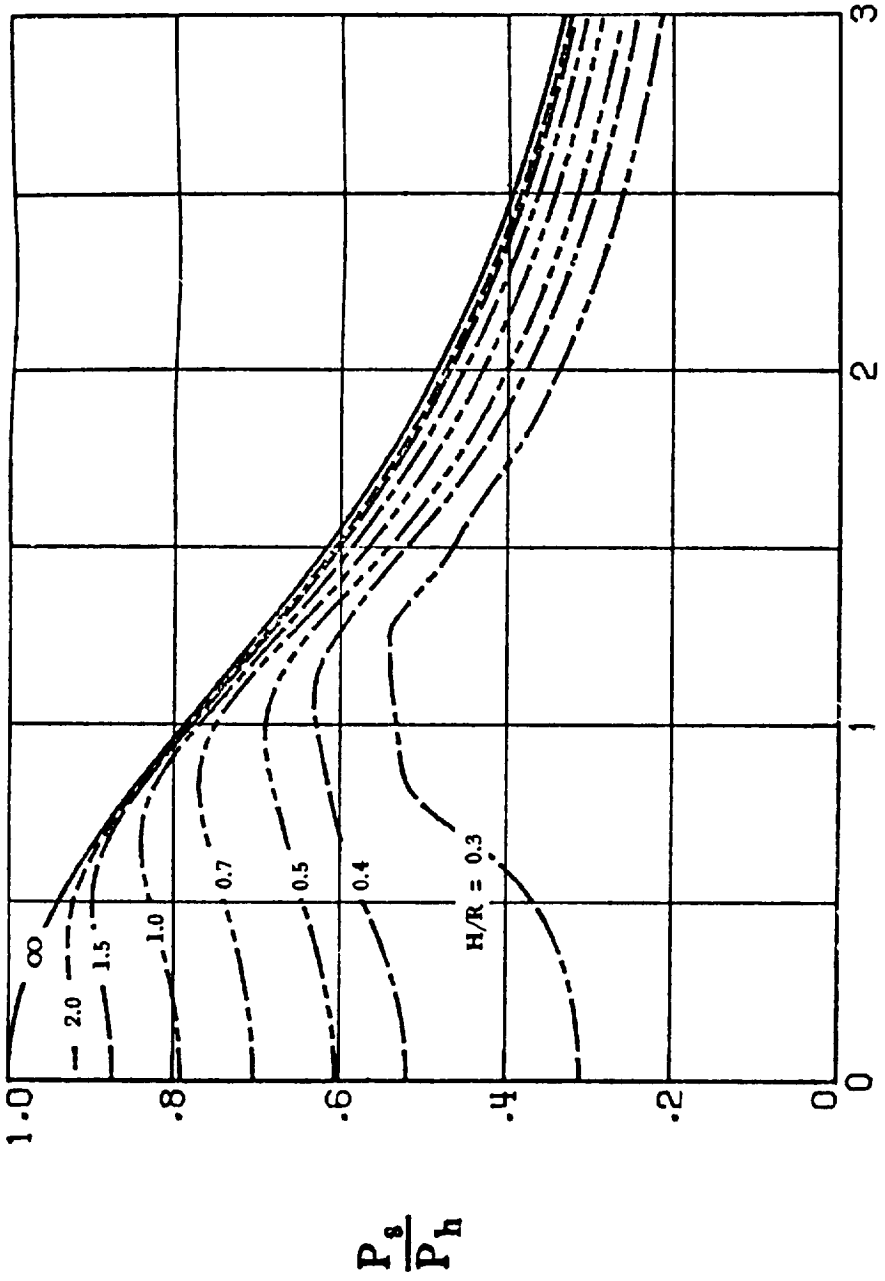

(b) $\alpha = 0^{o}$.

Figure 25. - Continued.

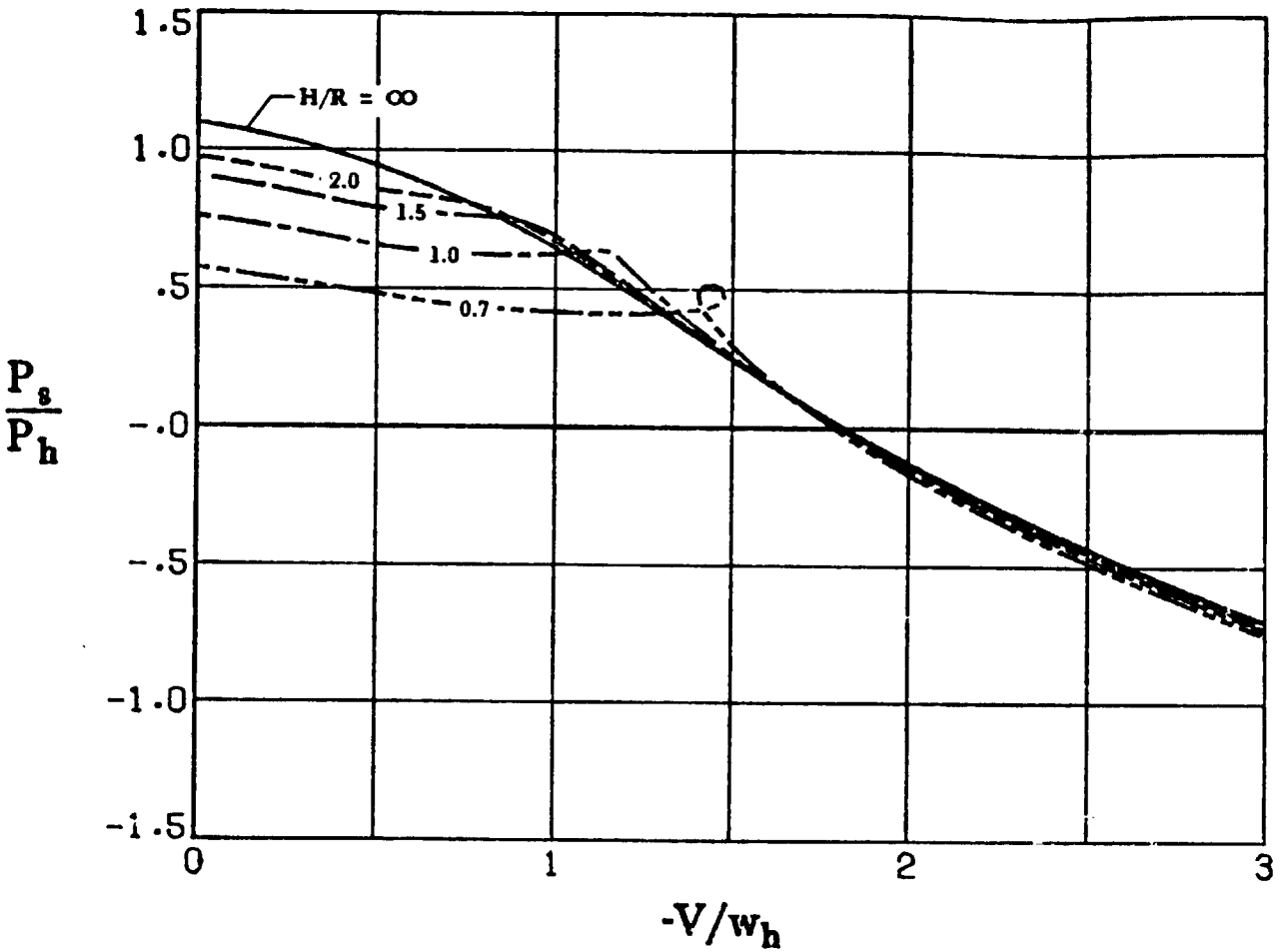

(c) $\alpha = 20^{o}$.

Figure 25. - Concluded.

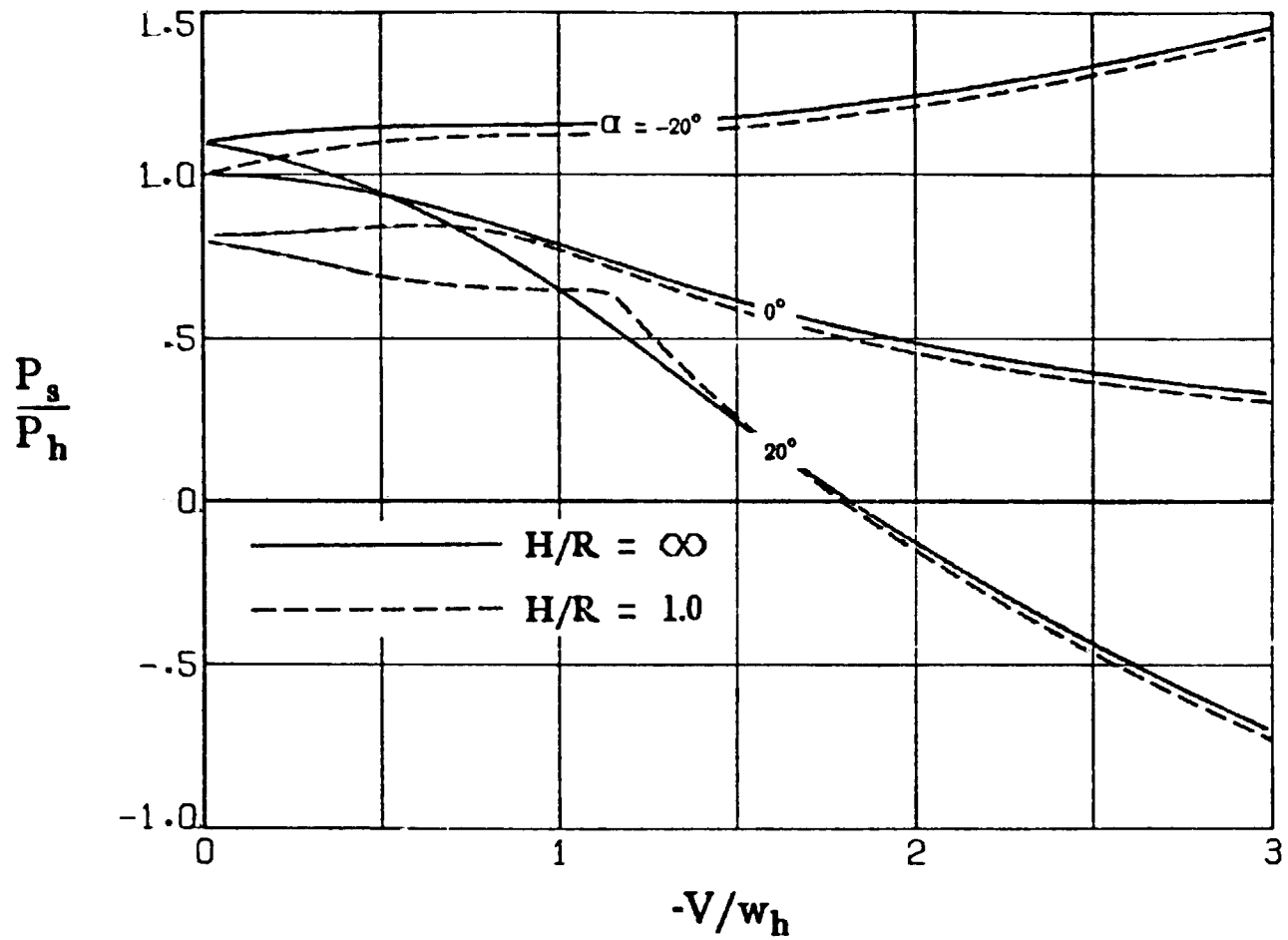

(a) Uniform disk-load distribution.

Figure 26. - Comparison of the induced shaft power required for accelerating and decelerating flight in free air and at a height of one radius above the ground.

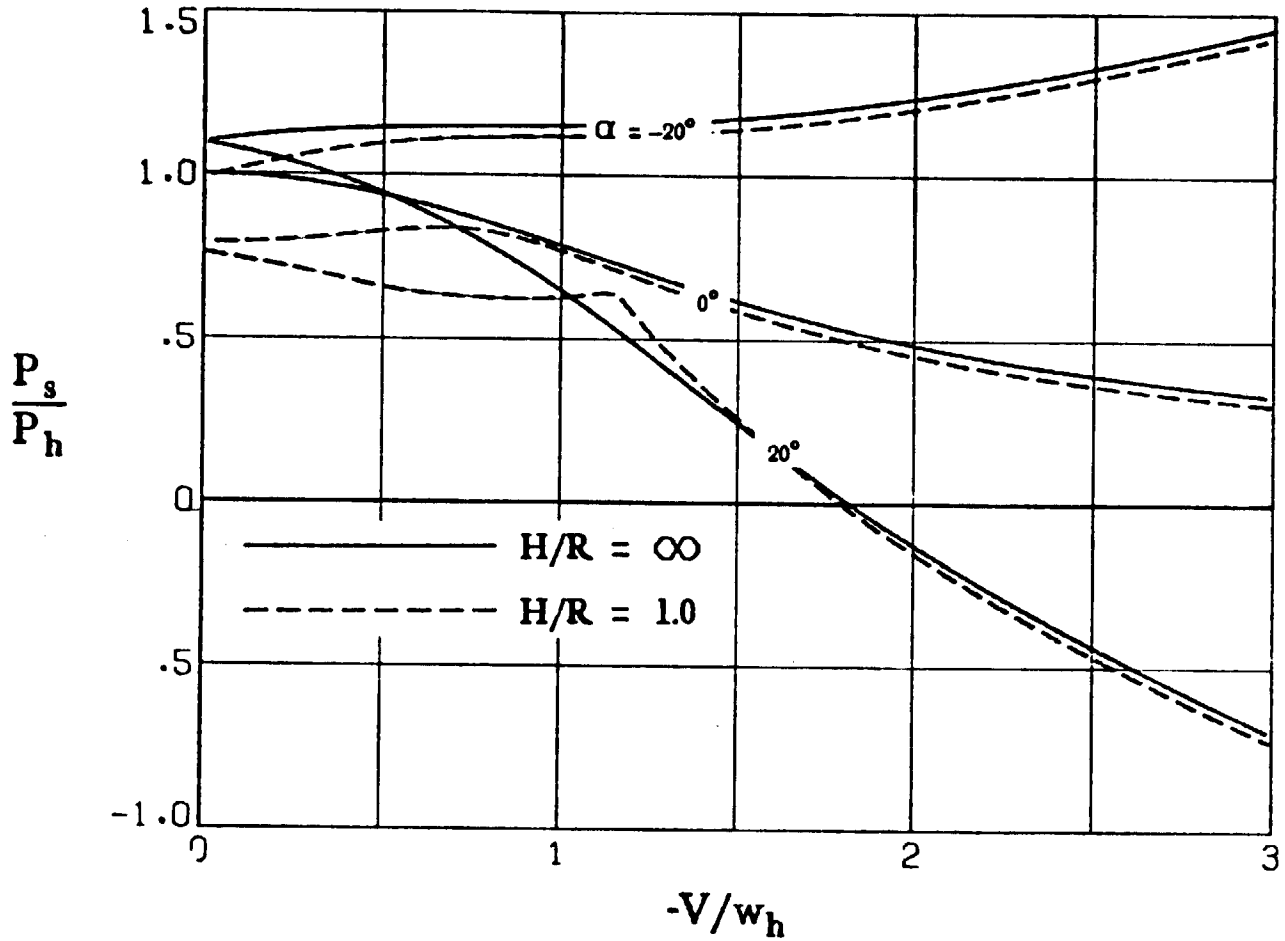

(b) Triangular disk-load distribution.

Figure 26. - Concluded.

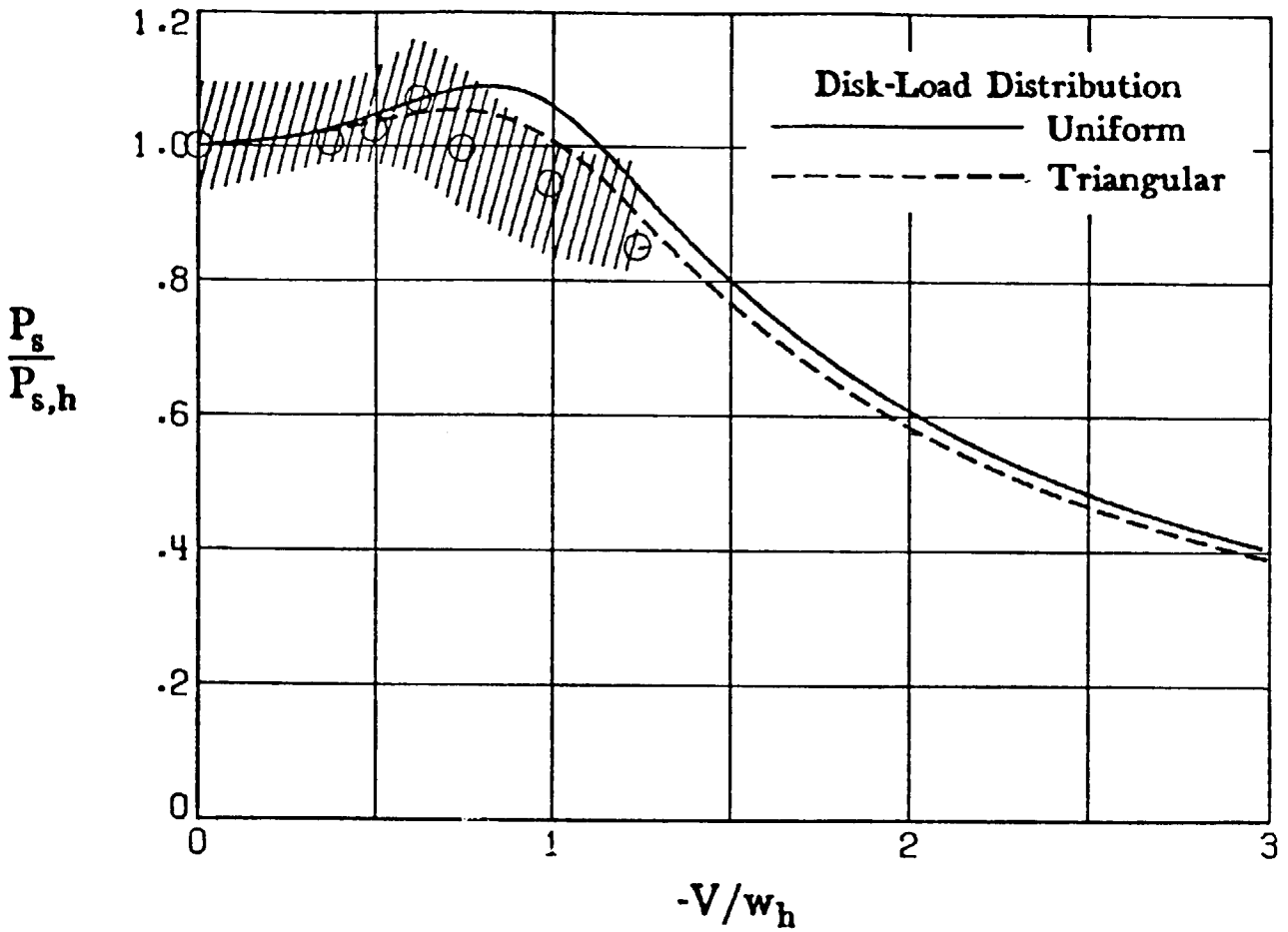

Figure 27. - Comparison of calculated shaft powers with the measured shaft powers of reference 5. The shaded region shows the range of measured powers and the symbols show the mean value of the measured power. H/R = 0.71.

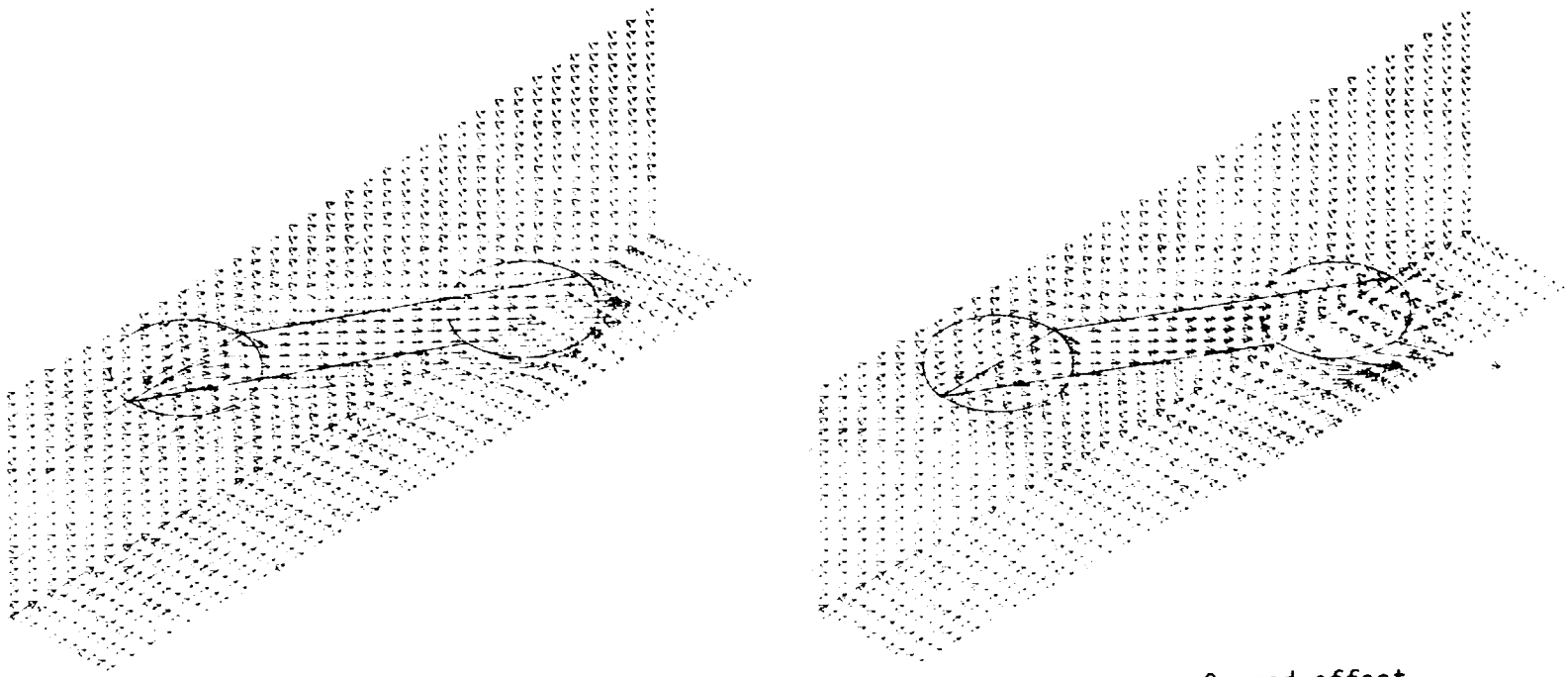

(a) $\chi = 70^{o}$

Figure 28. - Theoretically calculated flow vectors in the vicinity of a rotor in free air and in and in ground effect at H/R = 2.6. (Reference 23)

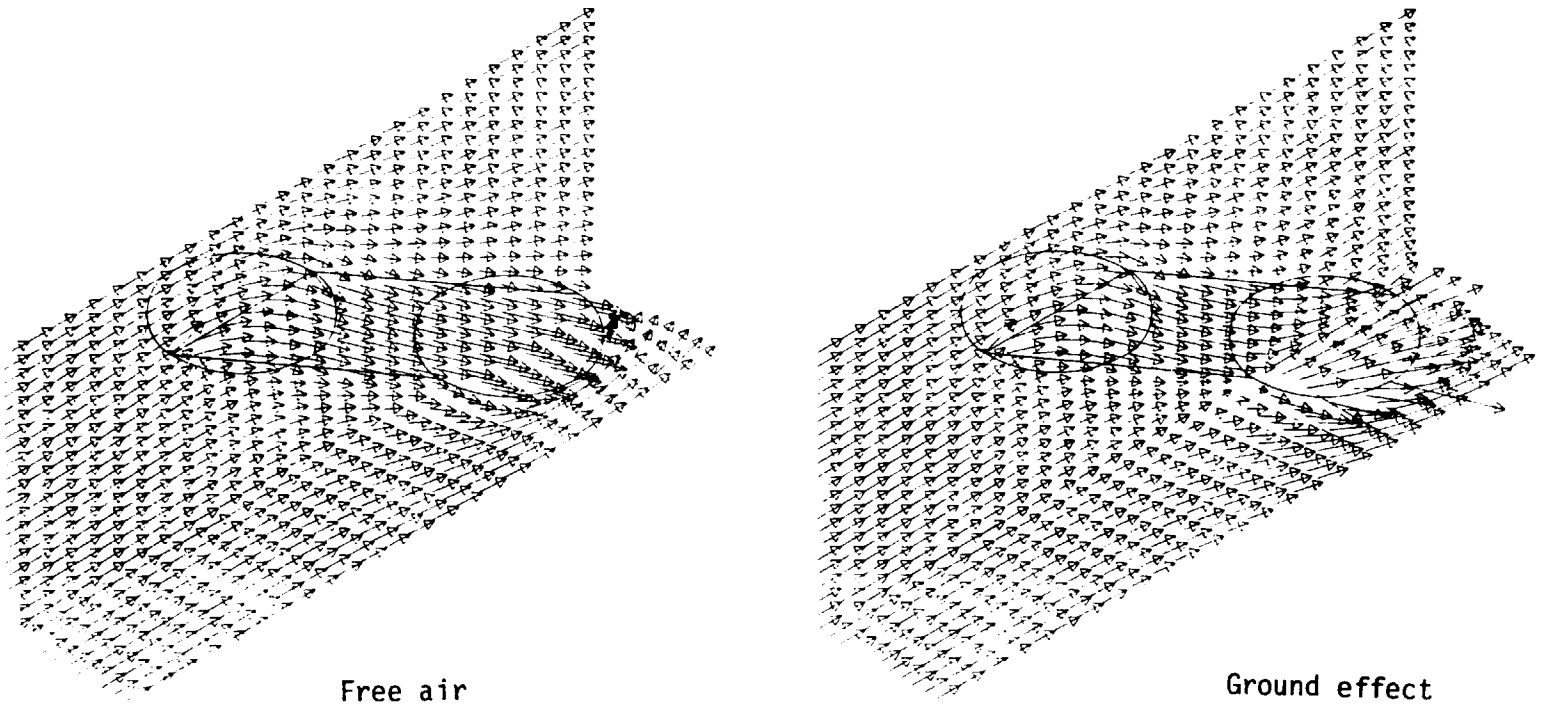

(b) $\chi = 60^{o}$

Figure 28. - Continued.

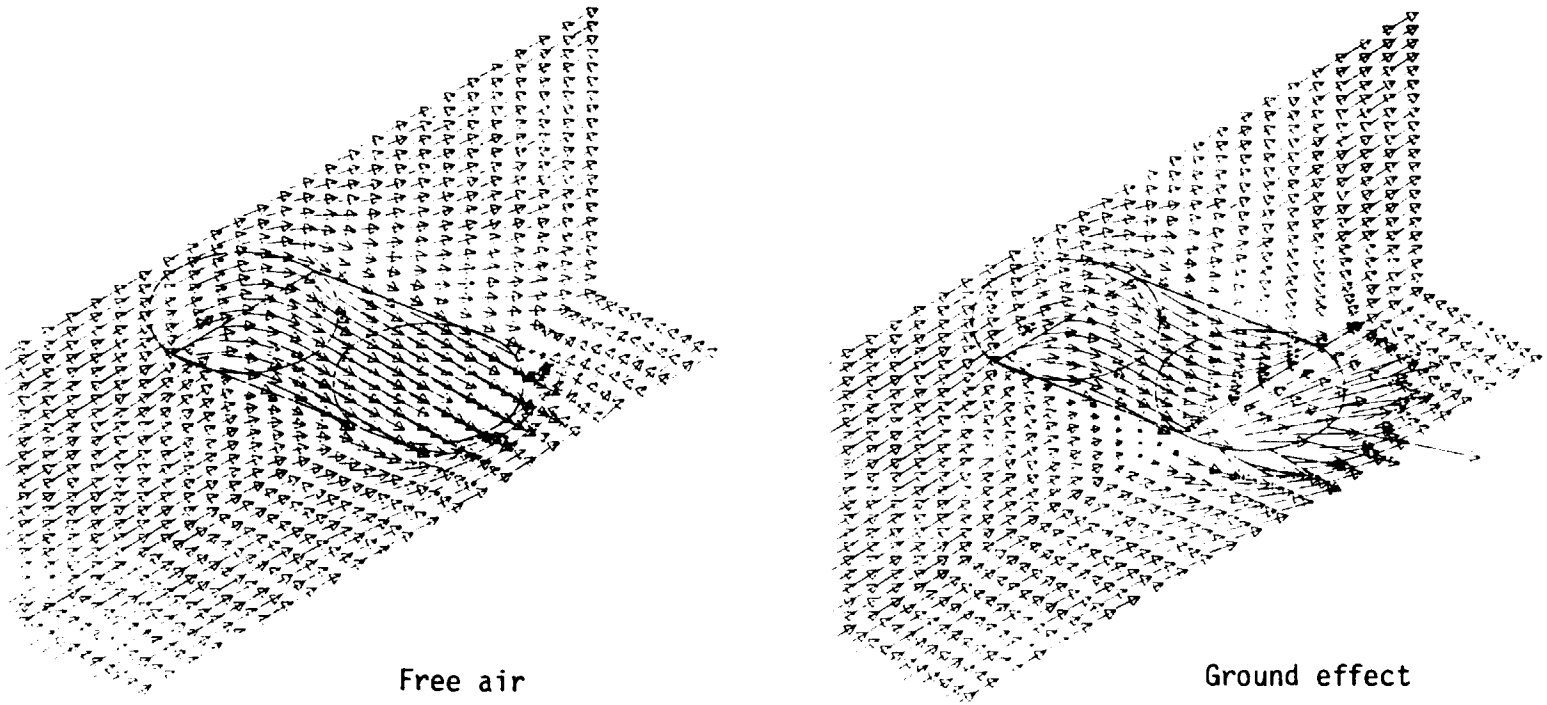

(c) $\chi = 50^{o}$

Figure 28. - Continued.

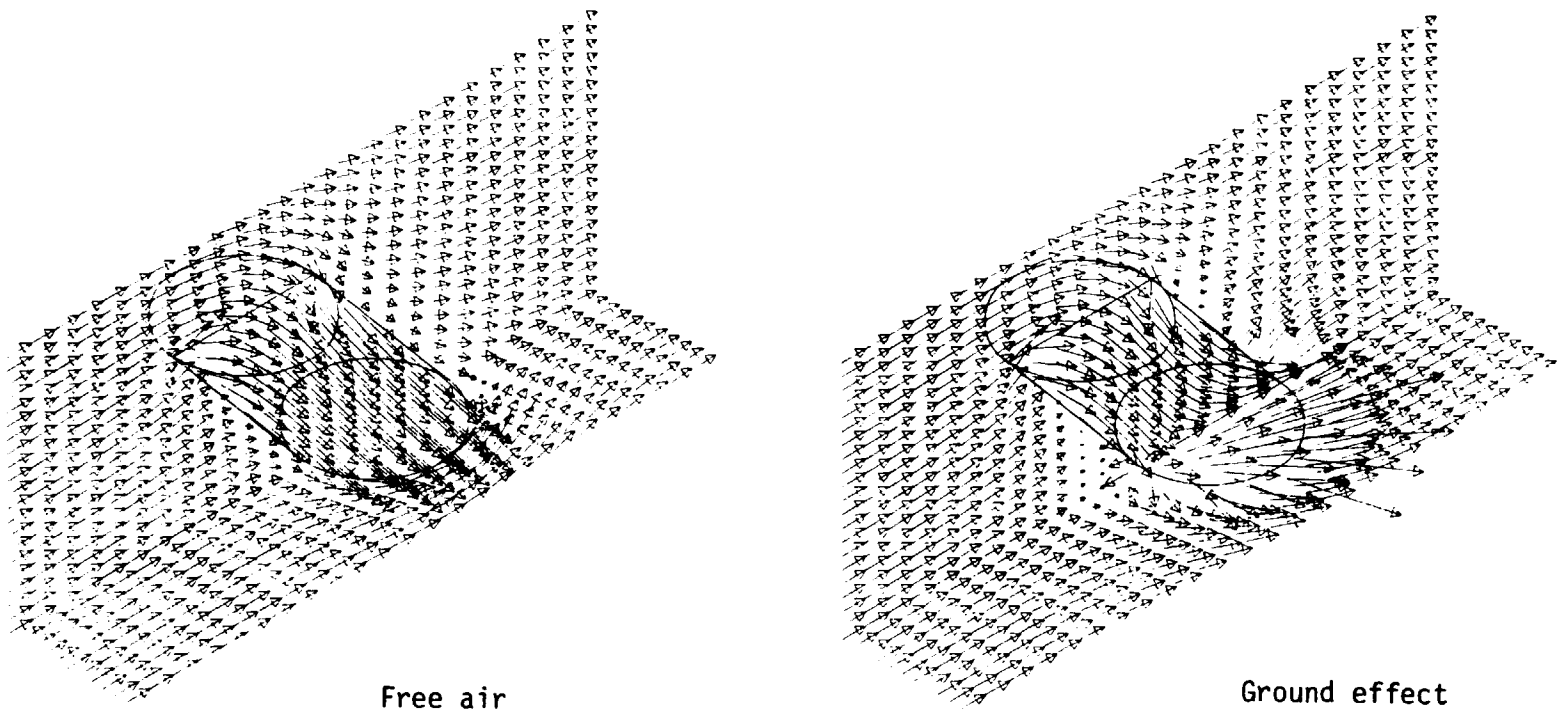

(d) $\chi = 40^{o}$

Figure 28. - Continued.

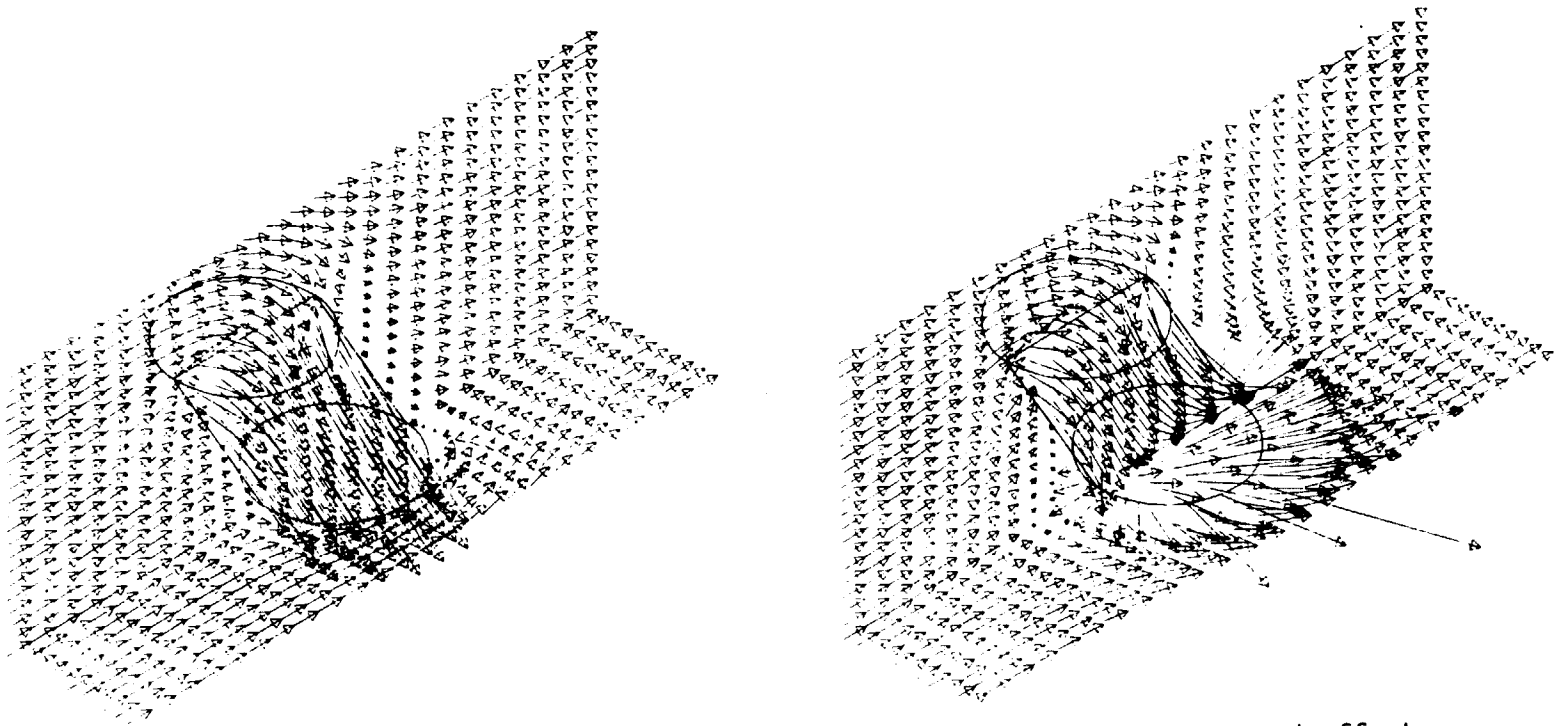

Free air

Ground effect

(e) $\chi = 30^{o}$

Figure 28. - Continued.

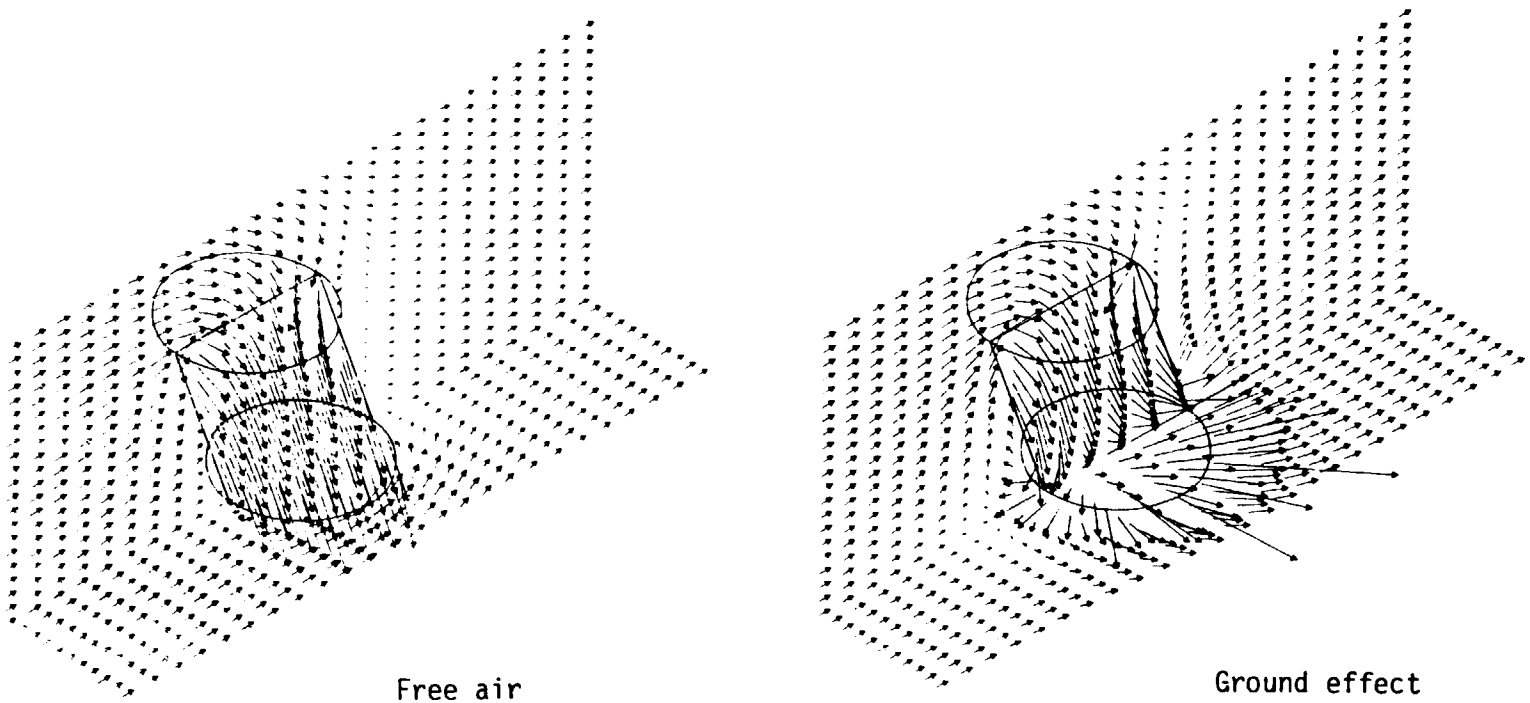

(f) $\chi = 20^{o}$

Figure 28. - Continued.

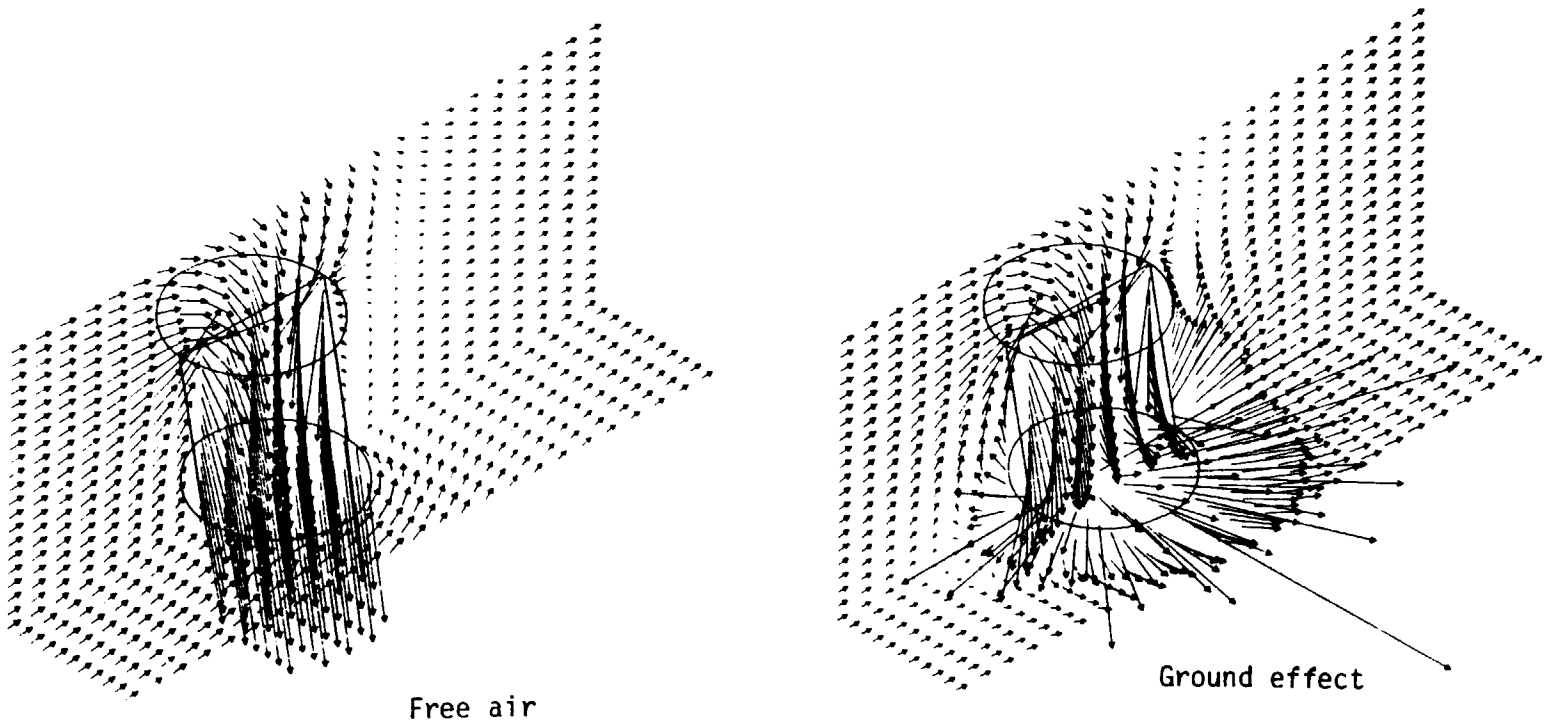

(g) $\chi = 10^{o}$

Figure 28. - Concluded.

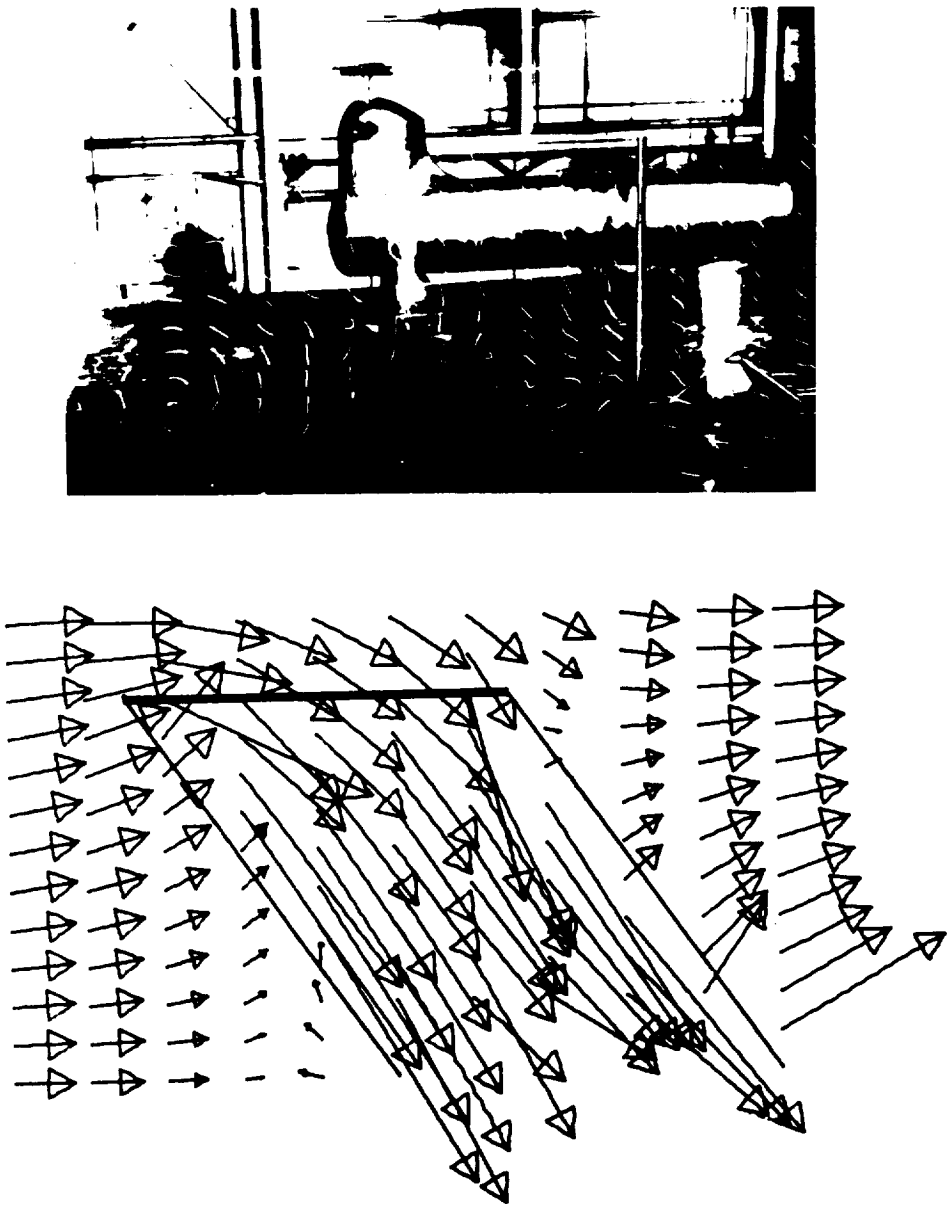

Figure 29. - Comparison (from reference 23) of the calculated flow field with a tuft-grid photograph from reference 40. Observe that the actual wake deformation is greater than the calculated deformation. Tuft grid and plane of calculation are 0.13 R to side of rotor. Calculations assume triangular load distribution. $H/R = 1.0$, $\chi \simeq 35^{o}$.

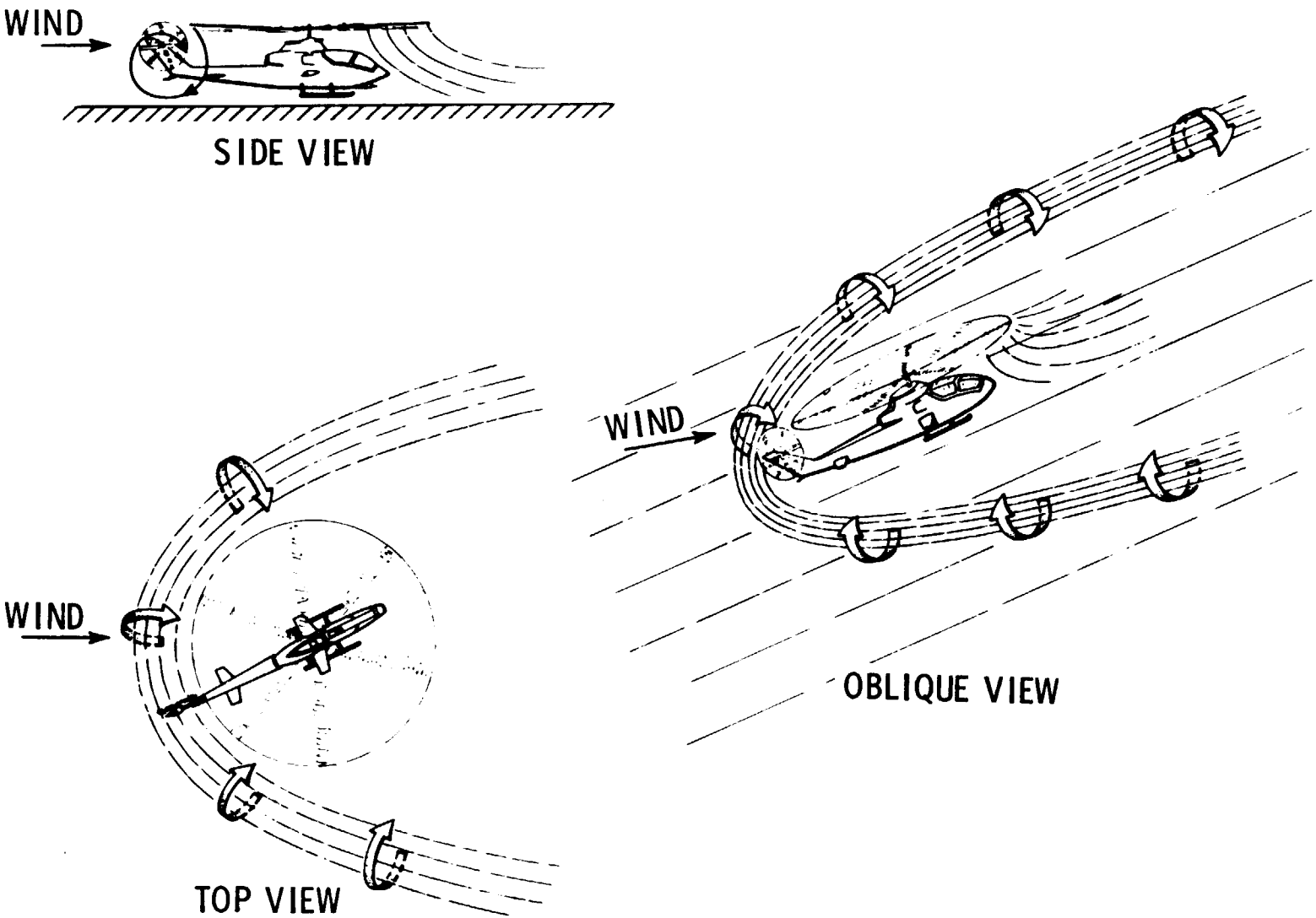

Figure 30. - Wake distortions which resulted in directional instability problems for helicopter hovering with tail winds in ground effect. (References 4 and 5)

NTIS does not permit return of items for credit or refund. A replacement will be provided if an error is made in filling your order, if the item was received in damaged condition, or if the item is defective.

Reproduced by NTIS
National Technical Information Service
U.S. Department of Commerce
Springfield, VA 22161

This report was printed specifically for your order from our collection of more than 2 million technical reports.

For economy and efficiency, NTIS does not maintain stock of its vast collection of technical reports. Rather, most documents are printed for each order. Your copy is the best possible reproduction available from our master archive. If you have any questions concerning this document or any order you placed with NTIS, please call our Customer Services Department at (703)487-4660.

Always think of NTIS when you want:
• Access to the technical, scientific, and engineering results generated by the ongoing multibillion dollar R&D program of the U.S. Government.
• R&D results from Japan, West Germany, Great Britain, and some 20 other countries, most of it reported in English.

NTIS also operates two centers that can provide you with valuable information:
• The Federal Computer Products Center - offers software and datafiles produced by Federal agencies.
• The Center for the Utilization of Federal Technology - gives you access to the best of Federal technologies and laboratory resources.

For more information about NTIS, send for our FREE *NTIS Products and Services Catalog* which describes how you can access this U.S. and foreign Government technology. Call (703)487-4650 or send this sheet to NTIS, U.S. Department of Commerce, Springfield, VA 22161. Ask for catalog, PR-827.

Name _____
Address _____
_____
_____
Telephone _____

- Your Source to U.S. and Foreign Government Research and Technology.